Physics – Uspekhi **37**(2) 185 – 217 (1994) ©1994 Uspekhi Fizicheskikh Nauk and Turpion Ltd

PACS numbers: 72.80. N

Amorphous semiconductors prepared by quenching under high pressure

S V Demishev, Yu V Kosichkin (deceased), N E Sluchanko, A G Lyapin

Contents

1. **Introduction** **185**
2. **Methods of solid-state amorphisation and amorphous semiconductors synthesised under high pressure** **186**
   2.1 Historical survey 2.2 Amorphisation during phase transitions under high pressure
3. **Theoretical aspects of the description of the kinetic characteristics of heterogeneous media** **189**
   3.1 Conductivity 3.2 Hall and Seebeck coefficients 3.3 Range of application of the models of multicomponent media
4. **Metal – insulator transitions in tetrahedral amorphous semiconductors synthesised under high pressure** **193**
   4.1 The metal – insulator transition in Cd – Sb, Zn – Sb, and Al – Ge alloys during amorphisation from a high-pressure phase 4.2 The MIT in a-GaSb synthesised by quenching under high pressure 4.3 Metal – insulator transitions in the a-GaSb : Cu system 4.4 Metal – insulator transitions in the a-GaSb : Ge system
5. **Crystallisation of the metastable phases of bulk amorphous gallium antimonide** **205**
   5.1 Variations of the structure of a-GaSb during crystallisation 5.2 Stability range and kinetics of phase transformations of the metastable phases in a-GaSb
6. **Metastable superconductivity in amorphous gallium antimonide** **210**
   6.1 Crystallisation and superconductivity in a-GaSb 6.2 Changes in the superconducting properties of the a-GaSb : Ge system 6.3 Critical behaviour of the conductivity of a medium containing superconducting inclusions. 6.4 Superconductivity in epitaxial GaAs layers
7. **Conclusions** **215**
   References **216**

Abstract. Amorphous semiconductors synthesised by high-pressure quenching (ASHP) are discussed as a new class of materials of potential value in explaining the mechanisms of solid-state amorphisation processes and in testing models of an effective medium and of the scaling theory and the percolation theory. The formation of multicomponent systems, the superconductivity induced by amorphisation, the stability regions of metastable phases, and the effect of doping on the physical properties of tetrahedral amorphous semiconductors have been studied by using a wide range of experimental methods capable of establishing the inter-relationship and the sequence of the phase transformations in ASHP produced by changes in the physical parameters. The bibliography contains 104 references.

S V Demishev, Yu V Kosichkin (deceased), **N E Sluchanko** Institute of General Physics, Russian Academy of Sciences, ul. Vavilova 38, 117942 Moscow. E-mail: demis@smp.gpi.msk.su.
A G Lyapin Institute of High-pressure Physics, Russian Academy of Sciences, Troitsk, Moscow Region

Received 21 October 1993
Uspekhi Fizicheskikh Nauk **164** (2) 195 – 230 (1994)
Translated by J I Carasso

1. Introduction

The study of the physical properties of amorphous semiconductors is one of the main endeavours in the modern physics of the condensed state. A group of now classical monographs published about 15 years ago effectively defined the scope of this field of study (see, for example, *Amorphous Semiconductors*, edited by M Brodsky, Topics in Applied Physics, Vol. 36, Springer, Berlin 1979). However, at that time (and, indeed, until very recently) amorphous semiconductors such as silicon, germanium, and $A^{III}B^{V}$ compounds were available only as films, and bulk amorphous materials of this type were effectively unknown to the scientific community: furthermore, the preparation of these materials was widely believed to be impossible in principle. Materials synthesised by solid-state amorphisation can be considered as an alternative to the traditional amorphous materials. Among the various solid-state amorphisation procedures, we shall examine the method which solves the 'insoluble' problem of producing bulk amorphous diamond-like semiconductors by using high pressures.

The method of synthesising amorphous semiconductors by using high pressures, which forms (with the study of the physical properties of these materials) the main topic of the present review, is not entirely new. The first report of the successful preparation of a bulk sample of an amorphous $A^{III}B^{V}$ semiconductor (GaSb) appeared in 1965 in a paper by

McDonald et al [1], who quenched the metastable GaSb II high-pressure phase (HPP) to liquid-nitrogen temperature. Subsequent heating at $p = 1$ bar led to amorphisation of the sample. Later work by Ponyatovskii and coworkers [2–5] on semiconductors of the ZnSb–CdSb system confirmed the formation of bulk amorphous materials under high-pressure conditions and produced the first reported measurements of their electrophysical characteristics. Why, then, did the field of research suggested by the results [1–5] fail (until quite recently) to stimulate the interest of scientists working on the physics of amorphous semiconductors? One possible explanation is that these studies of amorphisation effects [1–5] were aimed exclusively at phase transformations under high-pressure conditions, or alternatively that they were only a secondary result of a much wider study of phase transitions under pressure. This 'secondary' status of the results obtained for amorphisation under pressure led to their being treated as a scientific curiosity. In the second place, rapid developments in solid-state amorphisation (SSA) methods, which include high-pressure quenching [1–5], began in the early 1980s, and the importance of this field of study began to be understood only some 20 years after the publication of McDonald's pioneering paper [1]. Thirdly, the purely experimental difficulties of combining high pressures with cryogenic temperatures must also be mentioned.

It is now becoming accepted that SSA in the presence of high pressures can serve as a model of other SSA methods [6], and that an analysis for the structure and properties of amorphous semiconductors prepared at high pressures (ASHP) can provide an explanation of both the fundamental mechanisms of solid-state amorphisation and the special features in the behaviour of complex multiphase systems. Under these conditions, inclusions of submicron size formed during the synthesis of metastable phases are often found to have a controlling effect not only on the properties of the amorphous matrix but also on those of crystalline phases of binary and of ternary compounds.

Therefore the present review will be organised as follows. In the Section 2 we shall discuss current modifications of the scheme used in the synthesis of ASHP and the phenomenological models used in the description of SSA phenomena. Section 3 is devoted to a theoretical description of the electrophysical characteristics of heterogeneous media. In Section 4 we analyse the experimental results obtained for metal–insulator transitions formed in ASHP during their synthesis, doping, amorphisation, and crystallisation. The results of this section are widely used as the basis of study programmes on the formation of multiple phases in the ASHP a-GaSb. This problem is discussed in the next two sections, which give an analysis of the crystallisation of metastable phases in a-GaSb (Section 5) and of the metastable superconductivity process (Section 6).

2. Methods of solid-state amorphisation and amorphous semiconductors synthesised under high pressure

2.1 Historical survey

The term solid-state amorphisation (SSA) refers to a group of methods which do not require quenching of the liquid phase or deposition on a cooled substrate in order to produce amorphous material. Therefore the SSA methods offer an alternative to the standard technologies [7–9] conventionally used in the preparation of amorphous semiconductors (for example, a-Si). The SSA group includes solid-phase reactions [10, 11], mechanical melting [12–14], amorphisation under irradiation or ion implantation [15, 16], hydrogenation [17], and phase transitions at high pressures [18–28].

Published results [10–14] show that solid-phase reactions and mechanical melting can produce SSA in binary metallic alloys and in intermetallic compounds. Hydrogenation is also restricted in its applications to the specific range of compounds which can absorb hydrogen effectively [17]. Thus the only methods available for semiconductors are ion implantation and phase transitions under high-pressure conditions. The first of these methods is confined to the preparation of thin-film samples in which the amorphous layer has a thickness of a few mircometres [15].

Since the present review is aimed mainly at the bulk tetrahedral semiconductors, the high-pressure phase transitions are the only SSA methods which can be used to solve the experimental problems met in the synthesis of these materials [1–5, 29, 18–28]. We shall also analyse in detail the view currently held on this SSA mechanism. We note that the use of high pressures allows amorphous metals as well as amorphous semiconductors to be synthesised [29, 30]. SSA can take place under high-pressure phase transition conditions both during increases in the pressure p and while the high-pressure phase is relaxing to the normal temperature T and pressure p. In the former case an increase in p to $p > p_{tr}$ at $T =$ const converts the initial ordered phase (stable at $p = 1$ bar) into a disordered amorphous structure with a short-range order structure similar to that of the HPP rather than into an ordered HPP [where $p_{tr}(T)$ is the phase transition point] [31–35]. In the latter case the ordered crystalline HPP, stable at $p > p_{tr}(T)$, is converted into an amorphous phase with a short-range order structure similar to that of the initial ($p = 1$ bar) phase during its reversion to the normal conditions. The HPP of semiconductors such as silicon, germanium, and $A^{III}B^{V}$ compounds is a metal [6, 19] with a coordination number $Z = 6$, markedly different in its characteristics from the initial, tetrahedral semiconducting phase, which has $Z = 4$. Therefore in order to obtain bulk samples of ASHP we must use an SSA scheme in which the phase transition is HPP (metallic) $\rightarrow$ amorphous semiconductor.

Historically, the first observations of SSA during the relaxation of a high-pressure phase (metastable under normal conditions) were made by Stishov [36] in 1961 during a study of phase transformations in quartz. He found that heating stishovite (the metastable HPP) at $p = 1$ bar did not immediately induce the stishovite–quartz transition: a transition to a disordered phase was first observed. However, at that time this line of study (related to SSA) was not followed up, but the stishovite–amorphous SiO_2 transition was later studied in depth by several workers (see, for example, Stishov [36]). In the early work [1–5] the SSA phenomenon was not always interpreted as the achievement of an amorphous state. For example, the amorphisation of zinc antimonide was observed even in the first study reported by Ponyatovskii et al. [2], but the authors interpreted the amorphous phase not as amorphous zinc antimonide but as an undefined 'fine structure' resulting from the dissociation of ZnSb. A correct interpretation of the SSA phenomenon in the Zn–Cd–Sb system was given by Belash and Ponyatovskii [5], who first measured the electrophysical characteristics of these ASHP. It was found

that the conductivity of a-ZnSb is described by the activation law $\sigma \propto \exp(-E_a/k_B T)$ with an activation energy $E_a = 0.21$ eV, a Hall mobility μ not greater than ~ 5 cm^2 V^{-1} s^{-1}, and a Seebeck coefficient of sign corresponding to p-type conduction.

The 'recent history' of the ASHP stable at $T = 300$ K and $p = 1$ bar originated from the work of Mishima et al. [31], published in 1984, who proposed a model of SSA based on ice and used it to discuss the possibility of the amorphisation of various materials including tetrahedral semiconductors. It should be noted that SSA in solid-phase reactions and in mechanical melting had been detected a year earlier [10, 12]. Mishima's paper [31] stimulated the appearance of a still increasing number of publications on the problem of SSA through a high-pressure phase.

In 1985 Popova et al. [18] discussed the SSA of gallium antimonide by 'quenching the melt under high pressure'. They suggested the formation of a metallic glass with a short-range order structure similar to that of the metallic HPP (GaSb II) under conditions of fast cooling ($10-10^3$ K s^{-1}) at $p = 90$ kbar. When the pressure was lowered to $p = 1$ bar at $T = 300$ K the metallic glass was converted into a tetrahedral amorphous phase. More recent work [23] failed to confirm this hypothesis: as in the original publication [1] the amorphous a-GaSb phase was formed as a result of the GaSb II $\to$ a-GaSb phase transition. Unlike the other approaches known at the time, the SSA process used by Popova [18] did not require cryogenic temperatures for quenching the HPP: this simplified the synthesis and made samples of a-GaSb more readily available for physical investigations. In the same year Demishev and his coworkers began their continuing study of the electrophysical properties of a-GaSb [37].

In 1987 Ponyatovskii and Barkalov, with their coworkers, began publishing a series of papers [20–27] on the SSA accompanying phase transitions in the Al–Ge, Zn–Sb, and Cd–Sb systems. Special attention was paid to the thermodynamics of the HPP $\to$ amorphous semiconductor transformation, and also to the changes in the electric conductivity of the sample during the SSA. This group of studies has been discussed in a recent review [6]. We can see that up to the year 1987 the range of known ASHP had not been extended in comparison with the work carried out during 1965–1977, and was confined to the Ga–Sb, Zn–Sb, Cd–Sb, and Al–Ge systems. However, the progress made in the study of these ASHP stimulated a search for new tetrahedral semiconductors prepared by the SSA method. A paper by Clarke et al. [38] on the preparation of a-Ge and a-Si by using a diamond indenter appeared in 1988. The thickness of the ASHP samples obtained in this way was ~ 100 μm, and amorphisation was achieved only near the centre of the diamond needle. Obviously, these samples are no more than a laboratory curiosity, useless for serious studies. A similar state of affairs was reported for another industrial semiconductor: gallium arsenide. Vohra et al. [39] attempted to synthesise this material by the diamond anvil method, but they could not produce reasonably large samples. The synthesis of bulk samples of a-Si and a-Ge ASHP was reported only in 1992, by Brazhkin et al [28].

To conclude this brief historical survey we should note that the physics of ASHP is now a well established science. Since 1985 both a range of suitable materials and some fundamental concepts on the mechanism of SSA and on the genesis of the physical properties of ASHP have been developed. The trend towards a general increase in the number of investigations and towards an expansion of the range of experimental substances is growing steadily. The experiments briefly outlined in the present section do not amount to an exhaustive description of the history of the problem or of the large fund of physical phenomena now known to be characteristic of SSA: our aim at this stage was merely to identify the key events in the development of this field of studies.

2.2 Amorphisation during phase transitions under high pressure

The $p-T$ phase diagram shown in Fig. 1a is typical of substances displaying solid-state amorphisation through a high-pressure phase [6]. The line *ab* defines the equilibrium of the I $\to$ II phase transition [$p_{tr}(T)$]. The point *a* is the triple point, corresponding to the equilibrium between phases I and II and the melt. For the semiconductors discussed in this review (Ge, Si, $A^{III}B^V$ semiconductors, the ZnSb–CdSb system) phase I is the semiconducting phase (in the case of GaSb, a tetrahedral semiconducting phase with the zinc blend structure, $Z = 4$), and phase II is the metallic HPP (for GaSb a structure of the β-Sn type, $Z = 6$) [6, 19]. This group of substances melts with a negative change in the specific volume, like ice, and their liquid phase has a metallic character, with a short-range order structure similar to that of the HPP [40–42].

The synthesis scheme represented by the line *ABCD* in Fig. 1a was proposed as a means of preparing a bulk ASHP sample stable at $p = 1$ bar [1–5, 20–28]. The high-pressure phase (phase II, point *A*) was cooled to liquid-nitrogen temperature at $p = \text{const} > p_{tr}$ (point *B*). The pressure was then reduced to atmospheric at $T = $ const, bringing the HPP to a metastable state (point *C*). Lastly, at $p = 1$ bar, the temperature of the sample was raised (along the line *CD*), and amorphisation was obtained at a temperature $T = T_{am}$.

The phase diagram of CdSb (obtained [2] for $T \geqslant 250$ °C) and the amorphisation scheme used [20–27] to amorphise the alloy $Cd_{43}Sb_{57}$ are shown in Fig. 1b. The HPP (the γ phase in Ponyatovskii's terminology [6]) was subjected to the thermobaric treatment by the scheme $A \to B \to C$. Amorphisation was induced at $T_{am} \approx 50$ °C by heating the sample along the line *CD*; a further increase in temperature caused crystallisation of the amorphous sample in the region of $T \geqslant T_{cr} \approx 100$ °C. Under these conditions the excess of antimony was released in the form of inclusions in the semiconducting CdSb matrix.

Departures from stoichiometry were introduced into the ZnSb–CdSb system used by Ponyatovskii and coworkers [20–27] because small deviations from stoichiometry offer a more homogeneous HPP (the γ phase), and therefore they produce more uniform and perfect amorphous samples.

In a series of studies [20–27] by scanning calorimetry and dilatometry the thermodynamic characteristics of the SSA were measured with respect to the $A \to B \to C \to D$ process (Figs 2a and 2b). It was found that in the ZnSb–CdSb system the SSA produced by the relaxation of the HPP is an exothermic process (curve *1* of Fig. 2a), accompanied by expansion of the sample. A further increase in temperature results in crystallisation of the sample and in the appearance of a new exothermic peak (curve *2* of Fig. 2a). The sample is also slightly compressed in the region of $T > T_{cr}$ (Fig. 2b).

These observations were used as evidence for interpreting the SSA as a phase transition of the first kind. According to

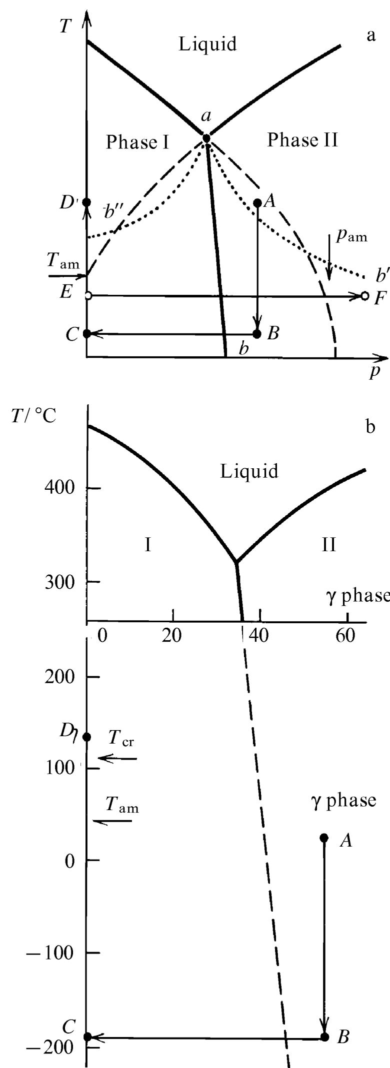

Figure 1. Scheme for the synthesis of the ASHP): (a) general case; (b) ASHP a-$Cd_{43}Sb_{57}$ (phase diagram for $T > 250$ °C taken from Ref. [6]).

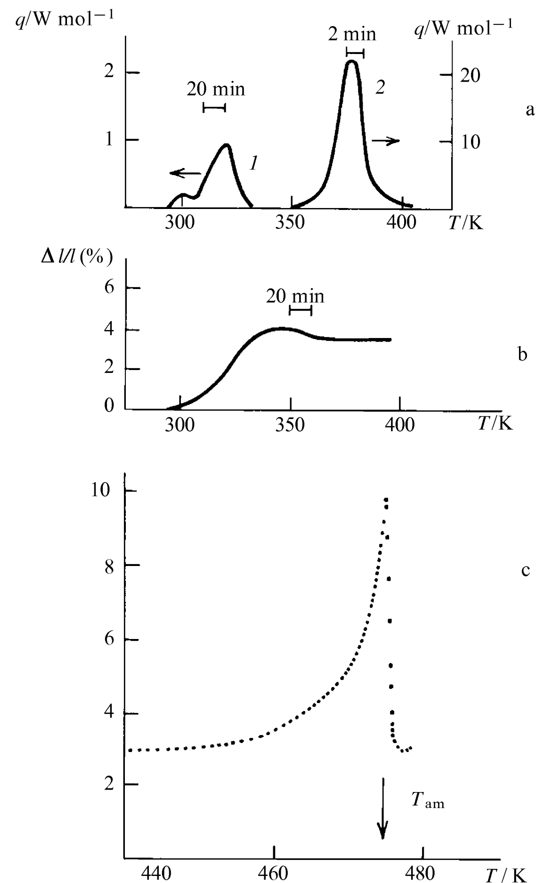

Figure 2. Thermodynamics of the SSA process: (a) heat evolution; (b) elongation (CdSb system) [6]; (c) specific heat ($Fe_2ErH_{3.4}$) [17].

Brazhkin et al. [43] the SSA is a phase transition of the first kind in which the growth processes are hindered, with bulk nucleation beginning at $T = T_{am}$. As a result of this hindrance the nuclei having the characteristic size $L_c \approx 10$ A cannot grow further, and the ordered phase I is replaced by an amorphous structure having the same short-range order as the ordered semiconducting phase.

However, the suggested explanation of the results in Figs. 2a and 2b cannot be used as a universal mechanism of the SSA process. It was shown [17] that in the amorphisation of the compound $Fe_2ErH_{3.4}$ the specific heat displays a singularity typical of phase transitions of the second kind (Fig. 2c). As a result the 'amorphous order parameter' of the SSA can be set in the bulk of the sample either smoothly (through nucleation and growth processes) or discontinuously.

There have been attempts to interpret the singularity in the specific heat in terms of the current theories of glass transition [44]. However, the validity of applying these theories, based on the quenching of a liquid phase, in the explanation of the SSA process is extremely doubtful.

Since the experimental data now available suggest that the various SSA schemes have a common physical origin, any theory proposed for this process must be able to account for the data in Figs 2a – 2c from a unified viewpoint, treating the manifestations of phase transitions of the first and the second kind as different limiting cases. However, as far as the present writers are aware, no such theory has so far been put forward.

One of the first models of SSA during phase transitions under high pressure was produced by Mishima et al. [31] on the basis of experimental data on the SSA of ice (the 'cold melting' model). Their approach was later called [6] the concept of the 'absolute instability line'.

Let us examine the $p - T$ phase diagram for a substance which melts with a negative volume discontinuity and whose HPP has a structure similar to that of a liquid (Fig. 1a). Following Mishima et al. [31] we shall extrapolate the melting curve of phase I to the pressure region above the triple point (broken line in Fig. 1a), and we shall call this the 'absolute instability line' [6, 31]. The following hypothesis was proposed [31]: if phase I is metastable in the vicinity of the absolute instability line, its intersection is equivalent to 'melting', which in the solid-phase variant corresponds to the formation of an amorphous phase.

Clearly, in order to realise a process of this kind the phase I → phase II transition must be kinetically hindered. In actual experiments this state of affairs is almost always encountered, since the I → II transition takes place on the *ab* equilibrium line only when the process responsible for the increase in pressure is infinitely slow.

If the rate of increase of the pressure is finite the I → II transition takes place at high pressures $p'_{tr} > p_{tr}$ (line ab').

We note that when the temperature is lowered, p'_{tr} must increase because of the decreased mobility of the atoms. An analogous nonequilibrium line (ab'') appears in a phase transition of type II $\rightarrow$ I at pressures $p''_{tr} < p_{tr}$ (Fig. 1a).

Thus according to Mishima et al. [31] SSA will take place on moving along the line *EF* (Fig. 1a) if the sample intersects the absolute instability line before it intersects the ab' line. This situation results in a disordered 'metallic' phase with a short-range structure similar to that of the HPP or of the liquid. Evidently, this behaviour can be reproduced by carrying out the phase transition process at sufficiently low temperatures.

Mishima's ideas [31] were tested on various systems (in particular, the molecular crystals SnI_4, GeI_4 [32], and graphite [33–35]) as well as on ice. Typical results on the solid-state amorphisation of graphite under elevated pressure, detected by the Raman scattering of light (with diamond anvils used to generate high pressures), are shown in Figs 3a and 3b. Increasing the pressure shifts the initial narrow line towards higher frequencies and broadens it substantially, denoting a disordering of the crystal lattice (Fig. 3a). It is interesting to note that the form of the 'amorphous spectrum' is not strictly defined and depends on the initial sample (Fig. 3b). We also note that SSA takes place at relatively high pressures in graphite, the amorphisation pressure being $p_{am} \approx 230$ kbar (Fig. 3a).

Similar ideas [31] were later developed by other workers [45, 46]. A slightly different approach was proposed by Fecht and Johnson [47], who treated the SSA point as an isolated critical point on the concentration–temperature phase diagram at which the difference between phase transitions of the first and the second kind disappears [47]. Evidently, this treatment assumes that the SSA is confined to binary or multicomponent systems, but the observations of SSA in elemental semiconductors [28, 38] highlight the limitations of this approach.

Attempts have been made [6, 19, 43] to extend the concept of an absolute instability line to the high-pressure phase $\rightarrow$ amorphous semiconductor transition (the process *ABCD* in Fig. 1a). It was suggested that in this case the extrapolation of the melting curve for phase II (Fig. 1a) plays the role of an absolute instability line. As in Mishima's work [31] amorphisation was observed when the sample intersects the absolute instability line before it intersects the nonequilibrium phase transformation line ab', and the amorphisation temperature T_{am} was defined as the intersection of the extrapolated melting curve with the T axis (Fig. 1a).

However, unlike the case of the *EF* process, this approach to the *ABCD* process is internally inconsistent. Thus, the quasimelting at the point T_{am} should correspond to the formation of a disordered metallic specimen (since a metallic melt is typical of all the compounds considered here), whereas in the experiment we observe the formation of an amorphous semiconductor rather than an amorphous metal. To resolve this contradiction it was suggested [6] that an amorphous metal is actually formed at $T = T_{am}$, but it is unstable and exists for a very short time before rapidly decomposing. Clearly, a product of this type would be undetectable in practice.

Thus in the case of the *ABCD* process there is no physical justification for constructing the absolute instability line by extrapolating of the melting curve. A more fruitful approach to the determination of the SSA point could be to identify the absolute instability with the softening of the phonon modes [43] or with singularities in the elastic moduli [48], which can be described in terms of the percolation of rigidity [49].

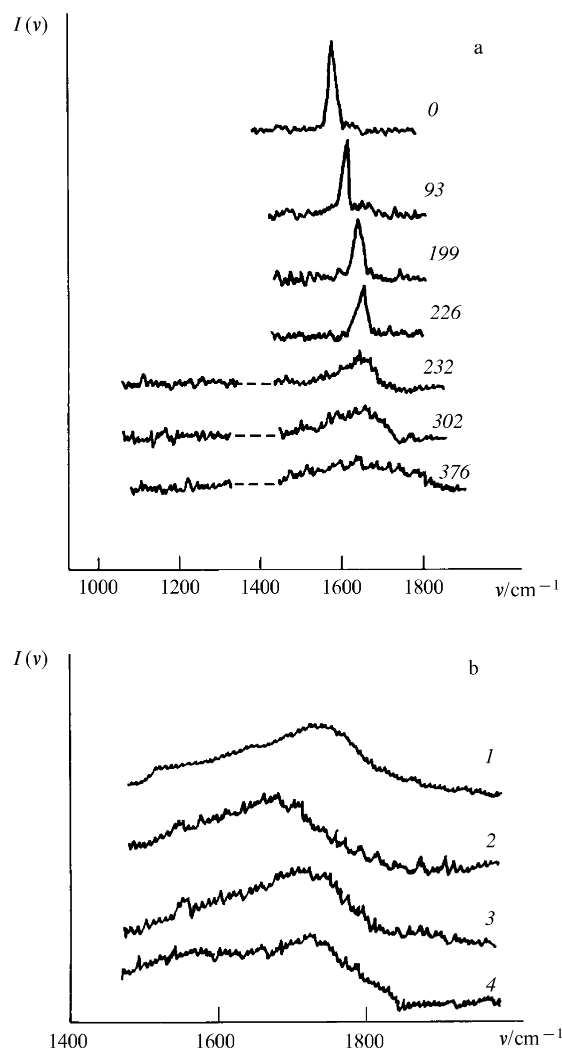

Figure 3. SSA on increasing the pressure in graphite: (a) transformation of the Raman spectra of monocrystalline graphite (curves numbered according to the pressure in kbar); (b) Raman spectra of a-C under pressure, obtained for different initial samples; (*1*) a-C (deposition), (*2*) monocrystal, (*3*) pyrolytic graphite, (*4*) vitreous carbon [33, 35].

Strictly speaking, similar comments apply also to the *EF* process, since none of the published discussions of the absolute instability line gives a physically sound justification for the extrapolation of the melting curve or defines the microscopic character of the lattice instability. Furthermore, no experiments under pressure have been reported to confirm the proposed [6, 19, 31, 43] behaviour of the instability line, especially in the vicinity of the triple point (Fig. 6a).

Thus, in spite of their simplicity and convenience, the concept of an absolute instability line and the 'cold melting' model still lack adequate theoretical foundations, and should be treated as possible phenomenological generalisations of a relatively small number of experimental facts.

3. Theoretical aspects of the description of the kinetic characteristics of heterogeneous media

The available results of experimental studies of the physical properties of ASHP and of the features of their synthesis

processes [6] suggest that materials of this type are not, in general, spatially uniform. Inhomogeneities can be produced by perturbations in the stoichiometry of the sample [6, 19] and by changes in its phase composition (for example, by varying the synthesis conditions [50, 51] or possibly by doping). Furthermore, when examining the solid-state amorphisation or crystallisation processes it should not be forgotten that during the intermediate stages of a phase transformation the sample is a mixture of phases: in the case of SSA a mixture of the HPP and of the amorphous semiconductor, and in the case of crystallisation a mixture of amorphous and of crystalline semiconductor.

Theoretical approaches to the description of the kinetic characteristics of these inhomogeneous media will be examined below: they include the conductivity, the Hall coefficient, and the Seebeck coefficient. The literature published on these topics is extensive, and includes various aspects of the fundamental problem of a spatially inhomogeneous medium. However, practically useful results applicable to real three-dimensional media (ie analytical models capable of describing experiments) are still few. Under these conditions precise results can be obtained either in the limit of low concentrations of inclusions or for an asymptotic behaviour in the vicinity of the percolation threshold [52–58].

3.1 Conductivity

Let us first consider the conductivity of a medium containing a small concentration of inclusions. We know that a polarisability tensor $\widehat{\alpha}$ analogous to the tensor used in electrostatics can be introduced into the problem of direct current flow. Then, in the limit of small concentrations of inclusions (n), we can write [53, 54]

$$\sigma = \sigma_0 \left(1 + \frac{4\pi}{3} n \, \mathrm{Sp} \, \widehat{\alpha} \right), \tag{1}$$

where σ is the effective (observed) conductivity, and σ_0 is the conductivity of the medium in the absence of inclusions. For ellipsoidal inclusions [53, 59]

$$\alpha^\nu = \frac{\sigma_1 - \sigma_0}{4\pi[\sigma_0 - (\sigma_0 - \sigma_1)\, n^\nu]} . \tag{2}$$

In the latter formula α^ν are the principal values of the polarisability tensor [$\nu = (x, y, z)$], n^ν are the depolarisation coefficients [59], σ_1 is the conductivity of the inclusions, and σ_0 is the conductivity of the matrix. For spherical particles $n^\nu = \frac{1}{3}$, and from (1) and (2) we obtain

$$\sigma = \sigma_0 \left[1 - n \, \frac{3(\sigma_0 - \sigma_1)}{2\sigma_0 + \sigma_1} \right]. \tag{3}$$

In the limit of low inhomogeneity $|\sigma_0 - \sigma_1|/\sigma_0 \ll 1$ and spherical inclusions we can calculate the next term of the expansion over concentrations [54]:

$$\sigma = \sigma_0 \left[1 - n \, \frac{\sigma_0 - \sigma_1}{\sigma_0} - \frac{1}{3} n(1-n) \left(\frac{\sigma_0 - \sigma_1}{\sigma_0} \right)^2 \right]. \tag{4}$$

However, finding the higher corrections ($\sim n^3$, n^4, ...) presents considerable difficulty and has not yet been attempted as far as we are aware. The discussion of higher concentrations (close to the percolation threshold, where the topological properties of a two-phase medium begin to change) requires a different physical approach based on percolation theory [52, 55].

Since the media studied most intensively in percolation theory have either $\sigma_1 = 0$ (dielectric inclusions) or $\sigma_1 = \infty$ (ideally conducting inclusions) we shall write expressions for σ following from formulae (1) and (2) for these limiting cases.

For ideally conducting ('superconducting') inclusions we find [53]

$$\sigma = \sigma_0 (1 + 3\beta_{\mathrm{M}} x_{\mathrm{M}}), \tag{5}$$

where $x_{\mathrm{M}} = n$ is the concentration of the ideally conducting metal, and

$$\beta_{\mathrm{M}} = \frac{1}{9} \sum_\nu \frac{1}{n^\nu} . \tag{6}$$

The factor β_{M} allows for the shape of the inclusions: for spherical inclusions [53] $\beta_{\mathrm{M}} = 1$.

In the case of dielectric inclusions in a conducting medium [53] we have

$$\sigma = \sigma_0 \left(1 - \frac{3}{2} \beta_{\mathrm{D}} x_{\mathrm{D}} \right) = \sigma_0 \left[1 - \frac{3}{2} \beta_{\mathrm{D}} (1 - x_{\mathrm{M}}) \right], \tag{7}$$

$$\beta_{\mathrm{D}} = \frac{2}{9} \sum_\nu \frac{1}{1 - n^\nu} . \tag{8}$$

In formula (7) we have used the notation $x_{\mathrm{D}} = n = 1 - x_{\mathrm{M}}$. The fraction by volume of the phase with the highest conductivity corresponds to x_{M} in (5) and (7). As in the case of the metal, $\beta_{\mathrm{D}} = 1$ for spherical inclusions [but Eqns (6) and (8) remain valid for ellipsoidal inclusions].

Let us calculate the geometric factors for the two limiting cases of an oblate and a prolate ellipsoid. In the former, inclusions such as platelets of diameter d and thickness l are modelled, with $l \ll d$. By using the expressions [59] for n^ν we find, after some simple algebra,

$$\beta_{\mathrm{M}} \approx \frac{8}{9\pi} \frac{d}{l}, \ \beta_{\mathrm{D}} \approx \frac{4}{9\pi} \frac{d}{l} . \tag{9}$$

It is interesting to note that in this case $\beta_{\mathrm{M}} = 2\beta_{\mathrm{D}}$, i.e. the effective conductivity of the medium is influenced more strongly by the form of the ideally conducting inclusions than by the form of the dielectric inclusions. We also note that in this case $l \gg d$, i.e. β_{M}, $\beta_{\mathrm{D}} \gg 1$. If (5) and (7) are used to calculate (or to estimate) the concentrations in a two-phase inhomogeneous medium, an inaccurate allowance for the geometric factor can lead to serious errors in the determination of x_{M} or x_{D}. Unfortunately, this situation is most often met in experiments, since information on the form of the inclusions is not usually available.

The other extreme case is used to model inclusions in the form of needles with a transverse diameter satisfying the equation $d \ll l$ (where l is the length of the needle). It is easily seen that the following asymptotic formulae are valid for these relative values of the parameters:

$$\beta_{\mathrm{M}} = \frac{l^2}{d^2 \ln(l/d)} , \quad \beta_{\mathrm{D}} = \frac{10}{9} . \tag{10}$$

Clearly, in the case of acicular inclusions the difference between the form effects of ideally conducting and of dielectric inclusions becomes even more marked: $\beta_{\mathrm{D}} \approx 1$, whereas $\beta_{\mathrm{M}} \gg 1$.

As x_{M} is increased in a medium containing ideally conducting inclusions the separate inclusions must eventually combine into an infinite cluster, i.e. percolation along an ideally conducting phase becomes possible [52], and the effective conductivity of the medium must tend towards

infinity. The critical concentration x_C at which this topological singularity takes place is called the percolation threshold. As reported [55], for $x_M \to x_C$ we can use the asymptotic formula

$$\sigma = \frac{\sigma_0}{[1-(x_M/x_C)]^q} \equiv \sigma_0 \tau^{-q}. \qquad (11)$$

Similarly, for a conducting medium containing dielectric inclusions, increasing the fraction by volume of the dielectric produces a state of affairs (at $x_D = 1 - x_C$) in which an infinite cluster of metallic inclusions connecting the opposite 'shores' of the two-phase system can no longer exist, and the system of conducting inclusions breaks up into separate regions [52]. Since the conductivity of the dielectric is zero in our model the effective conductivity of the medium also becomes zero at the point $x_D = 1 - x_{cr}$. According to the percolation theory [52] we have in the critical region

$$\sigma = \sigma_0 \left(\frac{x_M - x_C}{1 - x_C}\right)^t \equiv \sigma_0 \tau^t. \qquad (12)$$

Formula (12), like formula (11), is asymptotically exact. It is assumed that the exponents q and t are universal for a system of given dimensionality, i.e. that q and t are only slightly dependent on the form of the elementary inclusions from which the infinite cluster is formed. Evidently, the form effect of the inclusions should be most marked in the percolation threshold x_C. However, no reliable data on the character of this effect are available as far as we are aware. For example, it has been suggested [52] that x_C is only slightly influenced by the form of the inclusions, and that its value should be close to that of the percolation threshold for spherical inclusions $x_C = 0.15-0.17$ [52]. Obviously, this hypothesis is valid for dielectric inclusions, but not for 'superconducting' needles or filaments, since even for $x < x_C = 0.17$ we may easily find that the condition $\sigma = \infty$ is satisfied by a single filament bridging the gap between the 'shores'.

In general the parameter x_C should depend on the statistical distribution function of the characteristic dimensions of the inclusions. The validity of this assertion was recently confirmed by a study of a medium with two characteristic sizes. It was shown [60] that in systems of this type we can detect a large shift in x_{cr} as compared with its value for spherical inclusions.

However, even for the simplest (almost spherical) form of inclusions all attempts at deriving from first principles a formula for the effective conductivity of a medium which includes the asymptotic expressions (5) and (11) [or (7) and (12)] and the different limiting cases have been unsuccessful. Nevertheless in approximate calculations we can use the simplest interpolation formulae (as is done, for example, in the scaling theory of the metal–insulator transition [61]). For example, in the case of $\beta_D = \beta_M = 1$ we can write

$$\sigma = \sigma_0 \frac{1 + [3 - (q/x_C)]}{[1-(x_M/x_C)]^q} \qquad (13)$$

for ideally conducting inclusions, and

$$\sigma = \sigma_0 \frac{[(x_M - x_C)/(1-x_C)]^t}{1 + \left(\dfrac{3}{2} - \dfrac{t}{1-x_C}\right)(1-x_M)} \qquad (14)$$

for dielectric inclusions. The approximations (13) and (14) are illustrated in Fig. 4 as curves *1* and *2* respectively, whereas *1'* and *2'* are the linear asymptotes for $\beta_D = \beta_M = 1$.

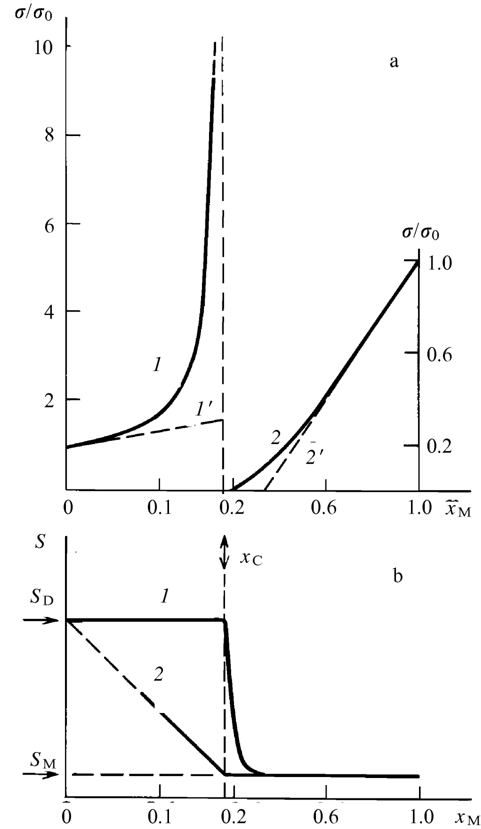

Figure 4. (a) Conductivity of a two-phase heterogeneous system: (*1*) ideally conducting inclusions, (*2*) dielectric inclusions (*1'* and *2'* are the low concentration limits); (b) critical behaviour of the Seebeck coefficient; (*1*) $K_M \gg K_D$, (*2*) $K_M \approx K_D$. The critical exponent values $q = 1$ and $t = 1.76$ have been used.

In order to apply the formulae (13) and (14) or the asymptotic expressions (11) and (12) to a spatially inhomogeneous medium we must know the critical exponents q and t. In the percolation theory the problem of dielectric inclusions in a conducting matrix is examined in detail, and we only need to know the critical exponent ν for the correlation radius of the infinite cluster in order to calculate t: this gives $t = 2\nu \approx 1.76$ for the three-dimensional case [52].

At the same time the expression for q contains an additional independent critical exponent, which characterises the similarity law in the critical region [55] or the fractal dimensionality of the superconducting inclusions [62, 63]. In the pioneering work of Efros and Shklovskii [55] it was assumed that $q = 1$ for $d = 3$ (where d is the dimensionality of the space). Subsequently Coniglio and Stanley [63], starting from the alternative concept of an 'unscreened perimeter' of the superconducting cluster, arrived at the formula

$$q = \nu\left[1 - \tfrac{1}{2}(d - d_f)\right] \equiv \nu\left(\tfrac{1}{2}d_f - \tfrac{1}{2}\right), \qquad (15)$$

where d_f is the fractal dimensionality of the superconducting sublattice ($d_f \leqslant 3$). By using the values $d_f \approx 2.54$ and $\nu = 0.88$ for the percolation cluster [64] we obtain $q = 0.68$.

Obviously, in the three-dimensional case q cannot be found by theory only, and experimental work is required. To the best of our knowledge the parameter q has never been determined in real inhomogeneous media: its value is totally unknown, unlike that of the critical exponent t, whose value

$(t \approx 2\nu)$ has been reliable confirmed by experimental data for three-dimensional two-phase systems [52]. The experimental determination of q will be discussed below in Section 6.

3.2 Hall and Seebeck coefficients

The critical behaviour of the Seebeck coefficient and of the Hall coefficient in the vicinity of the percolation threshold has been investigated [56–58] for the case of an inhomogeneous medium consisting of a mixture of 'metal' and of 'dielectric' with $\sigma_M \gg \sigma_D$ (where σ_M and σ_D are the conductivities of the 'metal' and of the 'dielectric', respectively.

It was found [56, 57] that the behaviour of the Seebeck coefficient $S(x_M)$ near the percolation threshold x_C depends on the relative values of the thermal conductivity of the 'metal' K_M and of the 'dielectric' K_D. If $K_M \gg K_D$ we find that $S(x_M)$ is indistinguishable from the Seebeck coefficient S_D of the 'dielectric' almost up to x_C, and in the close proximity of x_C it falls discontinuously to a value typical of the thermoelectric power of metals S_M (curve *1* of Fig. 4b). When $K_M \approx K_D$ we observe a critical behaviour similar to that of the electric conductivity [56, 57]:

$$S \approx (S_D - S_M)\tau^q + S_M \tag{16}$$

(curve *2* of Fig. 4b). In the above formula $\tau = 1 - x_M/x_C$.

An asymptotic expression, valid for $x_M < x_C$, was obtained [58] for the Hall coefficient in the vicinity of the percolation threshold:

$$R(x_M) = R_D(x_C - x_M)^{2q} + \frac{R_M}{[(x_M - x_D)^2 + \Delta^2]^{\nu/2}}\,, \tag{17}$$

where R_D and R_M are the Hall coefficients of the 'dielectric' and of the 'metal' respectively, and Δ is the size of the critical region (the 'blurred' region [55]). It follows from formula (17) that under certain conditions the Hall coefficient may have a resonance maximum at the percolation threshold, but this effect is purely topological and is not associated with changes in the microscopic characteristics of the components of the mixture. It should also be noted that for $x_M > x_C$ the first term in formula (17) vanishes.

For comparison with experimental data it is convenient to convert formula (17) into

$$\frac{R(x)}{R(0)} = \left[1 - \frac{A}{(\gamma^2+1)^{\nu/2}}\right]\tau^{2q} + \frac{A}{(\gamma^2\tau^2+1)^{\nu/2}}\,; \tag{18}$$

where $A = R(x_C)/R(0)$ is the reduced amplitude of the resonant increase in the Hall coefficient, and $\gamma = x_C/\Delta$. The quantities $R(x_C)$ and $R(0)$ are expressed in terms of the constants R_D and R_M [formula (17)]:

$$R(0) = R_0 x_C^{2q} + \frac{R_M}{(x_C^2 + \Delta^2)^{\nu/2}}\,, \quad R(x_C) = \frac{R_M}{\Delta^\nu}\,.$$

The dependence $R(x_M)$, predicted [58] for different values of A and $\Delta = 0.1x_C$, is shown in Fig. 5 (drawn for $q = 1$). It should be noted that though the expression (18) is formally defined for arbitrary values of x_M the validity region of (17) and (18) is confined to the vicinity of the percolation threshold.

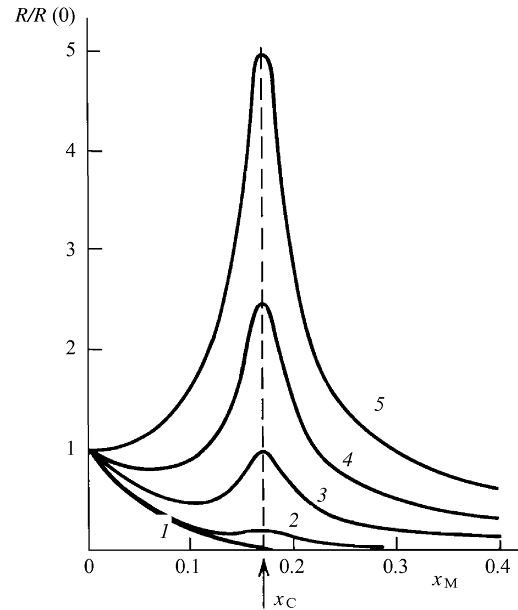

Figure 5. Resonance of the Hall coefficient at the percolation threshold for $q = 1$ and the following values of A: (*1*) 0, (*2*) 0.2, (*3*) 1.0, (*4*) 2.5, (*5*) 7.

3.3 Range of applications of the models of multicomponent media

The theory of the kinetic characteristics of heterogeneous media discussed above refers to strongly nonuniform media, with $\sigma_M \gg \sigma_D$. In a heterogeneous medium with $\sigma_M \approx \sigma_D$ the singularities and special features on the concentration dependences of the kinetic characteristics (Figs 4 and 5) become blurred, and various models of weakly inhomogeneous media could provide a better approximation [54].

Another limitation to the use of the results of the theory of heterogeneous media stems from their classical character. The treatment of inclusions of different phase composition as macroscopic regions having well defined microscopic parameters σ, R, and S assumes that the inequality $L \gg l_0$ applies, where L is the size of the inclusion and l_0 is the free path of the carriers. Evidently this is the condition which limits the application of the theory to crystalline doped semiconductors. For example, in crystalline gallium antimonide doped with tellurium and selenium l_0 lies in the range 200 Å $\leqslant l_0 \leqslant$ 3000 Å [65, 66], and the present theory is applicable only to relatively crude technological imperfections.

Therefore on the physically interesting nanometre scale the quantum effects will be predominant in doped semiconductors [65–67], and as a result the point for the anomaly of the kinetic characteristics (the mobility threshold) will not be related to the topological singularity at x_C [65, 66], and the critical exponent for the conductivity $(\sigma \propto \tau^t)$ is $t \approx 0.6$ [66, 67].

On the other hand, in amorphous semiconductors the free path is much shorter ($l_0 \approx L_{cor} \approx 10$ Å) [7, 61] and the restriction mentioned above is removed. We may hope that the classical theory of heterogeneous media will prove to be a convenient 'instrument' for the studies of physical inhomogeneities of widely different sizes, including almost the whole hierarchy of space scales found in the ASHP.

4. Metal-insulator transitions in tetrahedral amorphous semiconductors synthesised under high pressure

As was said above, one possible method of synthesising amorphous phases under pressure is solid-state amorphisation by heating a high-pressure phase [6]. Since the high-pressure phase (HPP) is usually a denser, metallic phase, the phase transition to the amorphous semiconducting modification is also a metal – insulator transition (MIT). The crystallisation of the amorphous matrix induced by further heating leads to the formation in the bulk of the sample of a crystalline phase with a metallic type of conduction, due to the presence of impurity atoms and of a large number of structure defects of various types (the case of heavy doping). Thus the crystallisation of a semiconducting amorphous phase also offers a way of studying specific MIT problems.

Furthermore, doping the amorphous matrix at the synthesis stage can itself create conditions favourable to controlled changes in the phase composition of the sample in the immediate vicinity of the MIT.

Therefore the remainder of this section will be devoted to the MIT in Cd – Sb, Zn – Sb, and Al – Ge alloys during amorphisation (Section 4.1), the effect of the conditions of synthesis (temperature and pressure) and of crystallisation of amorphous gallium antimonide in initiating the MIT (Section 4.2), and the doping of a a-GaSb at the synthesis stage with Cu and Ge additives, which also leads to the metal – insulator transition in this compound (Sections 4.3 and 4.4).

4.1 The metal – insulator transition in Cd – Sb, Zn – Sb, and Al – Ge alloys during amorphisation from a high-pressure phase

Since in these systems amorphisation takes place as a result of a structural transition from a high-pressure phase to a low-pressure phase, the latter having a higher resistivity than the initial HPP, we can expect a MIT in the system: for example, in the region of component concentrations where the fraction by volume of the HPP is close to the percolation threshold. At present the Cd – Sb, Zn – Sb, and Al – Ge systems have been most fully investigated [6, 19 – 27], and some preliminary results on the MIT in the GaSb system have been obtained [68].

In the case of Cd – Sb, the metal – insulator transition has been studied [26] by the 'stepwise amorphisation' method, which involves heating a sample of the high-pressure phase (held in a metastable state at liquid-nitrogen temperature) to approximately room temperature, and then cooling the sample once again. By controlling the heating the SSA process could be carried out through a sequence of intermediate metastable states (from the metastable metal through a mixture of metal and semiconductor to the amorphous semiconductor [26].

Normalised temperature dependences of the sample resistance $\rho(T)/\rho(T = 5; 6\,\mathrm{K})$, obtained for different heating – cooling cycles of the Cd – Sb alloy, are shown in Figs 6 and 7. The numbers on the curves of Fig. 6 correspond to the number of the cycle, and those in Fig. 7 give the logarithm of the normalisation constant

$$q_0 = \log_{10}(R_i/R_0)_{T=6\,\mathrm{K}}, \qquad (19)$$

where R_0 is the resistance of the sample in the initial state, and R_i is the resistance after the i-th anneal [26]. It can be seen that the metallic type of dependence ($q = 0$, initial sample),

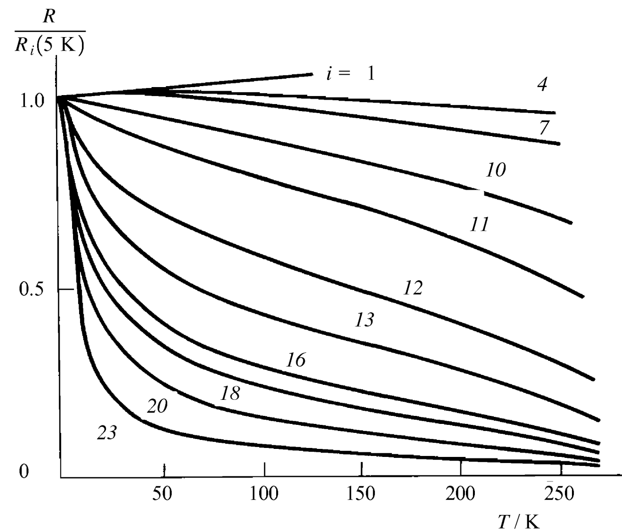

Figure 6. Changes in electric conductance during SSA in the Cd – Sb system. The curves are labelled with the number of heating – cooling cycles [26].

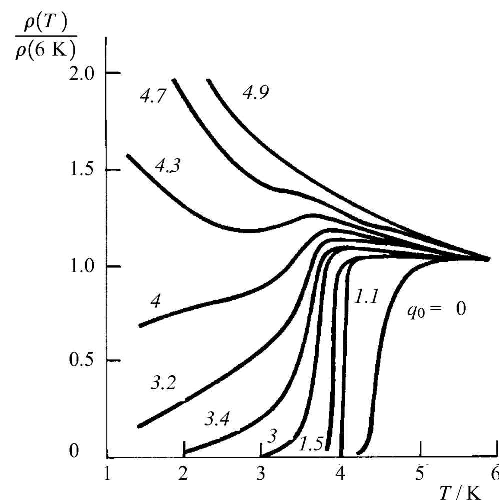

Figure 7. Superconducting transition in a Cd – Sb alloy on either side of the localisation threshold [27]. The parameter q_0 is defined in the text.

typical of the high-pressure phase, is replaced by the semiconductor type, and the superconducting transition which takes place during the anneal becomes blurred as the resistance of the sample increases (i.e. as q increases). At some point $q = q_{\mathrm{cr}}$ the metal – insulator transition takes place, and an activation-controlled $\sigma(T)$ dependence is observed (see Figs 6 and 7). The q_{cr} value was defined as the vanishing point of the parameter $\sigma(0)$, obtained by extrapolating $\sigma(T)$ to $T = 0$. This gave [26] $q_{\mathrm{cr}} \approx 3.9$. Thus in the vicinity of the MIT the resistance of the system at liquid-helium temperatures increases by about 4 orders of magnitude, and if the MIT in the system takes place by the percolation mechanism, the alloy being amorphised at $q = q_{\mathrm{cr}} \approx 3.9$ should be in a deeply critical region for $x_{\mathrm{M}} \approx x_{\mathrm{C}}$ [see formulae (12) and (14)]. However, the lack of structure data for these alloys during the SSA makes it impossible to estimate directly the extent of agreement between x_{M} and the classical percolation threshold.

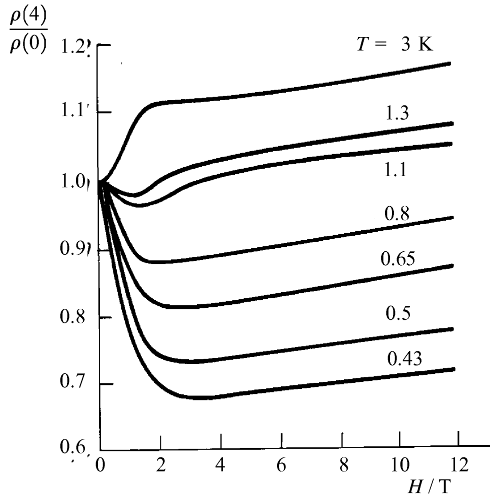

Figure 8. $R(T, H)$ magnetoresistance curves at different temperatures, normalised to $R(T, 0)$, for a Cd – Sb alloy characterised by $q = 4.9$ [27].

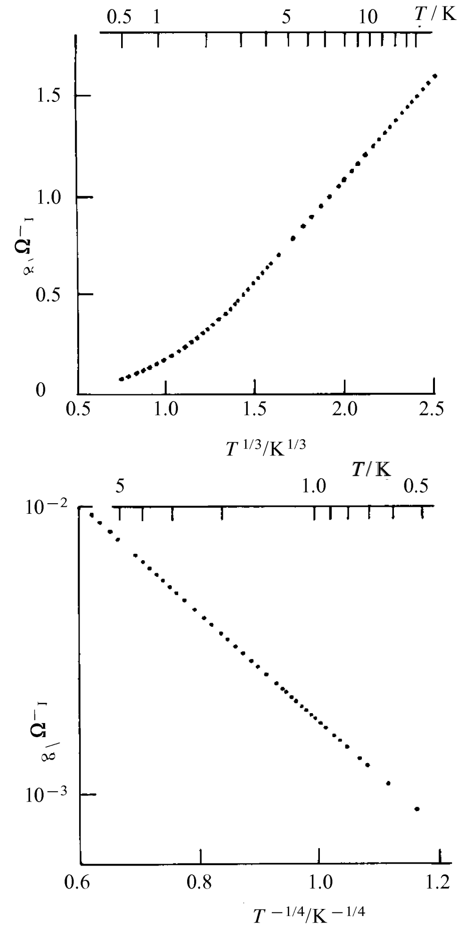

Figure 9. Temperature dependences of the conductance for a Cd – Sb alloying characterised by $q =$ 4.9 [27].

We note that transformations of a similar type were observed in the $\rho(T)$ curves during SSA in the GaSb and Zn – Sb systems [68, 24].

However, the MIT process during SSA is much more complex, and cannot be interpreted in terms of a simple percolation model of the mixture of phases [26]. In the Cd – Sb alloy with $q_0 = 4.9$, which is reasonably close to $q_{\rm cr}$, a strong ($\sim$30%) negative magnetoresistance (NMR) effect was detected, its amplitude increasing as the temperature was lowered (see Fig. 8) [69]. Furthermore in a Cd – Sb sample in this state the temperature dependence of the conductivity for $T > 5$ K is close to the power-law dependence

$$\sigma(T) \propto T^{-1/3}, \tag{20}$$

whereas for $T > 5$ K the $\sigma(T)$ dependence is replaced by the activation law

$$\ln\sigma(T) \propto -\left(\frac{T_0}{T}\right)^{1/4}, \tag{21}$$

characteristic of hopping conduction with a variable hopping range (see Fig. 9) [69].

These changes in the kinetic characteristics in the vicinity of the MIT were first observed in a study [66, 70] of a doped crystalline semiconductor GaSb : Se, and it was shown [66] that the behaviour can be explained adequately in terms of the scaling theory of the metal – insulator transition, which allows for the quantum effects rather than the classical effects (which are considered in the percolation theory).

Indeed, in the one-parameter scaling model the self-consistent Al'tshuler – Aronov system of equations [71] leads to the asymptotic relation $\sigma(T) \propto T^{-\alpha}$, where $\alpha = 1/d$ (d is the dimensionality of the space), so that in general the mobility edge does not coincide with the percolation threshold [70]. Near the mobility edge a strong NMR was observed ($\sim$30% for GaSb : Se at $T \approx 0.5$ K), increasing by a power law as the temperature was lowered [66, 70]. This is explained by the increase in the quantum interference effects near the localisation threshold (essentially, these effects induce the localisation [70]).

In addition, the alternation of the asymptotic relations (20) and (21) can also be explained in terms of the one-parameter scaling model [71, 66]. On the dielectric side of the transition the conductivity is described by the formula

$$\sigma(T) = \frac{e^2}{hL_T^{d-2}}\exp(-\gamma L_T), \tag{22}$$

where L_T is the coherence length of the phase of the wave function, limited by inelastic interactions with phonons, and γ is the reciprocal localisation radius. In the neighbourhood of the mobility edge γ is large, and a temperature range can be identified in which $\gamma L_T \ll 1$. Then only the pre-exponential factor is significant in formula (22), and since in the critical region for the three-dimensional case $L_T \propto T^{-1/3}$ [71], a power-law $\sigma(T)$ dependence will be observed. Lowering the temperature infringes the condition $\gamma L_T \ll 1$, and the exponential term in (22) can no longer be neglected. Therefore the asymptotic behaviour $\ln\sigma \propto (T_0/T)^{\alpha}$ should be observed, where α is defined either by the temperature dependence of the coherence length L_T ($\alpha = \frac{1}{3}$ or $\frac{1}{2}$, called the nonoptimal hopping regime [72]) or, if the condition $R_{\rm opt} \propto T^{-1/4} < L_T$ is satisfied, by the Mott hopping length, which leads to formula (21).

Thus the Cd – Sb system is very close to the predictions of the one-parameter scaling model for $d = 3$, leading to the conclusion [26, 69] of a spatially uniform sample structure in the vicinity of the metal – insulator transition.

However, this result is difficult to reconcile with current views on the mechanisms of SSA, according to which the system is markedly heterogeneous in the intermediate stages

of the process, and also with the results obtained by the same workers [25, 24] in a study of the MIT in the Zn – Sb and Al – Ge systems. An analysis of the temperature dependences of the conductivity while allowance for their evolution in the SSA process in Cd – Sb, Zn – Sb, and Al – Ge alloys showed that the $\sigma(T)$ data can be satisfactorily described in terms of the following model [24]. In these compounds the high-resistance amorphous phase begins to be formed as thin layers ('leaves') at the grain boundaries, with very little intersection of the 'growing leaves' as the volume of the semiconducting phase increases during the phase transformation.

As a result 'cactus-like' fractal structure, which is formed from the amorphous phase during the intermediate stages of the SSA [24], 'entangles' and distorts the permitted current trajectories in the metallic high-pressure phase. At some critical point the last current channel in the HPP between the sides of the sample is broken: this completes the metal – insulator transition, and transport in the dielectric region now proceeds by tunnelling (including thermally activated tunnelling) between the isolated metallic regions (the 'granular metal' case) [24].

It should be noted that some evidence of heterogeneity can also be seen in the Cd – Sb system: for example, the two contributions (positive, and negative) to the magneto-resistance (see Fig. 8) may be associated with the presence of inclusions having different phase compositions.

Let us now consider the types of temperature dependence of the conductivity in the critical region to be expected in the strongly inhomogeneous case. We shall stipulate that the space available for the current carriers is fractal rather than three-dimensional (a percolation cluster will be assumed in order to make the discussion more specific). It is known that the diffusion coefficient for a fractal depends on the space scale [64, 73, 74] $D \propto L^{-\vartheta}$, and therefore the conductance is expressed by the formula $g(L) \propto L^{d_{\mathrm{f}}-2-\vartheta}$ [73], where d_{f} is the dimensionality of the fractal. In the diffusion regime of transport on the fractal we have

$$\sigma \propto \frac{e^2}{hL_T^{d_{\mathrm{f}}-2}}\, g(L_T) \sim \frac{e^2}{hL_T^{\vartheta}} \sim T^{\,\vartheta/(2+\vartheta)} . \tag{23}$$

To determine the temperature dependence we assumed that $L_T \propto [D(L_T)h/T]^{1/2}$. For a percolation cluster in three-dimensional space [74] $\vartheta = 1.5$ and $\sigma \propto T^{\,0.43}$. In the region of localised transport formula (22) becomes

$$\sigma \propto \frac{e^2}{hL_T^{\vartheta}} \exp[-(\gamma L_T)^{d_{\varphi}}] , \tag{24}$$

where d_{φ} is the 'superlocalisation' exponent $(1 < d_{\varphi} < 1.35$ in the three-dimensional case [74]$)$. We should stress that the exact value of d_{φ} in real situations is not known: for $d = 2$ or 3 (two-dimensional or three-dimensional space) it is usually assumed that $d_{\varphi} = 1$, though in some cases this value has been modified [66] to allow for spatial nonuniformities. At the same time, if quantum effects are dominant in the scattering, in the presence of localisation and of only moderately thick dielectric interlayers ('leaves') we should expect a weak dependence of the asymptotic expression for the localised wave function on the conditions at the metal – dielectric interface. As a result we have $d_{\mathrm{f}} = 1$, in spite of the large change in the topology of the system during the SSA. We then find from (24) that in the regime of nonoptimal hopping $\ln\sigma \propto -(T_0/T)^{\alpha}$, $\alpha = 1/(2+\vartheta) = 0.28$. We note that the same exponent corresponds to Mott's law on the percolation fractal: $\ln\sigma \propto -(T_0/T)^{1/(d_{\mathrm{f}}+1)}$. For $d_{\mathrm{f}} = 2.54$ we [64] find $\alpha = 0.28$.

Thus, in a strongly inhomogeneous medium modelled by a percolation cluster, where the points for the topological transition and for the quantum localisation are close to each other, we observe only a moderately strong modification of the asymptotic expressions (20) and (21), and the corresponding critical exponents 0.43 and 0.28 are close to the values $\frac{1}{3}$ and $\frac{1}{4}$ observed experimentally [27] (see Fig. 9). In a real situation with a lower degree of inhomogeneity the observed difference will be even smaller, and whether the system is strongly heterogeneous or spatially uniform cannot be established unambiguously from the evidence of the critical exponents of the temperature dependence of the conductivity.

Therefore we conclude that the case of Cd – Sb, like that of Zn – Sb and of Al – Ge, corresponds to an MIT in a spatially inhomogeneous system, but (unlike Zn – Sb and Al – Ge) in the Cd – Sb system the quantum effects play a dominant role. Evidently, a detailed structure analysis of the SSA process would greatly help us to identify the origin of these differences in the behaviour of the alloys in the vicinity of the MIT.

Furthermore, the published results [24 – 27, 68, 69] make a new class of problems in the physics of metal – insulator transitions available for experimental study: transitions in a space of lower dimensionality, in which both topological and quantum effects can be important, and the point of the topological (percolation) transition and the localisation threshold for the electronic states can correspond to different values of the control parameter, which greatly complicates the picture of the physical processes. These problems call for the development of suitable theoretical approaches (for example, the validity of the one-parameter scaling procedure which has been used in some calculations is far from being self-evident). We can expect MIT similar to those discussed in this section to become one of the 'development points' in the fundamental understanding of the physics of disordered media.

4.2 MIT in a-GaSb synthesised by quenching under high pressure

The synthesis of amorphous bulk gallium antimonide under pressure has been reported [18, 37, 75 – 82]. In a-GaSb the intermediate high-pressure phase GaSb II (Fig. 10), used in the synthesis scheme, has the same stoichiometric composition as the amorphous GaSb. It has been shown [81] that the electrophysical properties of a-GaSb are almost totally determined by the synthesis temperature of the samples. Varying T_{syn} in the region of $T^*_{\mathrm{syn}} \approx 800$ °C markedly affects the resistivity ρ and its temperature dependence $\rho(T)$ (see Fig. 11). The quasimetallic type of conduction in samples synthesised at high temperatures $(T_{\mathrm{syn}} > T^*_{\mathrm{syn}})$ is replaced (at $T_{\mathrm{syn}} < T^*_{\mathrm{syn}}$) by the semiconductor type, producing a relative change with synthesis temperature of the resistivity (measured at liquid helium temperatures) of ten orders of magnitude.

Thus a change in the synthesis temperature T_{syn} can induce the metal – insulator transition (MIT) in a-GaSb.

On the dielectric side of the transition $(T_{\mathrm{syn}} < 800$ °C$)$ the temperature dependence of the resistivity at $T > 100$ K obeys the activation law

$$\rho \sim \exp\frac{E_{\mathrm{a}}}{k_{\mathrm{B}}T} . \tag{25}$$

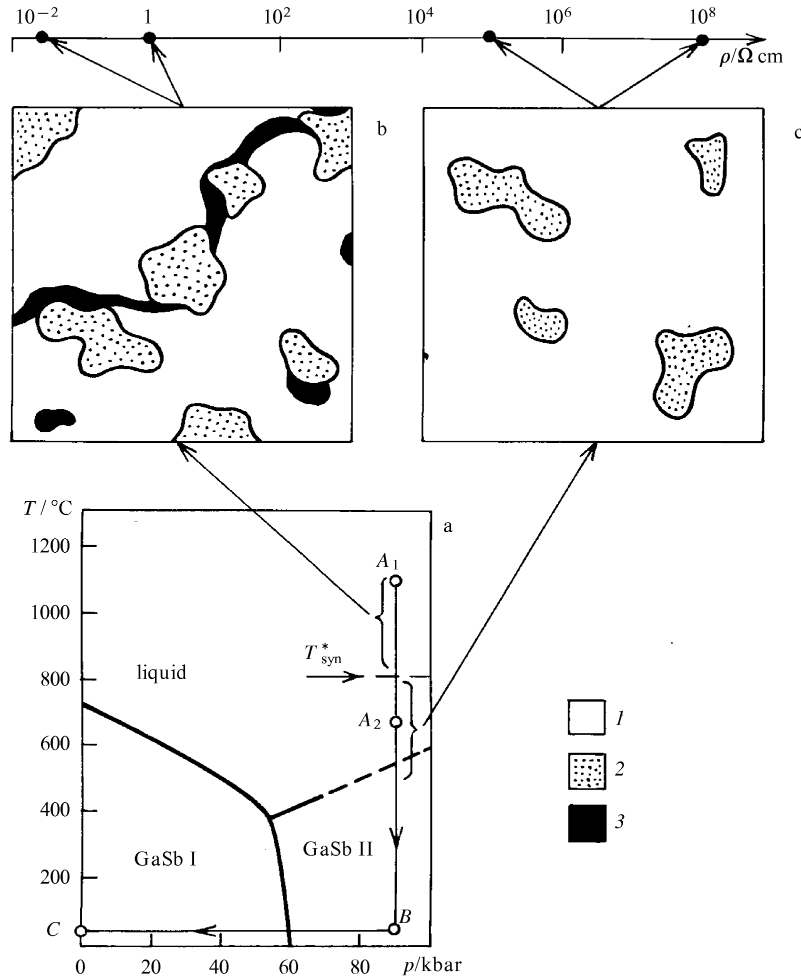

Figure 10. Scheme for the synthesis of bulk samples of amorphous gallium antimonide (a) and structure of the samples of a-GaSb obtained [84] at different synthesis temperatures (b, c). During the synthesis the initial GaSb sample of stoichiometric composition is transferred by pressure through the GaSb I – GaSb II phase transition line and is then fixed at p_{syn}. After being held at T_{syn} (point A) the sample is cooled to room temperature (point B), and the pressure is then removed (point C). The process $A_1 \to B \to C$ leads to amorphisation and to the formation of a metallic sample, and the process $A_2 \to B \to C$ leads to the synthesis of a dielectric (see text). Figures b and c correspond to the metallic and to the dielectric sample, respectively. A scale of electric conductivity for the dielectric and the metallic samples at $T = 4.2$ K is provided for comparison. The numbers refer to inclusions of different phase composition: (*1*) amorphous a-GaSb phase, (*2*) c-GaSb crystal, (*3*) Ga_xSb_{1-x} phase.

The activation energy stays almost constant ($E_a \approx 0.2$ eV) up to $T_{syn} \approx 750$ °C, but it falls off rapidly at $T_{syn} = T^*_{syn} \approx 800$ °C (Fig. 11).

At low temperatures ($T \leqslant 10$ K) the dependence (25) is replaced by Mott's law

$$\ln\rho \propto \left(\frac{T_0}{T}\right)^{1/4}, \qquad (26)$$

which is characteristic of variable-range hopping conduction (Fig. 12). The parameter T_0, which determines the slope of the parts of the $\rho(T)$ curve which are linear in $\ln\rho = f(T^{-1/4})$ coordinates, decreases when $T_{syn} \to 800$ °C from $T_0 \approx 2.9 \times 10^4$ K (curves *1* and *2* of Fig. 12) to $T_0 \approx 230$ K (curve *3* of Fig. 12).

This type of temperature dependence of the resistivity on the dielectric side of the MIT is consistent with the current views on the energy spectrum and on the charge transport in amorphous materials, which postulate the presence [7] in the energy gap of amorphous semiconductors of a band of localised states which contribute to the hopping conduction. Under these conditions a change in T_0 corresponds to a change in the parameters of the localised states as the system approaches the metal – insulator transition.

We note that the energy E_a obtained [81] in our laboratory (see Fig. 11) agrees well with the data reported for amorphous films of GaSb synthesised by deposition on a cooled substrate [83], whose activation energy lies between 0.14 and 0.25 eV. At the same time the Mott's law parameter T_0 for amorphous films of GaSb varies in the range $2.8 \times 10^8 - 3.1 \times 10^7$ K and greatly exceeds the highest values of T_0 for bulk samples of a-GaSb (see Fig. 12). This discrepancy is apparently produced by an increase (by about an order of magnitude) in the localisation radius for a-GaSb samples prepared at high pressures.

An analysis of x-ray structural results [81] shows that very weak lines from the crystal lattice of the initial c-GaSb phase are retained even in the most disordered samples of a-GaSb. According to estimates by the correlation procedure [81] the content of low-resistance metallic phase in samples of a-GaSb cannot be greater than $\sim 5\% - 10\%$, and therefore inclusions of the crystalline phase cannot be the only factor

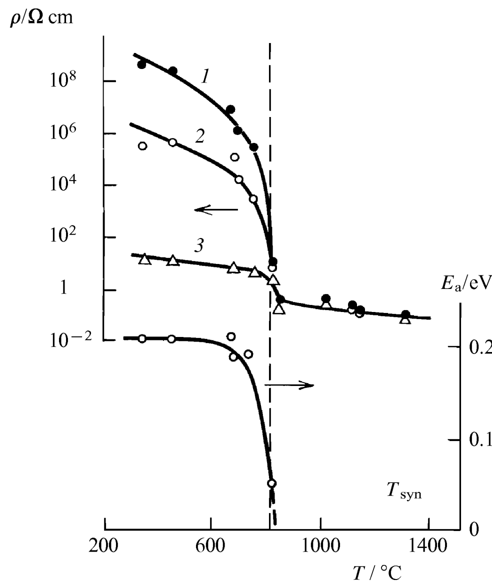

Figure 11. Change in the electrophysical properties of a-GaSb; the $\rho(T_{syn})$ curves were obtained by varying the synthesis temperature. (*1*) 4.2 K, (*2*) 100 K, (*3*) 300 K, (*4*) $E_a(T_{syn})$ dependence [81].

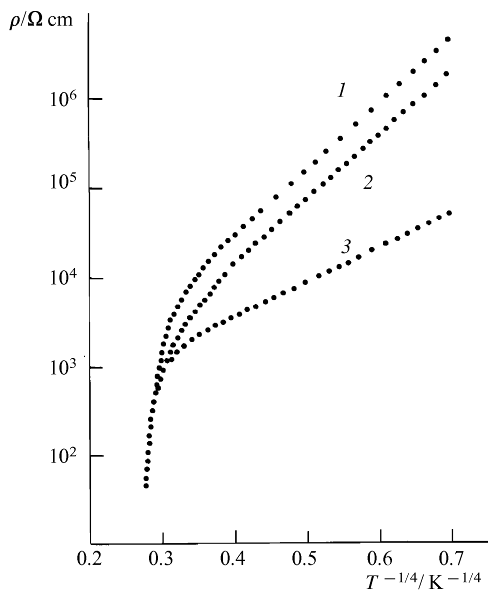

Figure 12. Hopping conduction in a-GaSb. (*1*) $T_{syn} = 350$ °C, (*2*) 450 °C, (*3*) 670 °C [81].

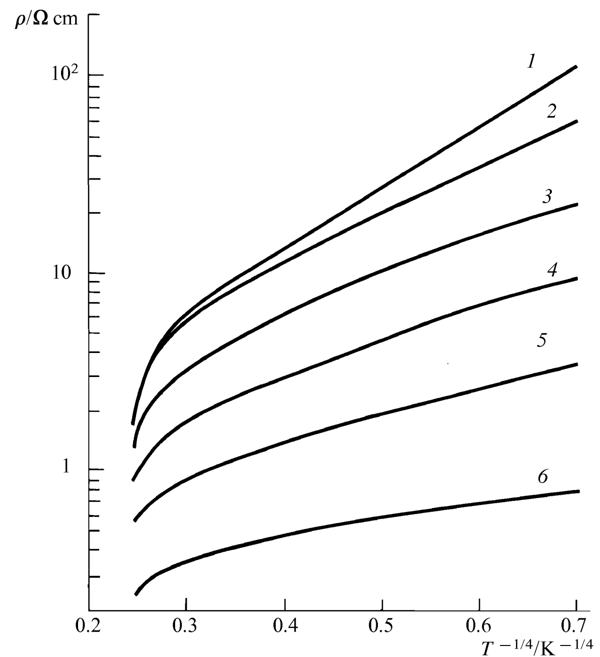

Figure 13. Changes in the hopping conduction parameters during annealing of a-GaSb ($T_{syn} = 350$ °C, $p_{syn} = 90$ kbar): (*1*) initial state, (*2*) $T_{an} = 70$ °C, (*3*) 80 °C, (*4*) 90 °C, (*5*) 100 °C, (*6*) 110 °C.

responsible for the MIT induced by variations in the synthesis temperature.

Detailed studies of the structural properties, of the character-istics of the superconducting state, of the stability region, and of the special features of the phase transformation of metastable phases in samples of a-GaSb showed [81, 84] that the main reason for the MIT resulting from changes in the conditions of a-GaSb synthesis is the departure from stoichiometry in the case of thermobaric treatment of the GaSb. The sub-micron superconducting inclusions of the metastable phase of nonstoichiometric composition Ga_xSb_{1-x} ($x > 0.5$), together with the submicron inclusions of the crystalline c-GaSb phase, form a sublattice of metallic conducting channels act as shunts in the dielectric amorphous matrix of a-GaSb. We shall consider these problems in greater depth in Sections 5 and 6.

The stepwise crystallisation of a-GaSb in samples from the dielectric side of the metal – insulator transition leads to a marked increase in the conductivity of the medium (Fig. 13). The largest changes in the parameter T_0 of Eqn (26) are seen in the initial stage of anneal at $T_{an} = 340-350$ K. As in our previous work [81] (see Fig. 12) the crystallisation of a-GaSb in this range of annealing temperatures lowered T_0 to values of $\sim$200 K.

However, it should be noted that smooth changes in conductivity during the crystallisation of dielectric samples of a-GaSb have not been observed in practice, because the small change in the resistance of the sample at the annealing temperature produces a large and irreversible increase in the low-temperature conductivity of the medium.

4.3 Metal – insulator transitions in the a-GaSb : Cu system

4.3.1 Doping of a-GaSb with copper. By analogy with amorphous films we can expect the introduction of an additional 'doping' element into the amorphous matrix to offer new possibilities of controlling the physical parameters of amorphous materials prepared at high pressures. In this sense, whereas at relatively low concentrations of the impurity (not exceeding a few mol%) we can envisage normal doping and the resulting changes in electronic properties, at higher concentrations the impurity begins to act as a structure-forming element. The best-known example of this behaviour is amorphous hydrogenated silicon a-Si : H, in which the concentration of hydrogen can be as high as 60 at% [9]. From the fundamental point of view one question remains unclear in the discussion of systems of this type (and in particular of a-Si : H): should they be treated as amorphous solid solutions or as multiphase systems [9]?

In the synthesis scheme used in our work [75–82] (see Fig. 10) the preparation of samples in the a-GaSb : Cu system from mixtures of c-GaSb and Cu powders required heating the sample to temperatures well in excess of the characteristic metallisation temperature T^*_{syn}. In this case the sample of the a-GaSb : Cu system with a zero concentration of copper ($x_{Cu} = 0$) has the structure shown schematically in Fig. 10b, and possesses superconducting properties owing to the presence of the Ga_xSb_{1-x} phase [81].

The evolution of the phase composition of a-GaSb : Cu samples resulting from an increase in x_{Cu} and the consequent changes in the physical characteristics of this complex multiphase system have been analysed [85]. All the samples were synthesised at $P_{syn} = 90$ kbar, $T_{syn} = 1100$ °C, and the copper content was varied in the range $0 \leqslant x_{Cu} \leqslant 47$ mol%.

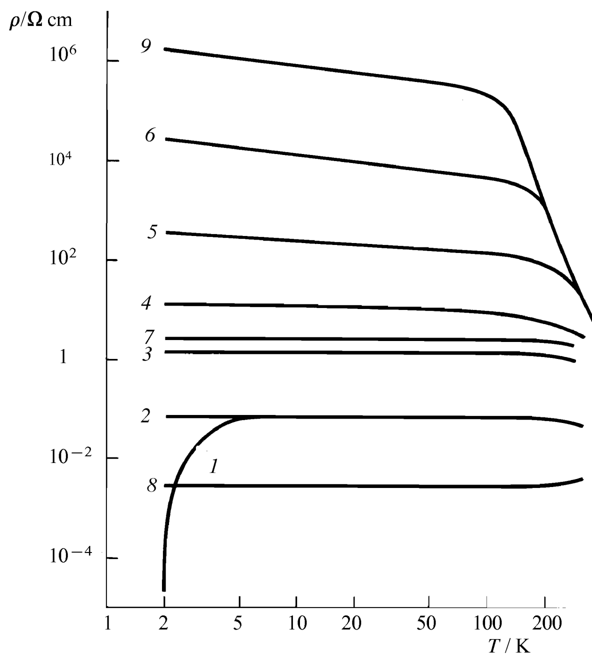

Figure 14. Temperature dependences of the resistivity of a-GaSb : Cu samples with different x_{Cu} concentrations: (*1*) $x_{Cu} = 0$ (undoped sample, $T_{syn} > T^*_{syn}$), (*2*) 3 at%, (*3*) 11 at%, (*4*) 14 at%, (*5*) 18 at%, (*6*) 27 at%, (*7*) 31 at%. The $\rho(T)$ dependence for an undoped sample of a-GaSb prepared at $T_{syn} < T^*_{syn}$ (curve *9*) is shown for comparison [85].

As reported [85], an increase in the concentration x_{Cu} induces a large change in the electric conductivity of the a-GaSb : Cu samples (Fig. 14). Initially we observe a suppression of the superconductivity at concentrations $x_{Cu} \approx 3$ mol% (curves *1* and *2* of Fig. 14), but the resistivity at $T > 10$ K is practically unaffected. After this, ρ begins to increase with x_{Cu} (curves *3*–*6* in Fig. 14), and in the region of $x_{Cu} \approx 10$ mol% the quasimetallic behaviour of $\rho(T) \approx$ const is replaced by activation control with an activation energy $E_a \approx 0.17-0.19$ eV. This value of E_a is consistent with data for undoped a-GaSb synthesised at $T_{syn} < T^*_{syn}$ [81].

The trend for an increase in $\rho(x_{Cu})$ persists up to $x_{Cu} \approx 27$ mol% (curve *6* of Fig. 14), beyond which the resistivity of the a-GaSb : Cu system decreases rapidly (curves *7* and *8* of Fig. 14), and in the region of $x_{Cu} \approx 50$ mol% it stabilises at the level of $\rho \approx 2 \times 10^{-3}\,\Omega$ cm. Under these conditions the semiconductor type of $\rho(T)$ dependence is again replaced by the metallic type.

It is interesting to note that the range of the increase in ρ which can be achieved by varying the copper content is a factor of $\sim 10^6$, which is about 2 orders of magnitude less than for the MIT in a-GaSb, due to the change in T_{syn} (see Fig. 14, where curve *9* corresponds to an undoped sample of a-GaSb prepared at $T_{syn} < T^*_{syn}$).

Therefore changes in x_{Cu} induce first a metal–insulator and then an insulator–metal transition in a-GaSb : Cu. A detailed x-ray structure analysis of these samples was carried out [85] in order to clarify the nature of this type of transformation in the electronic properties of a-GaSb : Cu.

4.3.2 Structure of the a-GaSb : Cu samples. The scattering structure factors $a(S)$ for some samples of the a-GaSb : Cu series, obtained by selecting the coherent part of the $I(S)$ x-ray scattering intensity curves, are shown in Fig. 15. In samples with a small copper contents ($x_{Cu} \leqslant 15$ mol%), as in the case of undoped a-GaSb, a small amount of the crystalline GaSb phase is retained. Estimates of the concentration of the crystalline phase (n_c) in samples of the a-GaSb : Cu system, made by the correlation method of analysis of the composition of phase mixtures [81], gave $n_c \approx 10\%$, in keeping with data for undoped a-GaSb. For samples in this range of x_{Cu} concentrations the peaks corresponding to crystalline GaSb (curves *I* in Fig. 15) are substantially broadened in comparison with the scattering from the unstressed monocrystal. This is because of the small size of the crystallites (~100–300 A).

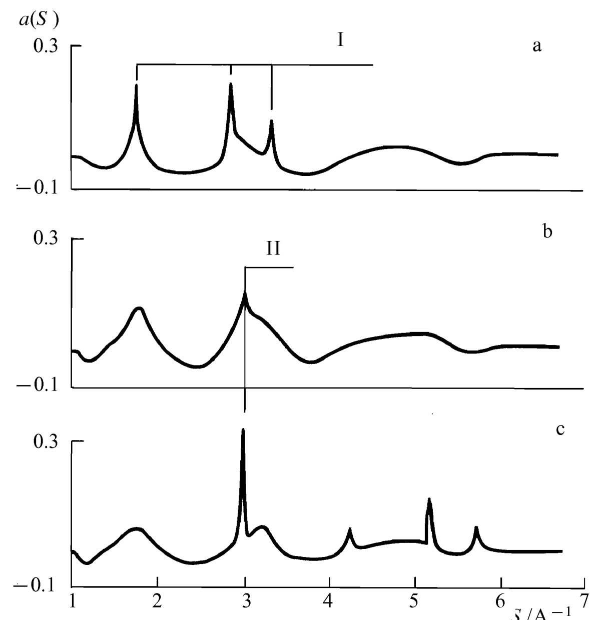

Figure 15. Structure factors for the scattering of x radiation (Cu K_α line, $\lambda = 1.5418$ Å) for a-GaSb : Cu samples with x_{Cu}: (a) at%, (b) 11 at%, (c) 27 at%; $S = (4\pi/\lambda) \sin\theta$. I, crystal lines, c-GaSb; II, Ga_4Cu_9 lines [85].

A further increase in the copper concentration produces the following changes in the structure of the a-GaSb : Cu samples. At concentrations $x_{Cu} \approx 10$ mol% the crystal lines in a-GaSb (Fig. 15, lines I) disappear, and a new line is formed at $S \approx 3$ Å (Figs 15b and 15c, line II), corresponding to the inclusion of a new crystalline phase (different from c-GaSb).

Increasing x_{Cu} in the range $x_{Cu} \geqslant 10$ mol% leads to a sharp increase in the amplitude of the new line, and for $x_{Cu} \geqslant 20$ mol% new lines with an intensity peak at $S \approx 3$ Å

can be resolved (Fig. 15c). This allows the new phase to be identified by assigning the group of lines in the region of $x_{Cu} \geqslant 10$ mol% to inclusions of the intermetallic Ga_4Cu_9 [86].

It is evident from Fig. 15 that, in addition to the contribution to $a(S)$ from the Ga_4Cu_9 inclusions, broad maxima corresponding to the amorphous a-GaSb phase appear over the whole range of x_{Cu} concentrations. Let us now consider the effect of copper doping on the structure of the a-GaSb phase itself.

The contributions from the amorphous a-GaSb phase were resolved from the $a(S)$ spectra of Fig. 15 and used to calculate the radial distribution function (RDF) of the atomic density and to estimate the correlation length L_{cor}. The RDF in a-GaSb : Cu was calculated by the standard method for a multicomponent system [87]. The coordinate of the first peak of the RDF for samples in the a-GaSb : Cu system ($R_1 = 2.6 \pm 0.1$ Å) was unaffected (within experimental error) by varying the copper content. The changes in the coordination number $n_1 = f(x_{Cu})$ calculated from the RDF are shown in Fig. 16 (curve *1* of Fig. 16a). The parameter n_1, which corresponds to the number of nearest neighbours in the a-GaSb : Cu structure, at first decreases smoothly from 3.71 ($x_{Cu} = 0$) to 3.66 ($x_{Cu} \approx 17$ mol%), then for $x_{Cu} \geqslant 17$ mol% it falls further to 3.61, and stabilises near this value for copper concentrations $x_{Cu} \geqslant 20$ mol%. The density of the a-GaSb : Cu samples (Fig. 16c) was used in the calculations of the RDF. The region in which the coordination number decreases smoothly corresponds to the concentration range $x_{Cu} < 20$ mol%, in which the pyknometric density of the samples stays constant ($\rho \approx 5.56$ g cm^{-3}).

The correlation length L_{cor} of the amorphous a-GaSb : Cu phase, which characterises the size of the regions in which the short-range order structure of the phase is retained, was calculated by the formula [88]

$$L_{cor} = \frac{0.9\lambda}{\Delta(2\theta)\cos\theta_0}, \tag{27}$$

where λ is the wavelength of the x-rays, and θ_0 and $\Delta(2\theta)$ are respectively the coordinate and the half-width at half-height of the first amorphous maximum. This estimate of the average size of the coherent scattering region of the amorphous matrix for the a-GaSb : Cu phase decreases monotonically as x_{Cu} is increased over the whole of the experimental range (Fig. 16b).

This x-ray structure analysis suggests the following scheme of phase transformations and of resulting changes in the morphology of the a-GaSb : Cu samples [85]. Initially (for $x_{Cu} \leqslant 10$ mol%) copper additions leads to the disappearance of the crystalline inclusions in the a-GaSb matrix. At this stage the copper being accommodated in the GaSb lattice acts as an 'amorphiser', ie as an agent which assists the disordering of the gallium antimonide structure. Thus, by treating the copper atoms as defects in the disordered a-GaSb lattice, we can expect them to be associated with additional distortions of the bond lengths and the bond angles, i.e. to produce additional disorder in the system. This behaviour should manifest itself as changes in the short-range order (i.e. in the average coordination number n_1) and in the intermediate-range order (i.e. the correlation length L_{cor}), as has been observed experimentally (Figs 16a and 16b).

In the region of $x_{Cu} > 10$ mol% we observe a qualitative rearrangement of the phase composition of the a-GaSb : Cu samples: the inclusions of c-GaSb disappear, and are replaced by the intermetallic Ga_4Cu_9. The most likely explanation is that at $x_{Cu} \approx 10$ mol% the 'solubility limit' of the copper in the amorphous a-GaSb phase is reached, and the excess of copper begins to react with the gallium and to be released as Ga_4Cu_9 inclusions. Upon further increasing x_{Cu} the volume fraction of the sample occupied by the Ga_4Cu_9 phase is increased, but according to the x-ray structure analysis results [85] there are no qualitative changes in the morphology of the system.

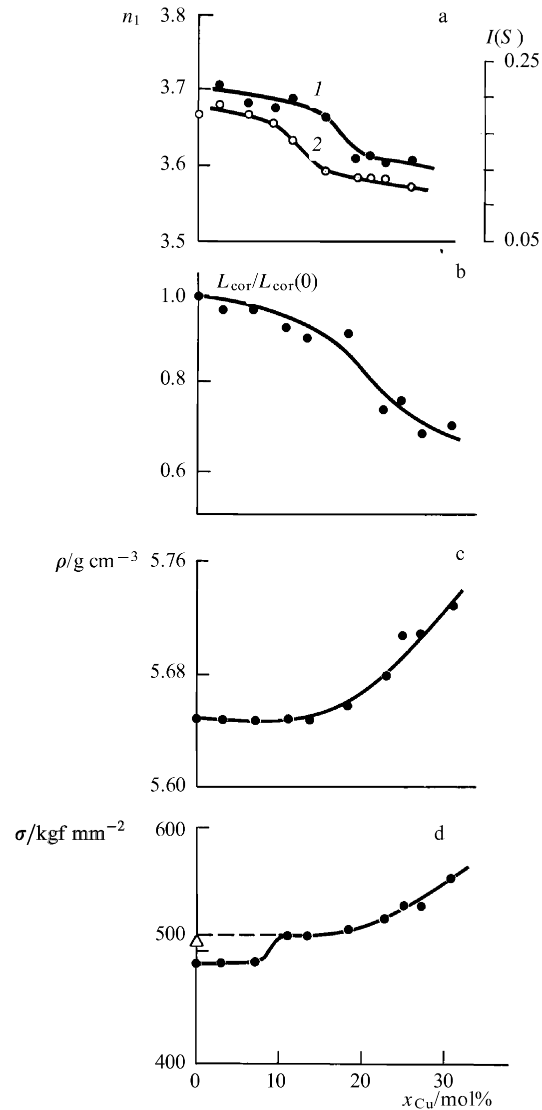

Figure 16. Concentration dependences: (a) coordination number n_1 (curve *1*) and amplitude of the first amorphous maximum (curve *2*); (b) correlation line L_{cor}; (c) pyknometric density ρ_0; (d) microhardness σ of the a-GaSb : Cu samples (the point △ corresponds to a sample prepared at $T_{syn} < T^*_{syn}$ with a minimal concentration of crystalline phase) [85].

It should be stressed that changes in characteristics of the amorphous a-GaSb : Cu phase itself take place over all the range of x_{Cu} values so far examined (Figs 16a and 16b), but above the 'solubility limit' their microscopic mechanism should differ qualitatively from that which applies when $x_{Cu} \leqslant 10$ mol%. Whereas in the latter case the copper is incorporated in the disordered a-GaSb lattice, when $x_{Cu} > 10$ mol% the formation of Ga_4Cu_9 inclusions becomes dominant. From the point of view of the amorphous matrix the

removal of gallium atoms (in order to form Ga_4Cu_9) should lead to the formation of vacancies in the gallium sublattice while keeping constant the concentration of copper atoms in the amorphous a-GaSb : Cu phase. It is reasonable to assume that this mechanism of defect formation must lead to a large amount of bond breaking, observed as a trend towards a decrease in the coordination number n_1. We note that when the concentration of vacancies exceeds a certain limit we can expect a relaxation of the short-range order structure in the disordered network, with a marked change in the first coordination number. It has been suggested [85] that this process is responsible for the large change in n_1 at $x_{Cu} \approx 17$ mol% (curve *1* and Fig. 16a).

This picture of the phase transformations in samples of a-GaSb : Cu is confirmed by a study of the concentration dependence of the microhardness $\sigma(x_{Cu})$ (Fig. 16d): $\sigma(x_{Cu})$ shows a discontinuity at $x_{Cu} \approx 10$ mol%, followed by a monotonic increase. In the region of $x_{Cu} > 10$ mol% the increase in the microhardness is attributed [85] to the formation in the bulk of the sample of denser and more rigid metallic inclusions, which also lead to a smooth increase in the density of the a-GaSb : Cu samples (Fig. 16c).

The jump in $\sigma(x_{Cu})$ at $x_{Cu} \approx 10$ mol% has been associated [85] with the disappearance of the crystalline inclusions of c-GaSb, and of their related phase boundaries, which can behave as the 'weak links' which set a limit to the strength characteristics of multiphase systems [89]. The amplitude of the jump in σ in the a-GaSb : Cu system corresponds exactly to the change in microhardness produced by varying the concentration of crystalline gallium antimonide in undoped a-GaSb (Fig. 16d) [85].

The effect of copper additions on the nonstoichiometric metastable Ga_xSb_{1-x} phase (Fig. 10a), which forms a network of metallic channels in the amorphous a-GaSb matrix as well as inclusions of c-GaSb, has been studied [85] also by recording the differential thermal analysis (DTA) curves of the a-GaSb : Cu system. It was found [85] that introducing even small quantities of copper ($x_{Cu} \approx 3$ mol%) makes the main exothermic peak narrower. In this concentration range the DTA abnormality at $T \approx 300$ °C was completely suppressed. Without attempting a detailed discussion of the DTA results obtained for these samples we shall note that they led the writers to the conclusion [85] that even at $x_{Cu} \geqslant 3$ mol% a nonstoichiometric Ga_xSb_{1-x} phase is not formed during the synthesis of a-GaSb : Cu.

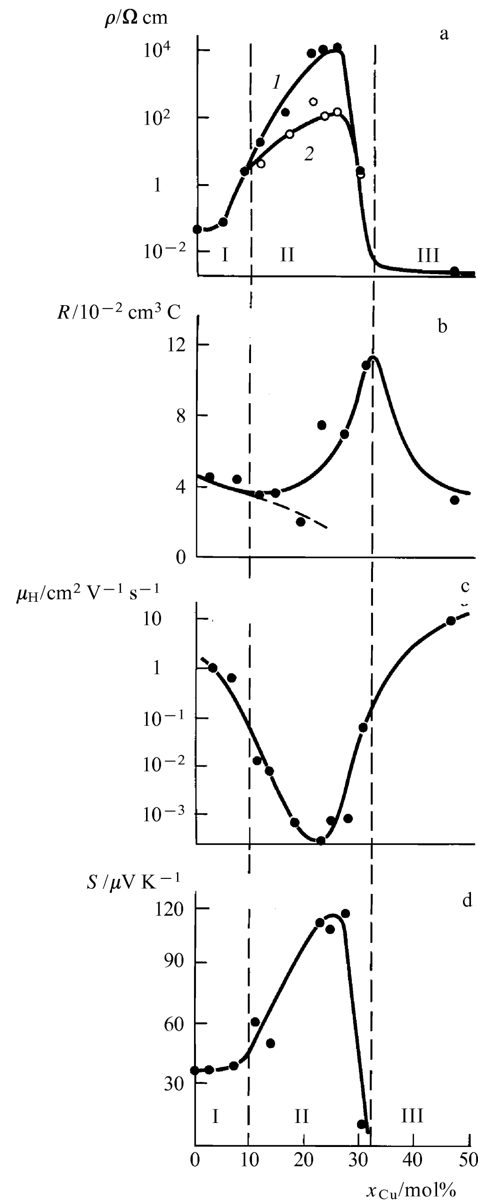

Figure 17. Concentration dependences: (a) resistivity $\rho(T, x_{Cu})$ (curve *1*, $T = 4.2$ K; curve *2*, $T = 300$ K); (b) Hall coefficient $R(x_{Cu}, 300$ K); (c) Hall mobility $\mu_H(x_{Cu}, 300$ K); (d) Seebeck coefficient $S(x_{Cu}, 300$ K) for a-GaSb : Cu samples. In Fig. 17b the full line represents the calculation by formula (18) on the basis of Shklovskii's theory, and the broken line defines the changes in R due to the doping of the amorphous matrix [85].

4.3.3 Effect of copper impurities on the galvanomagnetic and thermoelectric properties of a-GaSb. The data [85] on the structure of the a-GaSb : Cu samples were used to study the effect of copper impurities on the electrophysical, galvanomagnetic, and thermoelectric properties of these materials in order to identify the origin of the metal – insulator and insulator – metal transitions in the system. To this end we studied [85] the concentration dependence of the resistivity $\rho(x_{Cu})$, of the Hall coefficient $R(x_{Cu})$, of the Hall mobility $\mu_H(x_{Cu})$, and of the Seebeck coefficient $S(x_{Cu})$ (Fig. 17).

The characteristic ranges I, II, III of the parameter x_{Cu} (Fig. 17) locate the changes in structure and in physical properties of the a-GaSb : Cu samples. The boundary between the ranges II and III is set by the steep change in the resistivity (Fig. 17a), corresponding to the insulator – metal transition. During these transitions there is no qualitative difference between the structures of the samples in ranges II and III.

Since in the regions II and III an increase in x_{Cu} is accompanied by an increase in the fraction of the sample volume occupied by the metallic Ga_4Cu_9 phase we can reasonably attribute the insulator – metal transition to the development of percolation in the system of metallic Ga_4Cu_9 inclusions, whose resistivity ρ_M is much lower than the resistivity of the amorphous a-GaSb : Cu matrix (ρ_D).

Similarly there are no difficulties in the interpretation of the metal – insulator transition (the transition from region I and to region II), in which an increase in the copper concentration initially leads to the disappearance of inclusions of the low-resistance nonstoichiometric amorphous phase of Ga_xSb_{1-x} with $x > 0.5$, whereas when $x_{Cu} \approx 10$ mol% the crystalline inclusions disappear. In this way the low-resistance channels which provide an electric shunt in the amorphous matrix in samples prepared at $T_{syn} > T^*_{syn}$ are not formed [81], the resistivity increases, and the $\rho(T)$ curves

display the semiconductor form, typical of conduction in the amorphous a-GaSb phase (see Fig. 12). Under these conditions the superconducting properties of the samples are suppressed even at the low x_{Cu} concentrations of region I. It is evident from Fig. 17a that the boundary between regions I and II, which corresponds to a change in the structure of the system, coincides with the point of the metal–insulator transition (curves *1* and *2* of Fig. 17).

The behaviour of the a-GaSb : Cu sample is most complex in region II, where the percolation on the Ga_4Cu_9 phase is absent. We have a fairly wide concentration range ($10\ \text{mol\%} \leqslant x_{Cu} \leqslant 20\ \text{mol\%}$) in which the shunting effect of the metallic inclusions is not large and the change in the physical characteristics of the system is determined mainly by the properties of the amorphous a-GaSb : Cu phase itself. The situation is further complicated by the changes in these properties which take place in region II : simultaneous allowance is needed for the effects of the metallic inclusions and for the change in properties of the amorphous dielectric matrix.

As can be seen from Fig. 17a a large increase in $\rho(x_{Cu})$ (by 4 orders of magnitude at liquid helium temperatures and by 2 orders of magnitude at room temperature) takes place in region II. However, if the resistance ρ_D of the amorphous phase remained constant, the resistivity of the sample in this region would decrease rather than increase with x_{Cu} because of the shunting effect of the metallic inclusions with $\rho_M \ll \rho_D$.

Studies of the behaviour of the Hall coefficient R at $T = 300$ K and $H < 150$ kOe in a-GaSb:Cu revealed a complex nonmonotonic concentration dependence of R_H (Fig. 17b) [85], the coefficient R rising to a maximum at the boundary between regions II and III (the insulator–metal transition point, and the percolation threshold for the metallic Ga_4Cu_9 phase).

The $\rho(x_{Cu})$ and $R(x_{Cu})$ data (Figs 17a and 17b) for $T = 300$ K can be used to calculate the Hall mobility μ_H (Fig. 17c). Clearly, in the region $0 \leqslant x_{Cu} \leqslant 20$ mol% the parameter μ_H decreases by more than 4 orders of magnitude, reaching a minimum value $\mu_H \approx 10^{-4}\ \text{V}^{-1}\ \text{s}^{-1}$ at $x_{Cu} \approx 20$ mol%, beyond which it rises again to $\mu_H \approx 10\ \text{cm}^2\ \text{V}^{-1}\ \text{s}^{-1}$.

The concentration dependence of the Seebeck coefficient $S(x_{Cu})$ is shown in Fig. 17d. The $S(x_{Cu})$ curve is an almost exact replica of the $\rho(x_{Cu})$ (resistivity) curve, the only difference being that the amplitude of the change in the Seebeck coefficient in region II is

$$\frac{S(x_{Cu} = 25\ \text{at\%})}{S(x_{Cu} = 0)} = 2\ ,$$

in contrast to the change by two orders of magnitude in the conductivity of the system. The sign of $S(x_{Cu})$, like that of the Hall coefficient $R(x_{Cu})$, corresponds to p-type material.

Let us now examine the experimental results (Fig. 17) from the standpoint of the current theoretical ideas. Obviously, for $x_{Cu} > 10$ mol% (regions II and III) the discussion must be based on the model of a dielectric medium containing metallic inclusions. In this case, because of the condition $\rho_D \gg \rho_M$ which follows from the data in Fig. 17a, to a first approximation the metallic inclusions can be treated as ideally conducting.

By using the expressions (16)–(18) for the Hall coefficient and the Seebeck coefficient of a two-component medium of this type [56–58] we can assume that the fraction of the volume (x_M) occupied by the metallic phase in a-GaSb : Cu is proportional to $x_{Cu} : x_M = \alpha x_{Cu}$. We shall use the definition $\tau = 1 - (x_{Cu}/x_C)$, where x_C is the percolation threshold for the metallic phase.

It follows from formula (18) that under certain conditions $R_H(x_{Cu})$ can have a maximum in the vicinity of the mobility edge. However, when comparing formulae (11), (16), and (18) with experiment it should not be forgotten that in a-GaSb : Cu the parameters ρ_D, R_D, and S_D should also depend on x_{Cu}. To simplify the treatment we shall assume that $R_M = \text{const}$ and $S_M = \text{const}$. Furthermore it follows from Fig. 17d that the relationship $S_D \gg S_M$ holds for a-GaSb : Cu.

As can be seen from formulae (11), (16), and (18) the dependence of the characteristics of the amorphous a-GaSb : Cu matrix on the concentration of copper affects the physical properties of the system as a whole in different ways. This effect is most marked in the case of the resistivity ρ and of the Seebeck coefficient S, whereas in the expression for the Hall coefficient the term containing R_D decreases rapidly (as τ^{2q}) as the percolation threshold is approached, and in the percolation region the Hall effect is determined by R_M [see formula (18)]. Therefore in the model of the concentration dependence $R(x_{Cu})$ we can put $R_D \approx \text{const}$. We note that a calculation in this approximation allows only for the effect of inclusions, so that the degree of doping of the amorphous a-GaSb : Cu phase can be estimated from the deviation of the experimental points from the theoretical dependence (18).

In the context of these assumptions we must fix the two parameters A and γ in order to use formula (18) as an approximation to experimental data: the former can be calculated directly from the amplitude of the maximum in R, and in the case of a-GaSb : Cu its value is $A \approx 2.5$. This leaves γ as the only adjustable parameter: the best consistence between the model and experiment ($\Delta \approx 0.1 x_C$) was obtained by putting $\gamma \approx 10$. It is clear from Fig. 17b (where the full line corresponds to the calculation and the points to the experiment) that Shklovskii's model correctly describes the form of the $R(x_{Cu})$ curve over the whole range of copper concentrations, including the presence of a maximum in the Hall coefficient at the percolation threshold.

At the same time it was reported [85] that the decrease of the Hall coefficient in the region of $x_{Cu} \leqslant 20$ mol% is faster than suggested by steeper approximation (18). This behaviour is consistent with the model of defect formation in a-GaSb : Cu proposed in the previous section. Thus, in this range of x_{Cu} the concentration of Ga_4Cu_9 inclusions is not very great: their presence does not produce an appreciable shunting effect on the characteristics of the system, and the concentration dependence $R(x_{Cu})$ reflects the change in the carrier concentration. According to our assumptions the formation of a Ga_4Cu_9 phase is accompanied by the generation of defects of the vacancy type. We know [90] that in GaSb defects of this type act as a source of p-type carriers, and therefore the concentration of positive holes increases with x_{Cu}, and $R_D(x_{Cu})$ decreases. As a result the experimental $R(x_{Cu})$ points for $x_{Cu} \leqslant 20$ mol% lie below the theoretical curve (Fig. 17b).

Let us now examine the concentration dependence $\rho(x_{Cu})$ in region II. Our analysis shows that in this system $\rho(x_{Cu})$ increases in spite of the increase in the carrier concentration and of the shunting action of the inclusions with a metallic type of conductivity. This effect can be explained by considering the behaviour of the mobility $\mu_H(x_{Cu})$.

As could have been expected, in region II a very large decrease in the Hall mobility (by three orders of magnitude) is observed at concentrations up to $x_{Cu} \approx 20$ mol%. Since the shunting effect of the metallic inclusions is not very large we must assume that this decrease reflects a change in the character of the scattering in the amorphous a-GaSb : Cu phase. In the percolation region $x_{Cu} \leqslant 20$ mol% the effective mobility increases as a result of a gradual transition to conduction over the intermetallic Ga_4Cu_9 phase saturated with defects.

An analysis of the causes of the decrease in Hall mobility led to the conclusion [85] that in a-GaSb : Cu an increase in $x_{Cu} < 20$ mol% is accompanied by an increase in the scattering on localised defects and on fluctuations of the potential in the amorphous matrix. This conclusion is suggested by a decrease in the coordination number n_1 and in the correlation length L_{cor} (see Fig. 16) at these concentrations. The change in n_1 should be interpreted as a change in the number of defects in the amorphous network, i.e. the number of scattering centres for the current carriers, the number of scatterers increasing as the coordination number n_1 decreases. The correlation length L_{cor} characterises the spatial arrangement of the atoms while at the same time determining the space scale of the fluctuations of different physical characteristics in the amorphous medium (in particular, those of the random potential in which the charge carriers move). Therefore a decrease in L_{cor} means that the random potential has become more 'ragged', which further enhances the scattering.

We shall conclude this section by analysing the relationship between the $\rho(x_{Cu})$ and $S(x_{Cu})$ dependences. As reported [7], when the conductivity of the amorphous semiconductor is determined by activation on the mobility edge, ρ_D and S_D are related by the expression

$$\ln(\rho_D \sigma_{min}) = \frac{eS_D}{k_B} - 1 \,, \tag{28}$$

where e is the elementary charge, k_B is Boltzmann's constant, and $\sigma_{min} = 0.026e^2/\hbar L$ is the lowest metallic conductivity. (Here L is the characteristic length over which 'memory' of the phase of the wave function is retained.)

Obviously, the suggested conduction mechanism can correspond to samples with minimum mobility values, in which clearly defined activation-controlled regions can be distinguished on the $\rho(T)$ curves. To make the discussion specific we shall discuss a sample with $x_{Cu} = 27$ mol%, having $\rho(300\,\mathrm{K}) \approx 100\,\Omega\,\mathrm{cm}$. By using formula (11) we can easily show that in this case $\rho_D \approx 640\,\Omega\,\mathrm{cm}$.

If S_D is known, σ_{min} can easily be calculated by using Eqn (28). Since the relation between S and S_D depends on the ratio of the thermal conductivities K_D and K_M we may consider the possible alternatives. In the case of $K_D \ll K_M$ and $S \approx S_D$ we obtain $\sigma_{min} \approx 2 \times 10^{-3}\,\Omega^{-1}\,\mathrm{cm}^{-1}$ from expression (28), which corresponds to lengths L of approximately 3×10^{-3} cm (highly improbable in an amorphous semiconductor at the mobility edge). In the limit of $K_D \approx K_M$ we can calculate S_D by formula (16), from which it follows (for $S_D \gg S_M$ and $S \approx 120\,\mu\mathrm{V\,K}^{-1}$, Fig. 17d) that $S_D \approx 770\,\mu\mathrm{V\,K}^{-1}$. Using this value we obtain $\sigma_{min} \approx 4.3\,\Omega^{-1}\,\mathrm{cm}^{-1}$ and $L \approx 140$ Å. The latter estimate of σ_{min} agrees with the preexponential factor in the activation law for the resistivity $\rho = \rho_0 \exp(E_a/k_B T)$: according to the data in Fig. 14 $\rho_0^{-1} \approx \sigma_{min} \approx 2.3 - 5.5\,\Omega^{-1}\,\mathrm{cm}^{-1}$ in our concentra-tion region.

Thus in the case of a-GaSb : Cu the effect of metallic inclusions is described by similar percolation laws for ρ and S, which corresponds to the case of $K_D \approx K_M$. This effect, together with the linking condition (28), which is consistent with experimental data, is responsible for the similarity between the concentration dependences $\rho(x_{Cu})$ and $S(x_{Cu})$.

4.4 Metal – insulator transitions in the a-GaSb : Ge system

4.4.1 Doping a-GaSb with germanium. We know that in $A^{III}B^{V}$ semiconductors the Ge impurity is amphoteric [92], and the type of its electric activity depends on the type of atom which it replaces. In $A^{III}B^{V}$ compounds containing gallium, and in particular in GaSb, the germanium usually replaces the gallium, giving n-type conduction. Therefore the microscopic mechanisms of the changes in structure in the a-GaSb : Ge system can be inferred from the changes in the conduction type. Furthermore n-type samples of ASHP can be produced in this system. We should stress the fact that all the ASHP previously studied were, without exception, p-type conductors [5, 81, 85], which imposed severe limitations on their potential applications.

Thus the study of the a-GaSb : Ge system offers much wider possibilities of varying the properties of the semiconducting amorphous matrix [91]. Furthermore a detailed study of samples in the a-GaSb : Ge system synthesised by both the $A_1 - B - C$ scheme (see Fig. 10, metallic samples) and without additional heating ($A_2 - B - C$, dielectric samples) should make possible a sequence of metal – insulator transitions by varying the composition and the structure of the phases which form a network of metallic channels in the amorphous matrix.

4.4.2 Structure of the a-GaSb : Ge samples. A typical result for the structure factor of the intensity of the Cu K_α x-ray scattering [$a(S)$] for a-GaSb : Ge is shown in Fig. 18a. As reported [91], in the range of germanium concentrations $x_{Ge} < 23$ mol% we observe crystal lines (shown as broken curves in Fig. 18, I) in addition to the oscillatory $a(S)$ curve characteristic of the tetrahedral amorphous a-GaSb phase. The most interesting of these lines (set I) correspond to the c-GaSb phase, and the line II corresponds to crystalline germanium, c-Ge.

When the concentration of germanium is increased, the reduced amplitude of the c-GaSb crystal line I_c/I_0 (where $I_0 = I_c + I_a$ and I_a is the amplitude of the first amorphous maximum) slightly increases initially for the first maximum of the function $a(S)$, and then it begins to decrease at $x_{Ge} > 8$ mol% and vanishes at $x^*_{Ge} \approx 23$ mol% (see insert in Fig. 18a). A further increase in the concentration of germanium up to $x_{Ge} \approx 80$ mol% does not produce any new crystal lines, and the function $a(S)$ takes the form shown as a full line in Fig. 18a.

Thus an increase in x_{Ge} stimulates the evolution of the a-GaSb samples from the heterogeneous structure shown schematically in Fig. 10 to the spatially homogeneous a-GaSb : Ge random network. The situation is totally different from the case of doping with copper, since in samples of the a-GaSb : Cu system we find a limit to the solubility of the copper in the amorphous matrix [85]. In the case of the germanium dopant the opposite obtains: increasing x_{Ge} makes the system more uniform, and this behaviour persists up to $x_{Ge} \approx 80$ mol%.

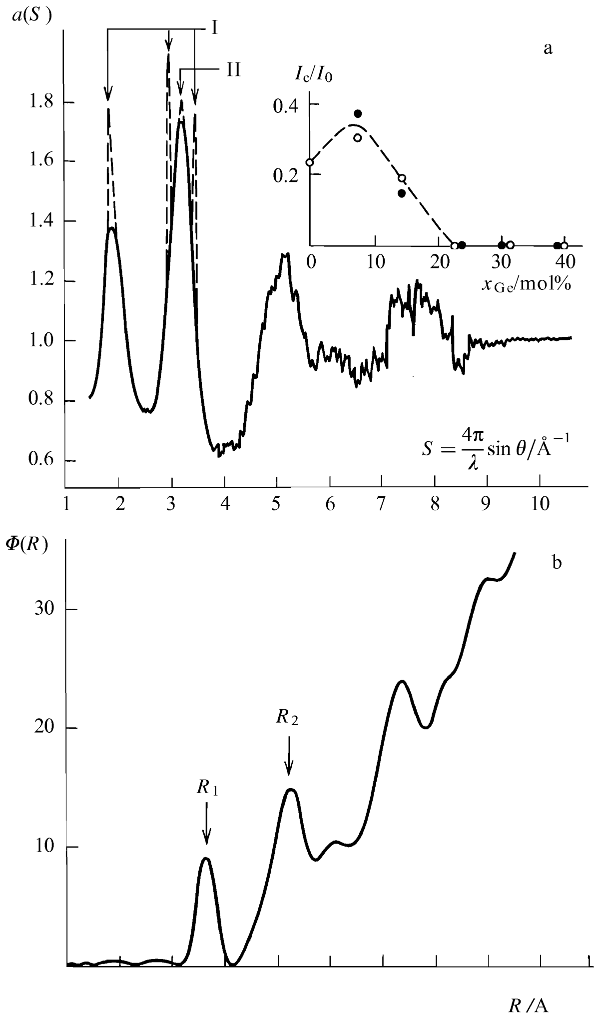

Figure 18. Structure of a-GaSb:Ge samples: (a) structure factor; (b) radial distribution factor for samples with $x_{Ge} = 36.7$ mol% ($T_{syn} = 400$ °C). The broken lines are the crystal lines for $x_{Ge} = 14.4$ mol% (I is the c-GaSb phase, II is the c-Ge phase). The insert shows the change in the relative amplitude of the crystal lines caused by alloying (metallic samples are shown as filled circles, dielectric samples as open circles) [91].

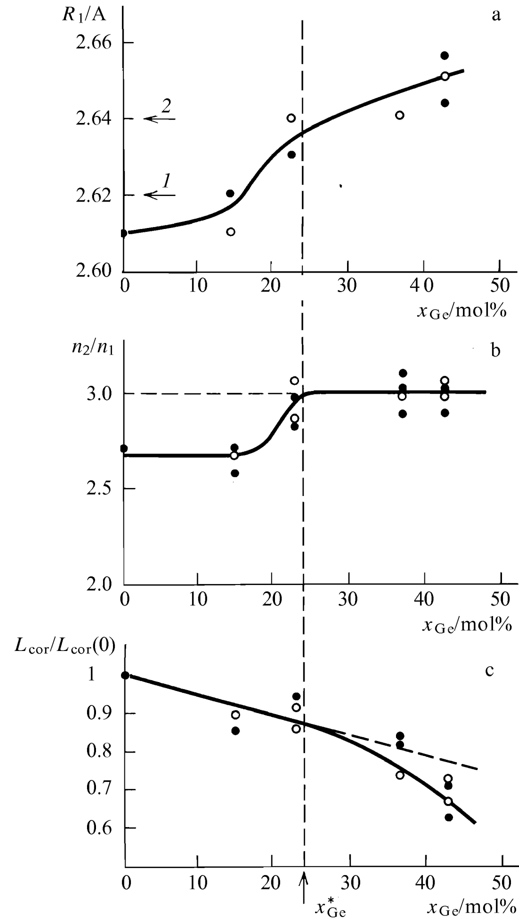

Figure 19. Concentration dependences of the structure parameters. The open circles are dielectric samples ($T_{syn} = 400$ °C), the filled circles are metallic samples ($T_{syn} = 1100$ °C) [91].

The concentration dependences of the radii of the first and the second coordination sphere R_1 and R_2 [the positions of the first and the second maximum of $\Phi(R)$] and the concentration dependences of the corresponding coordination numbers n_1 and n_2 [the area under the first and the second maximum in $\Phi(R)$] were also determined from an analysis [91] of the $a(S)$ curves in Fig. 18.

It was found [91] that in samples of a-GaSb:Ge with $x_{Ge} < 50$ mol% the coordination number is $n_1 \approx 4$ and the radius of the second coordination sphere is $R_2 \approx 4.22 \pm 0.01$ Å, almost independent of the concentration of germanium. The value $n_1 \approx 4$ corresponds to the tetrahedral character of the bonds in the amorphous a-GaSb : Ge network.

At the same time the parameters R_1, n_2, and L_{cor} are strongly dependent on the doping conditions (Fig. 19). The radius of the first coordination sphere R_1 increases with x_{Ge} from $R_1 = 2.61 \pm 0.01$ Å $(x_{Ge} = 0)$ to $R_1 = 2.65 \pm 0.01$ Å ($x_{Ge} \approx 42$ mol%) (Fig. 19a). Simultaneously (Fig. 3b) the ratio n_2/n_1 changes from 2.7 to $n_2/n_1 \approx 3$ (the latter value being characteristic of a perfect tetrahedral network, for which $n_1 = 4$ and $n_2 = 12$). In this concentration range the correlation length L_{cor} decreases by $\sim 30\%$, and (as reported earlier [85]) $L_C(x_{Ge} = 0) \approx 20$ Å.

It has been pointed out [91] that the increase in $R_1(x_{Ge})$ (see Fig. 19) is anomalous and inconsistent with the current views on the doping of semiconducting materials, since the covalent radii of the Ga, Sb, and Ge atoms ($R_c^{Ga} = 1.26$ Å, $R_c^{Sb} = 1.36$ Å, and $R_c^{Ge} = 1.22$ Å [92–94]), indicate (on average) a decrease in the interatomic distance as a result of adding germanium, because the covalent radius of the germanium impurity is smaller [94].

In the region of $x_{Ge} < 15$ mol% the parameter R_1 is close to the sum of the covalent radii $R_c^{Ga} + R_c^{Sb} = 2.62$ Å (Fig. 19a, *1*). This approximation to the bond length is too coarse for c-GaSb, for which $R_1 = \left(\frac{3}{4}\right)^{1/2} a = 2.64$ Å, where $a = 6.096$ Å is the edge length of the unit cube [95] (Fig. 19a, *2*). Therefore samples of amorphous gallium antimonide are more dense than samples with an unstressed defect-free crystalline lattice.

These results suggest [91] that the following mechanism is responsible for the anomalous change in the structure of the a-GaSb : Ge samples produced by an increase in the doping level. The initial $(x_{Ge} = 0)$ samples of a-GaSb contain a significant number of local regions where the bond length is shorter than its equilibrium value. This satisfies the inequality $R_1 \approx R_c^{Ga} + R_c^{Sb} < \left(\frac{3}{4}\right)a$. We can expect these structural perturbations to be associated with the interfacial region between the amorphous and the crystalline phase,

characterised by large changes in the order parameter, where the residual stresses are most likely to be concentrated. We note that the metallic Ga_xSb_{1-x} phase is located in the interfacial region in metallic samples [81, 85].

The addition of a germanium impurity causes an effective relaxation of the stresses in the amorphous GaSb network, and as a result R_1 increases towards the equilibrium value $R_1 \approx \left(\frac{3}{4}\right)^{1/2} a$. This structural change is accompanied by a redistribution of the atomic density between the first and the second coordination sphere (a change in the ratio n_1/n_2). The simultaneous relaxation of stresses in the amorphous network leads to the 'reamorphisation' of the inclusions in the crystalline phase. We note that this type of additional disorder in the amorphous structure has been observed previously in Cu–Sn and Cu–Al alloys during mechanical treatment [96].

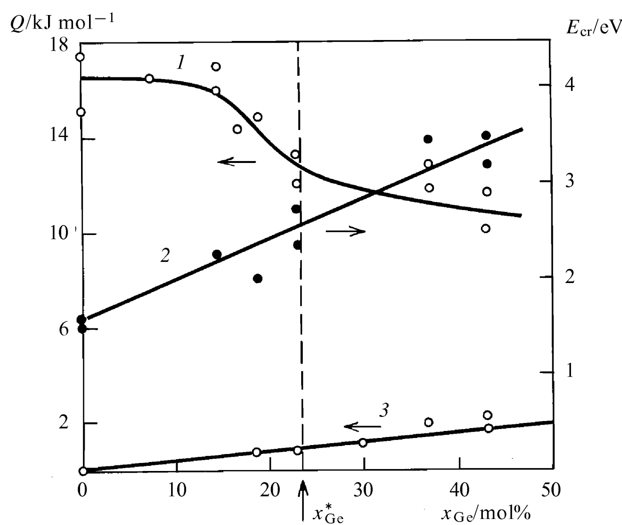

Figure 20. Heat of crystallisation (*1*) [91] and activation energy of crystallisation (*2*) for a-GaSb : Ge samples; (*3*) $Q(x_{Ge})$ data for the metastable $GaSb_{1-x}Ge_x$ solid solution formed by the crystallisation of a-GaSb : Ge [91].

Further evidence in favour of this model is provided by the concentration dependence of the heat Q and of the activation energy E_{cr} of crystallisation (Fig. 20). Obviously, during crystallisation the energy associated with disordering is evolved, including the energy stored in the amorphous phase in the form of local stresses of various types. A decrease in the volume fraction of stressed regions should lower Q, as is observed experimentally: $Q(x_{Ge})$ decreases as x_{Ge} increases (curve *1* of Fig. 20). At the same time the relaxation of stresses in the amorphous network should also stabilise the amorphous structure. As a result the barrier in the configurational space which separates the stable from the metastable states is increased. Therefore the activation energy crystallisation E_{cr} must increase when the concentration of germanium is increased (curve *2* of Fig. 20).

4.4.3 Special features of the concentration dependence of the kinetic characteristics of a-GaSb : Ge. The structural transition in a-GaSb : Ge which takes place at $x_{Ge} = x^*_{Ge}$ is most clearly seen in the concentration dependences of the kinetic coefficients for the samples examined (Fig. 21).

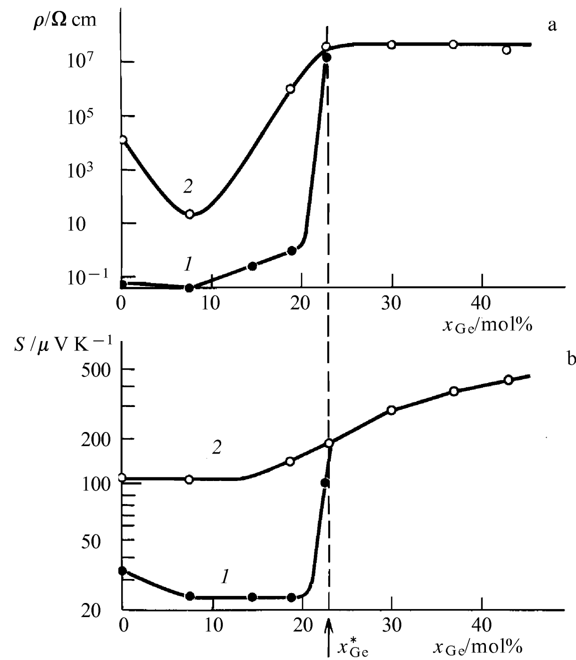

Figure 21. Concentration dependences of the resistivity (a) at $T = 100$ K, and of the Seebeck coefficient (b) at $T = 300$ K: (*1*) metallic samples, (*2*) dielectric samples [91].

A MIT is observed in a-GaSb : Ge in the vicinity of $x_{Ge} = x^*_{Ge}$: the resistivity of metallic samples suddenly increases by six orders of magnitude at $T = 100$ K, and beyond this point the resistivities of the metallic and of the dielectric samples are almost identical (Fig. 21a).

The concentration dependences of the Seebeck coefficient $S(x_{Ge})$ also show singularities at $x = x^*_{Ge}$. For metallic samples (curve *1* of Fig. 21b) a discontinuity is seen at the transition point: the coefficient S increases almost 100-fold. In dielectric samples (curve *2* of Fig. 21b) the thermoelectric power increases gradually from x_{Ge}, and a point of inflection in the $S(x_{Ge})$ curve is seen at $x_{Ge} = x^*_{Ge}$. In all the samples examined the sign of the Seebeck coefficient corresponded to p-type material.

One of the factors responsible for this behaviour of $\rho(x_{Ge})$ and $S(x_{Ge})$ is the disappearance, in the $x > x^*_{Ge}$ region, of the network of conducting channels, characteristic of the metallic samples (see Fig. 10) and consisting of c-GaSb, c-Ge, and Ga_xSb_{1-x} inclusions. However, it follows from the data in Figs 21a and 21b that the amplitude of the jump in ρ and S at $x = x^*_{Ge}$ exceeds the difference of the ρ and S values between metallic and dielectric samples at $x_{Ge} = 0$. This observation suggests that doping with germanium produces, in addition to a change in the phase composition of the samples, a change in the kinetic characteristics of the tetrahedral a-GaSb amorphous phase.

Thus in the region of $x_{Ge} = x^*_{Ge} = 23$ mol% the a-GaSb : Ge samples should be treated as multiphase systems, using as a first approximation a two-component medium consisting of a mixture of a 'dielectric' (the tetrahedral a-GaSb amorphous phase, doped with germanium) and a 'metal' (the inclusions of the crystalline c-GaSb and c-Ge phases and of the nonstoichiometric Ga_xSb_{1-x} phase). In a two-component medium of this type the behaviour of the Seebeck coefficient is determined by the relative values of the

thermal conductivity of the 'metal' K_M and of the 'dielectric' K_D [56–58]. In the case of $K_M \approx K_D$ the critical behaviour (and therefore the concentration dependence) of S should qualitatively mirror the critical behaviour and the concentration dependence of ρ (see Section 2); but if $K_M \gg K_D$, the thermoelectric power of the two-phase medium is determined by that of the dielectric up to the percolation threshold on the 'metal', and in our range of concentrations of 'metallic' inclusions it is independent of their volume fraction [56]. A comparison of the $\rho(x_{Ge})$ and $S(x_{Ge})$ curves (Figs 21a and 21b) shows that this case is indeed realised in a-GaSb : Ge. Thus, in dielectric samples ($T_{syn} = 400$ °C) there is no percolation on low-resistance crystalline phases, and their shunting effect is seen in the $\rho(x_{Ge})$ but not in the $S(x_{Ge})$ dependence. As a result the thermoelectric behaviour of dielectric samples of a-GaSb : Ge is determined by the Seebeck coefficient of the tetrahedral amorphous phase over the whole range of germanium concentrations.

Some preliminary measurements of the Hall coefficient in the a-GaSb : Ge system have been published. Unfortunately, only compositions on the metallic side of the MIT were studied. The change in the conductivity type of metallic samples of a-GaSb:Ge in the range of compositions $0 < x_{Ge} < 7.5$ mol% was pointed out [91]. This seems to have been the first experimental demonstration of the possibility of controlling the conductivity type of ASHP, which opened new prospects in the study of materials of this class and of their practical application. It was also pointed out [91] that the Hall mobility μ_H decreases as x_{Ge} increases. This result is consistent with the decrease in the characteristic length L_{cor} (see Fig. 19) as the doping level is increased.

The comparison of the data on the Seebeck coefficient and the Hall effect in metallic a-GaSb : Ge samples reveals a sign anomaly (characteristic of many noncrystalline materials [7]) at $x_{Ge} > 7.5$ mol%. However, this effect is usually observed in dielectric samples having activation-controlled or hopping conduction [7].

In a-GaSb:Ge the nature of the sign anomaly is apparently related to the multiphase nature of the samples. It has been suggested [91] that in the vicinity of the percolation threshold for the metallic phase both the conductivity and the Hall effect are determined by the low-resistivity inclusions [58], whereas the Seebeck coefficient is determined by the dielectric regions [61]. However, a combined analysis of the temperature dependence data for the resistivity, the Seebeck coefficient, and the Hall effect shows [91] that wholly satisfactory descriptions of these dependences cannot be produced by relying on existing models [7, 8, 61], that are commonly used to account for the properties of amorphous materials.

5. Crystallisation of the metastable phases of bulk amorphous gallium antimonide

In the discussion of the metal–insulator transitions in tetrahedral amorphous semiconductors we showed that one of the factors which stimulate the MIT in these substances is the formation at the synthesis stage of aggregates of defects in the amorphous phase as a result of the local breakdown of the initial stoichiometry. Furthermore, during amorphisation through a crystalline high-pressure phase we can expect structure defects to be generated also as a result of the local retention (in some domains of the sample) of the short-range order of the HPP. (The HPP is usually the phase with the lowest symmetry, characterised by a large coordination number.)

It has been shown [81, 85] that in amorphous gallium antimonide the associations of defects of the amorphous matrix (continuous random network), or in other words the inclusions of a metastable metallic phase of submicron size, exert a dominant effect on the properties of the substance, being responsible in particular for the superconductivity induced by amorphisation [78–81]. The formation of a network of conducting channels, partially or wholly shunting the high-resistance amorphous phase, is a universal feature of this method of synthesis, and is met in most of the 'multicomponent' amorphous semiconductors. Complex multicomponent systems of this type are still relatively new and nontraditional objects of study..

In this section we shall attempt to show, for the case of a-GaSb, that the study of structural relaxation and crystallisation processes in these substances, supplemented by the use of various low-temperature procedures, should provide an answer to questions on the origin, organisation, and physical characteristics of submicron metastable metallic inclusions in an amorphous semiconducting matrix.

5.1 Variations of the structure of a-GaSb during crystallisation

The a-GaSb samples from the metallic side of the metal–insulator transition, containing a network of conducting channels, were synthesised by quenching the melt under high pressure ($p_{syn} = 90$ kbar, $T_{syn} = 1100$ °C), and were then subjected to a series of isothermal anneals lasting ~50–100 min at temperatures in the range of 300–620 K (the 'stepwise crystallisation' method) [77, 81]. The x-ray scatter structure factors $a(S)$ $[S = (4\pi/\lambda)\sin\theta]$, corresponding to the initial sample of a-GaSb and to the states produced by each successive isothermal anneal, are shown in Fig. 22. As can be seen, the initial state of a-GaSb has a spectrum (curve *1* in Fig. 22) characterised by broad amorphous maxima, and against this background we find peaks corresponding to crystal line gallium antimonide. However, the crystal lines of GaSb are lower than the amorphous maxima, and are reliably recorded only for the first two coordination spheres (curve *1* in Fig. 22). A marked increase in the amplitude of the crystallines of GaSb is seen even at low annealing temperatures ($T_{an} \approx 350–380$ K; curves *2* and *3* of Fig. 22). A further increase in the annealing temperature T_{an} produces a large increase in the amplitude of the crystal lines of gallium antimonide for the temperature range $T_{an} \geqslant 420$ K (see Fig. 22) [84].

A detailed analysis [84] of the changes in structure of the a-GaSb samples during annealing leads to the following conclusions. The change in shape of the first diffraction maximum of $a(S)$ during stepwise crystallisation suggests that in the range $S \approx 1.5–2.2$ Å^{-1} the $a(S)$ curve is a superposition of three lines differing markedly in their width and position (Fig. 23). The shape of the crystal line is acceptably well described by the Gaussian function $I_c(S) = A_c \exp[-(S - S_0)^2/\gamma_c^2]$, whereas the residual concentration of crystalline phase in a-GaSb is proportional to $n_c \propto \int I_c(S)\,dS \propto A_c\gamma_c$.

The amorphous part of $a(S)$ in the vicinity of the first diffraction maximum is a superposition of two Gaussian functions of which the first corresponds to the region of the amorphous maximum and the second to the line edges, so

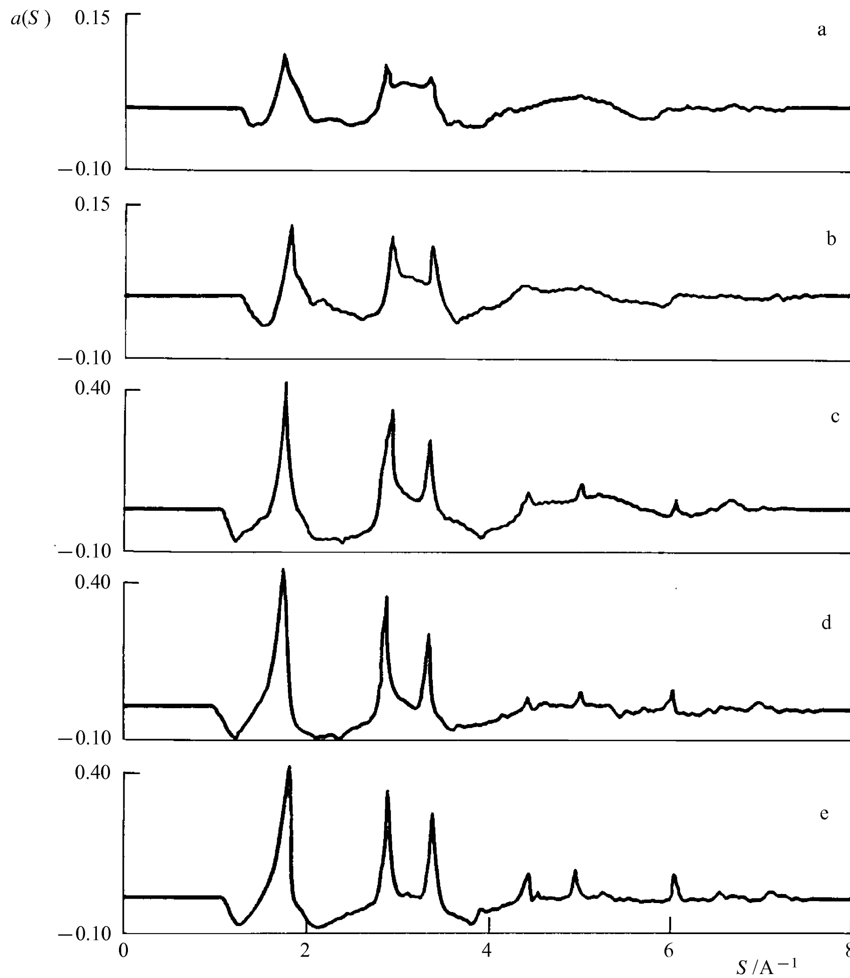

Figure 22. Changes in structure of metallic samples of a-GaSb ($p_{syn} = 90$ kbar, $T_{syn} = 1100$ °C) during sequential annealing at various temperatures: (a) 290 K (initial sample), (b) 350 K, (c) 380 K, (d) 400 K, and (e) 420 K [84].

that according to this model [84] the structure factor in the region of $S \approx 1.5-2.2$ Å^{-1} is described by the expression

$$a(S) = A_c \exp\left[-\frac{(S - S_c)^2}{\gamma_c^2}\right] + A_i \exp\left[-\frac{(S - S_i)^2}{\gamma_i^2}\right] + A_c \exp\left[-\frac{(S - S_a)^2}{\gamma_a^2}\right]. \quad (29)$$

In spite of the large number of free parameters in formula (29) the analysis of the experimental $a(S)$ curve is greatly simplified in the case of a-GaSb. First, for annealing temperatures $T_{an} \leqslant 450$ K the parameters S_c, S_i, and S_a (which define the position of the lines) remain constant, as well as the widths γ_c and γ_a. Because of the relationship $|S_c - S_i|$, $|S_c - S_a| \ll S_c$ the experimental amplitude of the change in the structure factor Δa_{max} provides the additional coupling condition $\Delta a_{max} = A_c + A_i + A_a$. Furthermore by treating this model as a simplified form of correlation analysis for determining component concentrations in a restricted range of the structure argument $S < 2.5$ Å [81], the parameters n_a, n_i, and n_c (having the meaning of relative concentrations) can be used [84].

$$n_{a,i,c} = \frac{A_{a,i,c}\,\gamma_{a,i,c}}{A_a\gamma_a + A_i\gamma_i + A_c\gamma_c}, \quad (30)$$

with $n_a + n_i + n_c = 1$. Use of this relationship [84] to approximate the experimental data by formula (29) reduces the number of adjustable parameters to two and accordingly simplifies the mathematical treatment. It is evident from

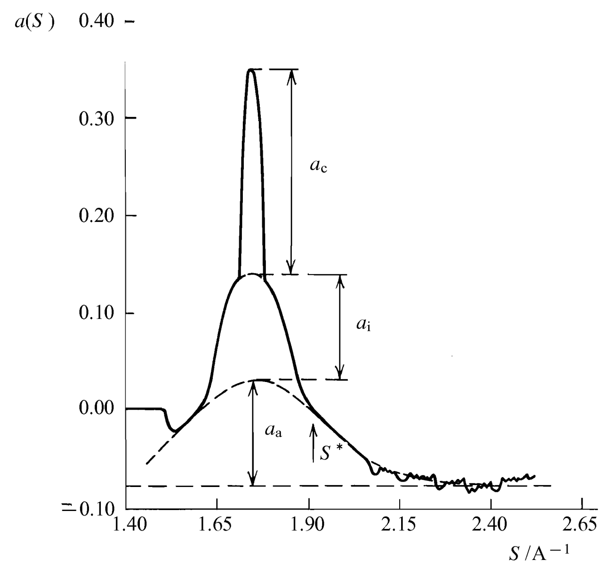

Figure 23. Structure of the first maximum $a(S)$ for a-GaSb (data obtained after annealing at 380 K are shown [84]).

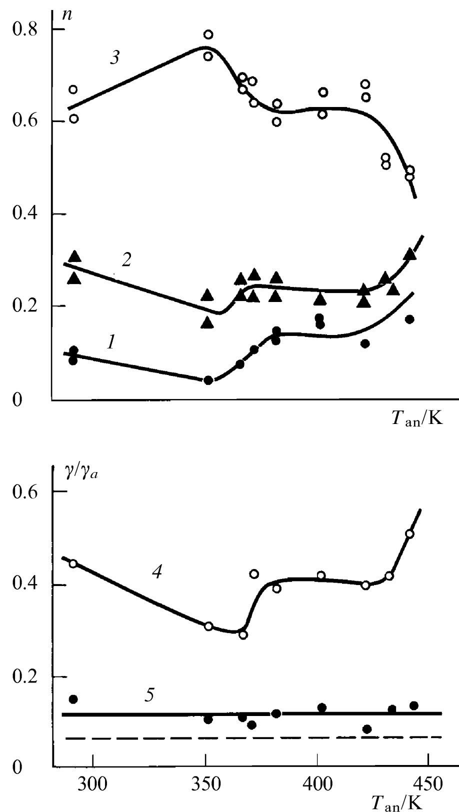

Figure 24. Changes in the parameters n_c (*1*), n_a (*3*), and n_i (*2*) and in the ratios γ_i/γ_a (*4*) and γ_c/γ_a (*5*). The parameters are defined in the text. The broken line shows the apparatus limit on the line width [84].

Fig. 23 that the procedure suggested in Ref. [84] procedure satisfactorily describes the shape of the first peak of $a(S)$.

The behaviour of the parameters n_a, n_i, n_c, and also γ_i and γ_c during the annealing process is shown in Fig. 24. The qualitative similarity between the contributions from n_i and n_c to the annealing process has been pointed out [84] (see Fig. 24). Furthermore in the initial state of annealing ($T_{an} < 350$ K) the crystal concentration decreases and the parameter n_a increases. If this process is identified with the structural relaxation characteristic of the majority of amorphous materials (including a-GaSb [77]) it is natural to associate the decrease in n_c with a kind of 'reamorphisation' of the system produced by the relaxation of the stresses at the boundary between the amorphous and the crystalline phase. Therefore the quantity n_a and its contribution to formula (29) reflect the presence of the amorphous a-GaSb phase itself. The decrease in n_a at the onset of intensive crystallisation ($T_{an} > 430$ K) is consistent with this interpretation.

This discussion allows us to identify the contribution bearing the subscript i with the presence of an intermediate region between the crystalline inclusions and the amorphous matrix, so that n_i corresponds [84] to the volume fraction of this boundary region (see Figs 23 and 24).

The correlation length (i.e. the characteristic range over which the relative ordering of the amorphous matrix is retained) can be calculated by using formula (27).

Within the present model [84] the parameter γ_a is defined by the correlation length L_{cor} of the disordered a-GaSb amorphous network; γ_c is given by the crystallite size L_c, and γ_i is given by the size of the boundary region L_i in which the transition from an ordered arrangement of atoms in the crystallite to a disordered arrangement in the amorphous network takes place. By using formula (27) and the $a(S)$ data (see Figs 22 and 23) we calculate [84] $L_{cor} \approx 20$ Å = const, $L_c \approx 200$ Å, and $L_i \approx 50$ Å [84].

It has been pointed out [84] that γ_c (and therefore also L_c) stays almost constant during the annealing process (see Fig. 24). Thus, at temperatures in the range of $T \leqslant 450$ K the dominant process in the crystallisation of a-GaSb is the formation of nanocrystals of c-GaSb. At higher annealing temperatures ($T_{an} > 450$ K) the characteristic size of the c-GaSb crystallites begins to increase while the parameter γ_c decreases. It follows from Fig. 24 that the crystallisation of a-GaSb takes place in two stages: in the range $350 \leqslant T \leqslant 380$ K and at $T_{an} > 430$ K. A steep decrease in the boundary region is observed in both the first and the second temperature range (the parameter γ_i increases). This behaviour suggests that processes at the boundaries of inclusions play a dominant role in the crystallisation of metastable phases in a-GaSb.

According to current views [81, 84] the intermediate region between the crystalline inclusions and the amorphous matrix (the contribution with the subscript i in Fig. 23) is uniquely connected with the nonstoichiometric Ga_xSb_{1-x} amorphous phase and is therefore located at the boundary between the amorphous and the crystalline phase (Fig. 10b). Under these conditions the changes in the boundary region are associated with changes in the phase composition of the samples, and in particular with the amount of the Ga_xSb_{1-x} phase in the bulk of the sample and with the parameter x, which defines the deviation from stoichiometry.

5.2 Stability range and kinetics of phase transformations of the metastable phases in a-GaSb

The structure analysis method described in the previous section is most effective in the region of annealing temperatures where the amplitudes A_i, A_a, and A_c are of the same order of magnitude. Since in the region of $T_{an} \geqslant 450$ K we observe a transition from the condition ($A_c \approx A_i$, A_a) to ($A_c \gg A_i$, A_a) a reliable analysis of the changes in phase composition of the samples, including the evolution of the boundary region, is impossible. Therefore the crystallisation and relaxation of a-GaSb were studied [84] by other methods: differential thermal analysis (DTA) and the temperature and time dependences of the electric conductivity of the samples, $\rho(T, t)$.

It should be noted that these methods are very different from the point of view of their ability to characterise phase transitions quantitatively. Thus, the electric conductivity method is most sensitive to phase transformations in the network of conducting channels in the a-GaSb samples, whereas the DTA method is more sensitive to changes in the bulk characteristics, and in particular to the crystallisation of the amorphous GaSb phase. Therefore the experimental methods used in the earlier work [84] are complementary: the $\rho(T, t)$ measurements gives the fullest and most detailed description of the electrically conducting c-GaSb and Ga_xSb_{1-x} inclusions (phase composition and geometric form), whereas the DTA data quantitatively characterise the volume fraction of the metastable phases (Ga_xSb_{1-x} and a-GaSb) in samples of amorphous gallium antimonide.

The kinetics of phase transformations have been studied [84] by resistance measurements from the relaxation curves $\rho/\rho_0 = f(t)$, where $\rho_0 = \rho(t = 0)$, obtained in a series of isothermal anneals at 300–600 K (Fig. 25a). Furthermore

the temperature dependence of the resistivity was measured (between $T = 1.8$ K and $T = T_{an}$) before each successive anneal at a predetermined temperature T_{an} exceeding the temperature of the previous anneal, and the field dependences of the magnetoresistance $\rho(H, T)$ were also determined. The galvanomagnetic characteristics of the a-GaSb samples obtained in these experiments will be discussed in Section 6. The time dependences $\rho/\rho_0 = f(t)$ (Fig. 25a) were monitored [84] for 50–120 min, depending on the extent of the phase transformation required (determined from the resistivity of the sample). In the crystallisation temperature range (350–470 K) and for a fixed annealing temperature $T_{an} = \text{const}$, the time dependence of the resistivity is determined by the change in the content of the metastable phase Z_ρ in the structure of conducting channels of the a-GaSb samples. According to the approach now widely accepted in the kinetics of phase transformations [97, 105] the fractional amount of transformed phase Z_ρ is linearly related (to a first approximation) to the physical parameter being measured:

$$Z_\rho = \frac{\rho(T_{an}, t) - \rho_\infty(T_{an})}{\rho_0(T_{an}) - \rho_\infty(T_{an})}, \tag{31}$$

where $\rho_\infty(T) = \lim_{t\to\infty} \rho(T, t)$ and $\rho_0(T_{an}) = \rho(T_{an}, 0)$.

Noting that relation (31) applies, firstly, to a two-component medium consisting of a metastable and a crystalline phase, and, secondly, when the system is beyond the critical region corresponding to the percolation threshold, we have used it only as an initial approximation

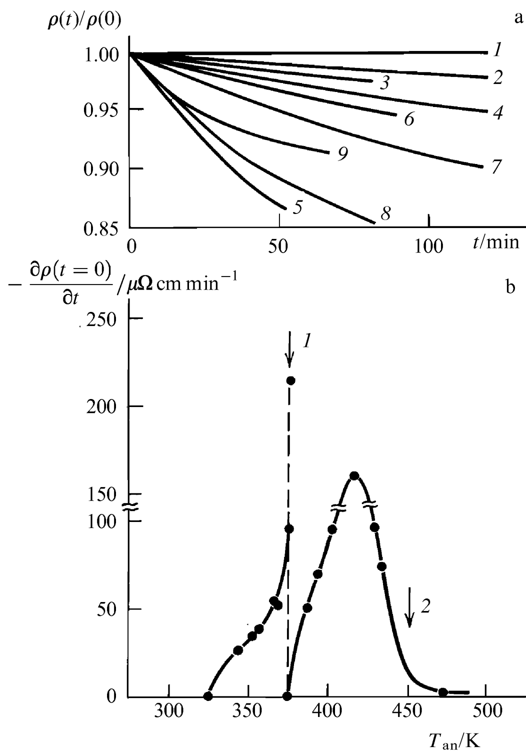

Figure 25. Time dependences of the resistivity [84] during isothermal annealing (a) and changes in the relaxation rate of the resistance at different annealing temperatures (b): (*1*) 330, (*2*) 340, (*3*) 350, (*4*) 360, (*5*) 370, (*6*) 380, (*7*) 390, (*8*) 410, and (*9*) 430 K. The arrows denote the characteristic temperatures: *1*, structure anomaly at 370 K; *2*, completion of steep resistance changes at 450 K.

[84]. In this approach [84] the characteristic time of the phase transformation $\tau = -Z_\rho/\dot{Z}_\rho$ can be written

$$\tau = -\frac{\rho(T_{an}, t) - \rho_\infty(T_{an})}{\partial\rho(T_{an})/\partial t}. \tag{32}$$

It can be seen from Fig. 25a that the derivative $\partial\rho/\partial t$ is finite in the limit of $t \to 0$, and therefore we have considered [84] the quantity $\tau = \tau(t = 0)$. This approach is justified within the Avrami–Kolmogorov approximation

$$Z_\rho = \exp\left[-\left(\frac{t}{\tau}\right)^n\right], \tag{33}$$

often used in the description of nucleation and growth processes [97]. Thus it follows from (33) that a finite value of $\dot{Z}_\rho$ and $\partial\rho/\partial t < 0$ are achieved for an Avrami exponent of $n = 1$. The experimental dependence [84]

$$\left.\frac{\partial\rho}{\partial t}\right|_{t=0} = f(T_{an})$$

is shown in Fig. 25b: in accordance with x-ray diffraction measurements two sections can be identified for $\partial\rho/\partial t$ in the whole range of annealing temperatures.

A detailed analysis of the data from resistance measurements leads to the conclusion (Fig. 25) that a-GaSb crystallises in two stages involving two different metastable phases. In the first of these phases crystallisation begins at ~330–350 K, and complete crystallisation can be achieved by a lengthy isothermal anneal at $T \approx 370$ K. The crystallisation of the second phase begins at $T_{an} \geqslant 370$ K.

When two different crystallisation channels are present we have

$$\rho(T_{an}, t) = \rho_\infty(T_{an}) + \Delta\rho_1 e^{-t/\tau_1} + \Delta\rho_2 e^{-t/\tau_2}, \tag{34}$$

As can be seen from the isothermal annealing results, $\tau_2 = \infty$ for a-GaSb with $T_{an} \leqslant 370$ K, and $\Delta\rho_1 = 0$ for $T_{an} > 370$ K. These conditions allow the contributions to the relaxation to be separated, and the characteristic times of the phase transformation to be determined for the two separate crystallisation processes. The results of this analysis of the data in Fig. 25 are shown in Fig. 26a, where the $\tau_{1,2}(T)$ results are plotted in Arrhenius coordinates. Tt can be seen that the asymptotic experience of the type $\tau_{1,2} = \tau_{1,2}^0 \exp(E_{a1,2}/k_B T)$ are substantially different for τ_1 and τ_2. In the former case $\tau_1^0 \approx 0.4$ s and $E_{a1} \approx 0.4$ eV, whereas for the crystallisation of a-GaSb we find $\tau_2^0 \approx 0.3 \times 10^{-13}$ and $E_{a2} \approx 1.41$ eV.

Let us now consider the results obtained [84] by differential thermal analysis. Typical heat evolution curves for metallic samples of a-GaSb (containing inclusions of the nonstoichiometric Ga_xSb_{1-x} amorphous phase) and for dielectric samples (practically free from nonstoichiometric inclusions) are shown in Fig. 26b as curves *1* and *2*, respectively. As has been pointed out [81, 84], in the sample from the metal side of the metal–insulator transition the main exothermic peak is much broader than the heat evolution maximum in the dielectric sample, and is shifted downwards by about 30 K. Another distinctive feature is seen in the DTA curves of the metallic a-GaSb samples: an additional broad maximum at $T_{an} \approx 550$–600 K.

By comparing the results of structure investigations of a-GaSb samples [81, 84] (see also Fig. 10) and of DTA studies (curves *1* and *2* of Fig. 26b) it was established [84] that the presence of a nonstoichiometric Ga_xSb_{1-x} amorphous phase leads to the formation of anomalies in the

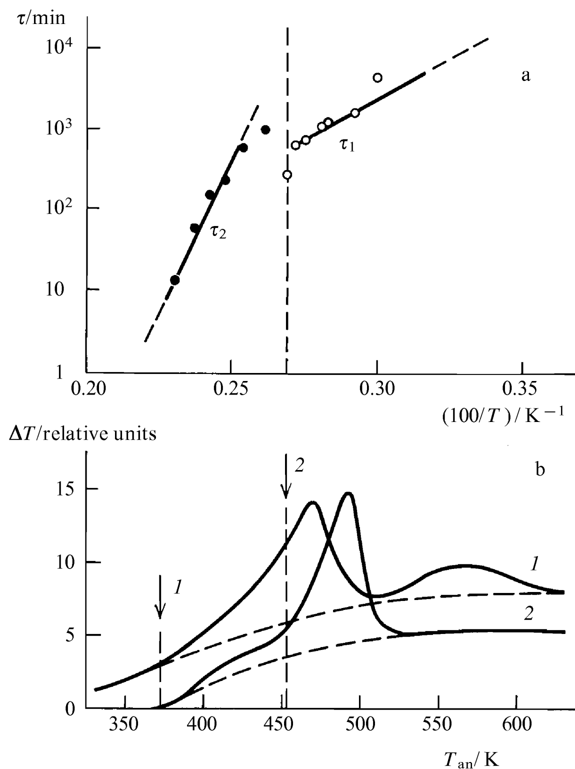

Figure 26. Characteristic crystallisation time as a function of annealing temperature, obtained from resistance measurements (a) and heat evolution curves for metallic (*1*) and for dielectric samples (*2*) of GaSb (b) [84] (the base lines in the DTA method are shown as broken curves). The vertical broken lines separate the regions of $T < 370$ K (τ_1) from those of $T > 370$ K (τ_2). The numbered arrows correspond to the same temperatures as those in Fig. 25.

DTA curves in two separate regions of temperature: $T_{an} \approx 370-430$ K (a broadening of the DTA peak) and $T_{an} \approx 500-620$ K (an additional heat evolution maximum).

By varying the temperature scanning rate of the main exothermic peak [43] the activation energy of the crystallisation and the Avrami exponent were determined. The activation energies were $E_a \approx 1.2$ eV for the metallic samples and $E_a \approx 1.4$ eV for the dielectric samples. In both cases the Avrami exponent was $n \approx 1 \pm 0.1$.

As reported [84] the main exothermic peak in Fig. 26b is due to the crystallisation of the amorphous a-GaSb phase itself. By comparing the Avrami exponents and the activation energies obtained by the DTA method with the results of resistivity measurements it was concluded [84] that the phase transformations in the structure of conducting channels and in the bulk of the a-GaSb samples on the metal side of the transition are essentially identical, and therefore both methods can be used in this case to describe the phase transformation. The crystallisation process of the metastable phases in a-GaSb is naturally separated into two stages, and the Ga_xSb_{1-x} inclusions crystallise in the temperature region preceding the onset of the crystallisation of the tetrahedral amorphous a-GaSb phase.

The crystallisation of the amorphous phase of gallium antimonide has a characteristic time $\tau_{02} \approx 10^{-13}$ s and is a polymorphic transformation controlled by processes at the interface between the amorphous and the crystalline phase. Since the fraction of the crystalline phase in these samples is relatively large, nucleation processes are unimportant and it is reasonable to consider only the growth processes, the Avrami exponent $n \approx 1$ corresponding [97] to the growth of crystallites after the exhaustion of the nucleation sites on the grain boundaries.

According to the same classification [97] the crystallisation of nonstoichiometric inclusions of Ga_xSb_{1-x} belongs to the group of preferred crystallisation processes. In this case a concentration gradient of the components (Ga and Sb, depending on the initial composition of the inclusion) is produced ahead of the crystallisation front, and atoms diffusing over large distances are included in the diffusion-controlled process. As a result the preexponential factor τ_{01} corresponding to the crystallisation of the Ga_xSb_{1-x} inclusions (Fig. 26b) is substantially greater than τ_{02}, namely $\tau_{01} \approx 0.14$ s.

The Avrami exponent observed in the study of the relaxation of the resistivity at 340–380 K is unity [84]. As reported [81], the concentration of nonstoichiometric superconducting inclusions of Ga_xSb_{1-x} in samples of a-GaSb is $n_c \approx 3\% - 5\%$, whereas the fraction of the sample in the crystalline state is $\sim 5\% - 10\%$ in the bulk of the sample (see Fig. 24). These observations suggest [84] that the diffusion-controlled growth of the crystal during the preferential crystallisation of Ga_xSb_{1-x} is determined by the growth of the particles having a relatively large initial volume [97], so that in this case the value $n \approx 1$ indicates quasi-one-dimensional growth of the GaSb crystallites.

The reduced dimensionality of the growth in GaSb, leading to small values of the Avrami exponent, arises apparently from the dominant role of the interfacial boundary between the amorphous and the crystalline regions during the crystallisation process. This result is consistent with the structure analysis data (Fig. 24), from which it follows that any change in the phase composition of the samples produces a change in the structure of the boundary region.

It has been noted [84] that some discrepancies exist between the structure analysis, DTA, and $\rho(T_{an}, t)$ results for the crystallisation processes in amorphous gallium antimonide. First of all, comparing the characteristic temperatures $T_{an} \approx 370$ K (structure anomaly, sharp maximum in $|\partial\rho/\partial t|$) and $T_{an} \approx 450$ K (completion of the relaxation changes in electric conductivity, $\partial\rho/\partial t = 0$) with the DTA curve for the metallic sample shows that a marked heat evolution takes place only after the first metastable phase has crystallised, and furthermore that the crystallisation in a-GaSb continues beyond the point when $\partial\rho/\partial t = 0$. Thus the DTA data are relatively insensitive to the crystallisation anomalies in the region of $T_{an} \approx 370$ K.

Several reasons for this state of affairs have been pointed out [84]. First, there is a systematic deviation between the characteristic temperatures obtained by stepwise isothermal anneal and by DTA methods, dependent on the scanning rate and on the characteristic time of the phase transformation [77]. In a-GaSb at scanning rates of 5–20 K min^{-1} this effects leads to a shift of $\Delta T \approx 10-25$ K, and therefore this value of ΔT should be added to the characteristic temperatures when comparing data obtained from the isothermal process with DTA data [77].

Secondly, allowance must be made for the structural organisation of the inclusions of different phase composition in a-GaSb. Published data [81, 85] show that inclusions of the Ga_xSb_{1-x} phase together with the crystalline phase form a network of conducting channels which determines the topology of the current lines and defines the

effective value of the electric conductivity, although the volume fraction of these inclusions is not large. Therefore quite small concentration changes of the Ga_xSb_{1-x} phase, which has a metallic conduction [81, 85], can strongly influence the conductivity of the system, even though the associated heat evolution features are small (the DTA signal is proportional to the mass of the corresponding metastable phase).

Similarly, the completion of the isothermal changes in the conductivity of the samples at a fixed annealing temperature before the achievement of complete crystallisation can be attributed to the formation of an infinitely large cluster of the crystalline phase at $n_c^* \approx 0.15-0.17$, which provides electric shunts in the high-resistance amorphous material. It is reasonable to expect an infinite cluster to be formed from the network of conducting channels, giving crystallites with a characteristic size determined by the cross-section of the conducting channels ($\sim$250 A) [81]. This assumption is confirmed by the results of structure studies, according to which the crystallite size ($L_c \approx 200$ Å) stays constant in the temperature range $T \leqslant 450$ K. Furthermore according to the data in Fig. 24 the critical value $n_c = n_c^*$ is reached at $T \approx 420-430$ K, where all further resistivity changes are suppressed ($\partial\rho/\partial t = 0$) (see Fig. 25b).

Thus the differential thermal analysis data and the $\rho(T, t)$ data [84] are complementary. The concept of the proximity of the a-GaSb samples to the percolation threshold of the crystalline phase for annealing temperatures $T_{an} \geqslant 370$ K also explains the steep dependence of the parameter $d\rho/dT$ on the annealing temperature in this temperature range (see Fig. 25). Obviously, in the critical region (where $n_c \to n_c^*$) we can expect small changes in the concentration of the crystalline phase to induce large changes in the electric conductivity of the system.

In the vicinity of the percolation threshold, formula (31) is invalid, and we must use the percolation model to determine Z_ρ. Starting from a model of the medium containing low-resistance inclusions in a conducting matrix [19] we can show that the formulae (31) and (32) give the product $\tau\delta$ instead of τ, where $\delta \cong (n_c^* + Z_\rho - 1)/(1 - n_c^*)$. As a result the $\ln[\tau_2(T)]$ data in Fig. 26a are shifted by $\ln\delta$. Under these conditions the character of the $\tau(T)$ curve is not affected qualitatively, and the activation energy is also unaffected, but the parameter τ_{02} increases to $\sim 5\times10^{-13}$ s.

6. Metastable superconductivity in amorphous gallium antimonide

Published studies [78–81] of the low-temperature characteristics of amorphous gallium antimonide have shown that samples from the metal side of the metal–insulator transition pass into a superconducting state when the temperature is decreased to $T < 9$ K. As reported [81], the appearance of superconductivity in amorphous gallium antimonide is due to the presence of the metastable nonstoichiometric phase Ga_xSb_{1-x} with $x > 0.5$: at temperatures $T < 1.8$ K the volume fraction of the superconducting phase V_s exceeds the percolation threshold V_c and the sample attains a state of zero resistance.

The study of the evolution of the superconducting properties of a-GaSb during the annealing process (‘stepwise crystallisation’) is closely related to the topic discussed in the previous section, and provides a useful test and exact specification of the results. The change in the parameters of the superconducting state in the preferential crystallisation of the Ga_xSb_{1-x} inclusions in the a-GaSb matrix are compared with the results of studies of the metastable superconductivity of Ga_xSb_{1-x} films [98], giving additional information on the change in the composition x of inclusions of the nonstoichiometric phase. The results of these investigations are discussed in Section 6.1, while in Section 6.2 we examine the behaviour of the super conductivity of the phases in the a-GaSb : Ge system and in Section 6.3 the three-dimensional percolation theory for conducting media containing superconducting inclusions is studied experimentally for the case of bulk amorphous gallium antimonide a-GaSb containing superconducting inclusions of the nonstoichiometric metastable Ga_xSb_{1-x} phase. The recent discovery of superconductivity in epitaxial films of GaAs is considered in Section 6.4 in the context of the results obtained for GaSb.

6.1 Crystallisation and superconductivity in a-GaSb

Since the development of semiconductivity in amorphous gallium antimonide is due [81, 85] to the presence of the Ga_xSb_{1-x} phase with $x > 0.5$ a study of the evolution of the superconducting properties of a-GaSb should offer a means of testing and verifying the results obtained in Section 5.

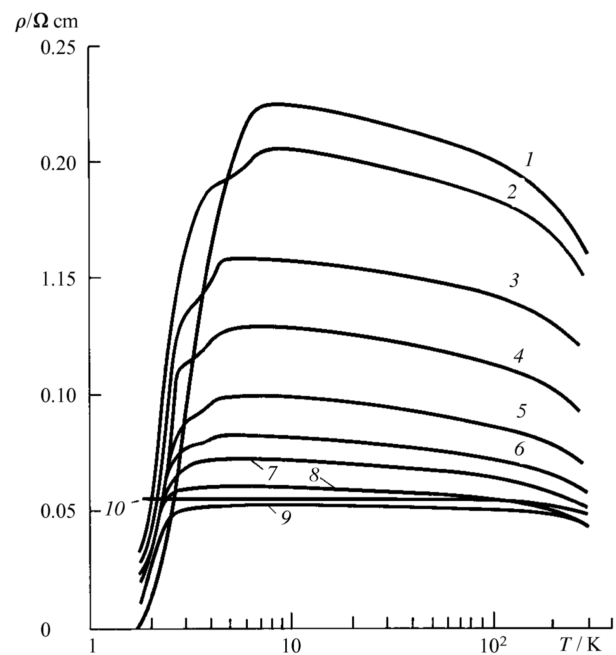

Figure 27. Changes in the superconducting transition in a-GaSb in a series of sequential isothermal anneals at different temperatures [84]: (*1*) 290 K (initial sample), (*2*) 360, (*3*) 370, (*4*) 400, (*5*) 420, (*6*) 440, (*7*) 450, (*8*) 470, (*9*) 520, (*10*) 570 K.

The change in the resistance characteristics of the superconducting transition in a-GaSb during the annealing process [84] is illustrated in Fig. 27. The width of the superconducting transition in the initial sample (curve *1*) greatly exceeds the more typical values: the resistance smoothly falls to zero in the range $1.8 \leqslant T \leqslant 8$ K. This behaviour is attributed [98] to the dispersion of the composition of the nonstoichiometric inclusions and to the associated dispersion of the critical temperature T_c. As a result, at $T_c \approx T_m \approx 8$ K the inclusions with the highest

critical temperature become superconducting; as the temperature is lowered, the resistance of inclusions for which $T_c > T$ vanishes, and at $T = T_p$ the superconducting inclusions form an infinite cluster and the sample reaches a state for which $\rho = 0$. A detailed analysis of the percolation character of this superconducting transition has been given [81, 82].

Increasing the annealing temperature lowers the absolute value of the resistivity $\rho(T > T_m)$, and at the same time all the superconductivity features are shifted towards lower temperatures (see Fig. 27). After an anneal at $T_{an} \approx 330-340$ K the state with $\rho = 0$ is not reached, and the resistivity remains finite at all temperatures $T \geqslant 1.8$ K.

It can be seen from the data [84] in Fig. 28a that the annealing of the metastable superconductivity of the Ga_xSb_{1-x} inclusions takes place in two stages. Initially, at annealing temperatures $T_{an} \approx 370$ K, the superconductivity of the inclusions for which $4 \leqslant T_c \leqslant 10$ K is suppressed, and at annealing temperatures $T_{an} > 370$ the $\rho(T = 10$ K) and $\rho(T = 4.2$ K) (curves *1* and *2* in Fig. 28a) are almost indistinguishable. The superconductivity of the inclusions with $T_c < 4$ K is retained even for anneals in the temperature range $370 < T_{an} < 500$ K. Complete suppression of the superconducting properties is reached after annealing at $T_{an} > 500$ K (curve *3* and *1* of Fig. 28a). Thus the metastable superconductivity of a-GaSb is completely annealed [84] once the tetrahedral gallium antimonide amorphous phase has completely crystallised (Fig. 26).

In Fig. 28 we show the behaviour [84] of the maximum critical temperature of the superconducting transition T_m as a function of the annealing temperature T_{an} in a-GaSb. By using the known [98] change in the superconductivity characteristics of the Ga_xSb_{1-x} phase, the concentration dependence of the critical temperature and of the electric conductivity of the inclusions $T_c(x)$ and $\rho(x)$ was regenerated [84], and the characteristic values of x corresponding to the two components of the nonstoichiometric metastable phase having different physical properties were determined (Fig. 28b). It can be seen from the $T_c(x)$ data at $T \leqslant 350$ K that the superconductivity of inclusions with $x > 0.8$ containing a maximum amount of gallium in the Ga_xSb_{1-x} phase and having the highest critical temperature is completely suppressed, and that the inclusions with $x \approx 0.8-0.7$ and a maximum critical temperature of $T_c \approx 4$ K are the most stable. The superconductivity of inclusions of this type can be suppressed by annealing at $T_{an} \approx 570$ K (Fig. 28c).

The physical explanation suggested [84] for this type of $T_c(x)$ dependence is a change in the short-range order structure of the Ga_xSb_{1-x} phase. Thus, in the vicinity of $x \approx 1$ the amorphous gallium structure should be dominant in Ga_xSb_{1-x}, and at $x \approx 0.5$ the dominant structure should be a different (tetrahedral) form of GaSb. Therefore there is a critical concentration, corresponding to the transition from one of these types of short-range order to the other, at which the physical characteristics of the system show a singularity in the behaviour of T_c and ρ for $x \approx 0.8$ (see Fig. 28).

Additional information on the nature of the superconductivity in a-GaAs was obtained [84] by analysing the field and temperature dependences of the magnetoresistance $\Delta\rho/\rho = f(H, T)$ and their evolution during the annealing process. It has been previously shown [81] that for $T < T_m$ the positive magnetoresistance (PMR) of a-GaSb is due mainly to the suppression of the superconductivity of the inclusions, whereas the contribution from the normal kinetic mechanisms is small because of the small value of the mobility μ. Under these conditions the inequality $\mu_H \ll 1$ is valid in the range of magnetic fields $H < 150$ kOe [81].

The field dependence $\rho(H)$ of the resistance at different temperatures is shown in Fig. 29a for the initial (unannealed) sample. It can be seen that at $T \leqslant 4$ K the shape of the $\rho(H)$ curve becomes more complex, and two regions can be distinguished on the experimental curve, corresponding to the disappearance of two different superconducting phases with different critical fields (H_{c2}). When the suppression of the superconductivity by the magnetic field has gone to completion we observe a weak, linear increase in the resistance of the sample with magnetic field (Fig. 29a).

Thus in general the $\rho(H)$ data can be represented as a superposition of several contributions (curves *1–3* of Fig. 29b). For $T \leqslant 4$ K we first observe the suppression of the inclusions with minimum critical parameters, and the corresponding component of the $\rho(H)$ curve rises to a

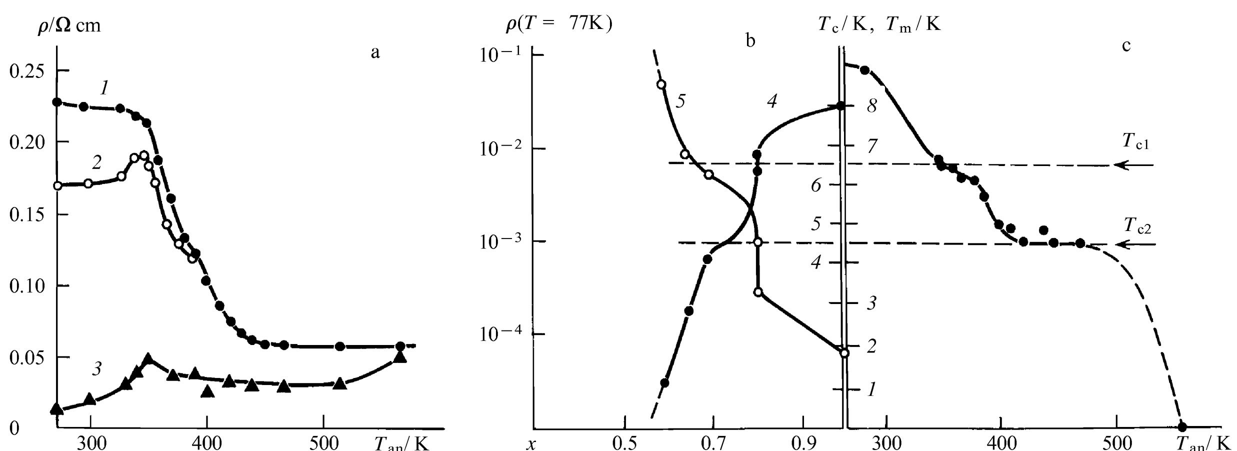

Figure 28. Changes in electric conductivity of a-GaSb samples as a function of the annealing temperature; the numbering of the curves defines the measurement of ρ after the successive anneals at different temperatures: (*1*) 10 K, (*2*) 4.2 K, (*3*) 2 K [84]; (b) changes in the critical temperature (*4*) and in the resistivity at $T = 77$ K (*5*) during variations in the composition of the Ga_xSb_{1-x} inclusions; (c) evolution of the characteristic critical temperature of the inclusions during annealing. The experimental data on $T_c(x)$ and $\rho(x)$ were taken from Hauser [98].

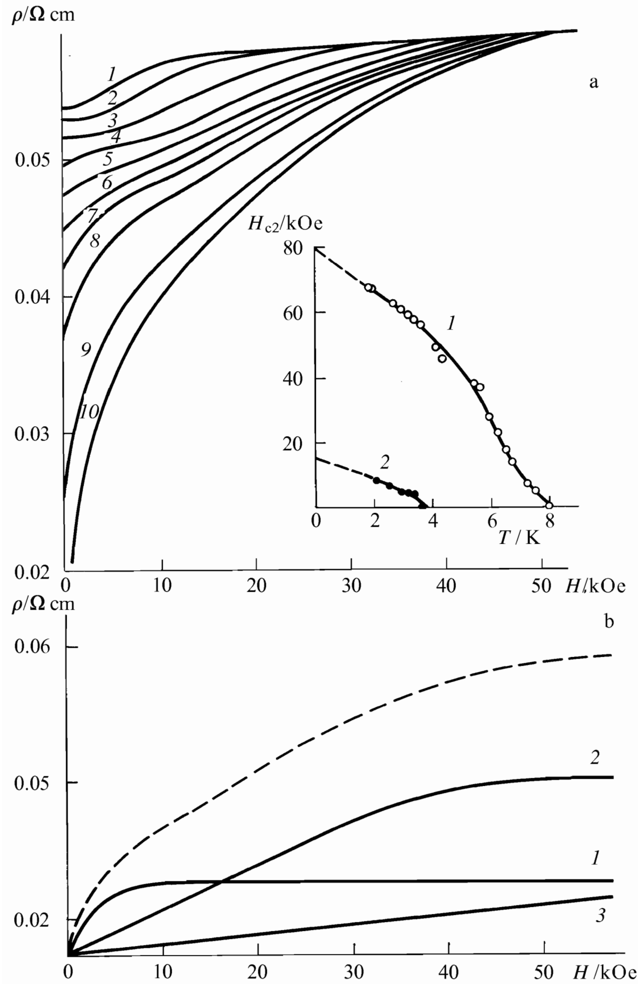

Figure 29. (a) Field dependences of the resistivity $\rho(H)$ for the initial unannealed (metallic) a-GaSb sample at different temperatures (K): (*1*) 6.6, (*2*) 6.3, (*3*) 5.5, (*4*) 4.1, (*5*) 3.5, (*6*) 3.2, (*7*) 2.9, (*8*) 2.6, (*9*) 2.1, (*10*) 1.9; the temperature dependences of the critical field H_{c2} are shown in the insert for inclusions with $x > 0.8$ (open circles) and $x < 0.8$ (filled circles). (b) Structure of the field dependence of the magnetoresistance for $T = 2.6$ K.

saturation level (curve *1*). The component corresponding to the other superconducting phase (with higher critical parameters) behaves in a similar way (curve *2*). The third contribution to the $\rho(H)$ curve, corresponding to a linear plateau and observed in strong magnetic fields, is due to the magnetoresistance of the nonsuperconducting a-GaSb matrix. Evidently, at $T > 4.2$ K only two contributions (analogous to curves *1* and *3* of Fig. 29b) are needed to describe the $\rho(H)$ curve.

By reconstructing from Fig. 29 the critical parameters H_{c2} and T_c for both superconducting phases defined above the $H - T$ superconductivity diagram for a-GaSb was constructed [84] and the characteristic values were determined [$T_c \approx 8$ K and $H_{c2}(0) \approx 80$ kOe for the first superconducting phase and $T_c \approx 4$ K and $H_{c2}(0) \approx 14$ kOe for the second, see insert in Fig. 29].

The value [84] $H_{c2}(0) \approx 80$ kOe for the first phase is consistent with the $H_{c2}(0)$ value reported [99] for amorphous gallium (~ 100 kOe). Furthermore the high values of $H_{c2}(0)$ for the second phase [84] make this feature of the PMR of a-GaSb impossible to interpret by assuming the presence of a disordered metallic phase (high-pressure GaSb II) or of metastable superconducting antimony phases as inclusions in the bulk of the sample. Indeed, it has been reported [100, 101] that these phases have critical temperatures close to those observed in a-GaSb, but their critical fields H_{c2} are much lower (not greater than ~ 5 kOe).

The parameter T_m and the corresponding value of H_{c2} given above are characteristics of a superconducting inclusion with maximal critical temperature and field. When the superconducting parameters are dispersed the system of superconducting inclusions cannot be described fully by fixing only T_m. Introducing the distribution function of the volume of the inclusions with respect to the critical temperature $\varphi(T_c)$ gives the following formula for the volume of the sample occupied by the superconducting phase at the given temperature:

$$V_s(T) = \int_T^{\infty} \varphi(T_c)\, dT_c\,, \qquad (35)$$

where $\varphi(T_c \geqslant T_m) \equiv 0$. It has been shown [84] that to a first approximation the magnetoresistance of a-GaSb is $\Delta\rho/\rho \propto V_s(T)$. (This condition is violated only in a narrow temperature interval adjacent to T_p, where an infinite cluster is formed from the superconducting inclusions.) Therefore the changes in $\Delta\rho/\rho$ in a fixed magnetic field can be used [84] to determine the nature of the changes in V_s and in $\varphi(T_c)$ during the annealing process (Fig. 30). Under these conditions the $\Delta\rho/\rho = f(T_{an})$ curve measured at the lowest temperature $T \approx 2$ K (curve *1* of Fig. 30) describes the total change in the volume of the a-GaSb sample occupied by superconducting phases.

It would appear that the $\Delta\rho/\rho = f(T_{an})$ data measured at $T \approx T_{c1} \approx 4$ K give the change in the volume V_s caused by

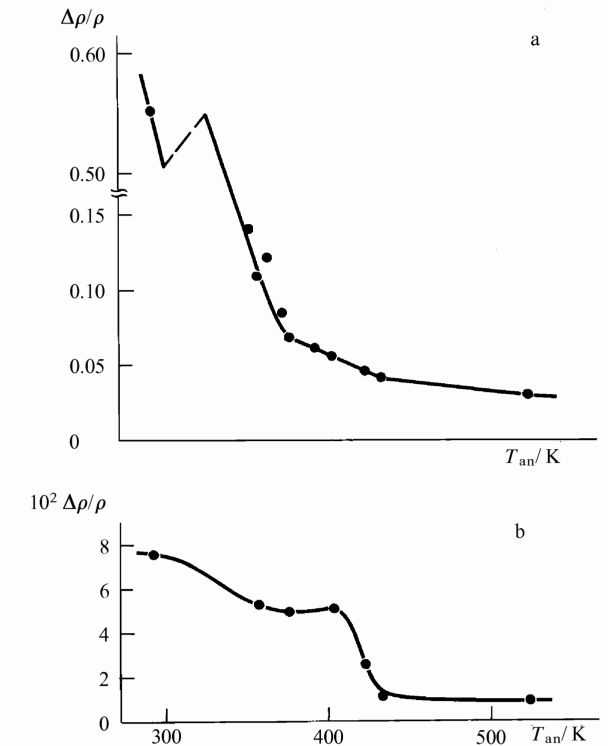

Figure 30. Changes in magnetoresistance in the field $H = 45$ kOe during annealing. Measurements at (a) 2 K, (b) 4.2 K.

the predominant anneal of the first superconducting phase: Ga_xSb_{1-x} with $x > 0.8$ ($T_c \geqslant 6.5$ K). As can be seen from curve 2 of Fig. 30, annealing at $T_{an} \approx 350$ K decreases the volume of inclusions for which $x > 0.8$, and beyond this point (for $T_{an} \approx 370$ K) the rate of crystallisation of this nonstoichiometric metastable phase decreases. Raising the annealing temperature to $T_{an} \approx 400-430$ K suppresses the superconducting inclusions with $x > 0.8$, and after this the superconductivity of a-GaSb is determined essentially by the inclusions of Ga_xSb_{1-x} with $x < 0.8$ [84].

6.2 Changes in the superconducting properties of the a-GaSb : Ge system

The low-temperature properties of a-GaSb : Ge samples were studied [91] with the aim of explaining the effect of germanium additions on the superconductivity of the metastable phases in amorphous gallium antimonide.

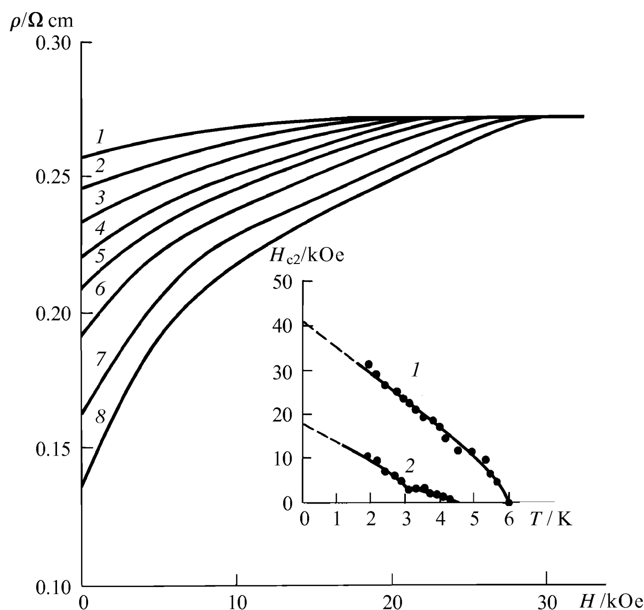

Figure 31. Suppression of the superconductivity by a magnetic field in a metallic sample with $x_{Ge} = 14$ mol% [91]. $H_{c2}(T)$ data for $x > 0.8$ (*1*) and $x < 0.8$ (*2*) are shown in the insert. The $\rho(H)$ curves correspond to the following temperatures (K): (*1*) 4.2, (*2*) 3.7, (*3*) 3.3, (*4*) 2.9, (*5*) 2.7, (*6*) 2.4, (*7*) 2.2, (*8*) 1.9.

The $\rho(H,T)$ data on the suppression of the superconductivity by an external magnetic field in a sample with $x_{Ge} = 14$ mol% are shown in Fig. 31. It has been pointed out [91] that, as in the undoped system, two characteristic regions of changes in ρ can be distinguished on the $\rho(H)$ curve for $T \leqslant 4$ K (see Fig. 31). By using $\rho(H,T)$ data the $H_{c2}(T)$ dependences have been plotted for two superconducting phases (see insert in Fig. 31) in the bulk of the a-GaSb : Ge sample, and the parameters T_c, $H_{c2}(T = 0)$, and dH_{c2}/dT $(T \to T_c)$ of the superconducting state of both phases have been obtained (Fig. 32).

Several important conclusions follow from the results [91] in Fig. 32. First, the large difference between the concentration dependences of the superconductivity parameters in phases I and II confirms that we are dealing with two different superconducting phases. Second, the presence of concentration dependences for the parameters T_c, $H_{c2}(0)$, and dH_{c2}/dT, given by the characteristics of the energy spectrum of the superconductor, the carrier concentration, and the mean free path [102], suggests that the structure phases responsible for the superconductivity of a-GaSb are doped by germanium. Third, the superconductivity of the metallic samples is retained up to the point of the structure transition $(x_{Ge} = x^*_{Ge})$.

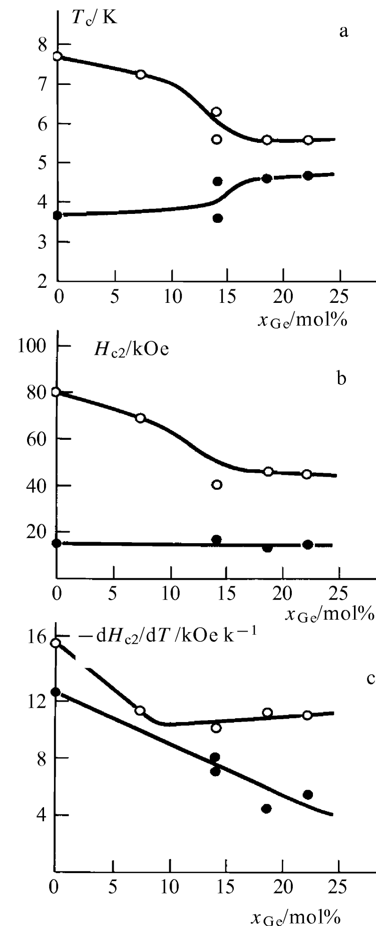

Figure 32. Concentration dependences of the superconductivity parameters of a-GaSb : Ge. Open circles for $x > 0.8$, filled circles for $x < 0.8$. (a) $T_c(x_{Ge})$, (b) $H_{c2}(0)$, (c) $(-dH_{c2}/dT,\ T = T_c)$ [91].

6.3 Critical behaviour of the conductivity of a medium containing superconducting inclusions

Very little is known at present on the value of the critical exponent q in real materials (see Section 2), and therefore the choice of the model (Ref. [55] or Ref. [62]) which best describes the critical behaviour of the superconducting inclusions is not straightforward. One of the few reported studies in this area [82] used bulk samples of amorphous gallium antimonide (a-GaSb) synthesised by quenching under high pressure as the experimental material.

In the preceding sections we showed that under certain conditions (temperature and pressure used for the synthesis) inclusions of the nonstoichiometric metastable Ga_xSb_{1-x} phase with $x > 0.5$, which show superconductivity, are formed in the bulk of the a-GaSb phase. The characteristic size of these inclusions is ~250 A [81], and the dispersion of x produces dispersion of the critical temperature T_c. As a result the superconducting transition in a-GaSb is strongly extended (see Fig. 29): initially, at $T = T_m \approx 8$ K, the resistance of the inclusions with a maximal critical temperature $T = T_c$ vanishes, and at $T = T_p \approx 1.8$ K an infinite cluster is formed

from the superconducting regions, and the stage $\rho = \sigma^{-1} = 0$ is reached. Thus in the case of a-GaSb the temperature is a convenient parameter for smoothly controlling the amount of the superconducting phase V_S in the samples, and amorphous gallium antimonide can be used as a model material in studies of percolation over the superconducting inclusions.

We shall express the $V_s(T)$ dependence in the form of (35), where $\varphi(T_c)$ is the distribution function of the clusters with respect to T_c. From expressions (11) and (35) we arrive at the following formula for the resistivity $\rho(T) = \sigma^{-1}$:

$$\frac{1}{\rho}\frac{\partial\rho}{\partial T} = q\frac{\varphi(T)}{n_c}\left(\frac{\rho}{\rho_0}\right)^{-1/q}; \qquad (36)$$

where $\rho_0 = \sigma_0^{-1} \approx \rho(T \geqslant T_m)$ is the resistance of the medium in the absence of inclusions (Fig. 33). Therefore, if the function $\varphi(T)$ has no steep singularities [as shown by the smooth outline of the $\rho(T)$ curve at $T < T_m$] we can rewrite the experimental data in the coordinates

$$\ln\left(\frac{1}{\rho}\frac{\partial\rho}{\partial T}\right) = f(\ln\rho)$$

and find the exponent q from the slope of the linear part. The main advantage of this method is that a knowledge of the percolation threshold and of the parameter V_s (whose experimental determination is often difficult) is not needed.

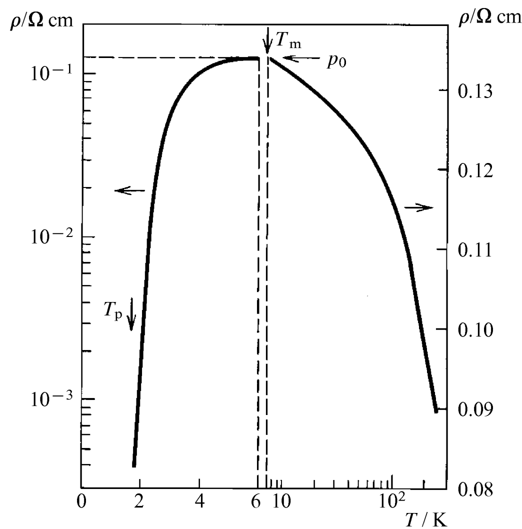

Figure 33. Temperature dependence of the resistivity and the superconducting transition for samples of a-GaSb. Measurement current $I = 0.5$ mA [82].

The experimental $\rho(T)$ dependence for $T < T_m$ in the above coordinates is shown in Fig. 34. The presence of an extended linear part for $\rho \leqslant 6 \times 10^{-2}\,\Omega$ cm, corresponding to the asymptotic relation (11), is noteworthy. Under these conditions the parameter q is found to be $q = 1 \pm 0.01$, which agrees with the Efros–Shklovskii hypothesis [55] but is incompatible with the Coniglio–Stanley model [62]. Thus, for the experimental value $q = 1$ we find from formula (12) that $d_f \approx 3.27 > d = 3$, and the fractal dimensionality greatly exceeds the dimensionality of the space. We consider this extremely unlikely.

As can be seen from Fig. 34, lowering the temperature still further $(T \to T_p)$ infringes the condition (11). In the region of $\rho < 4.5 \times 10^{-3}\,\Omega$ cm the quantity

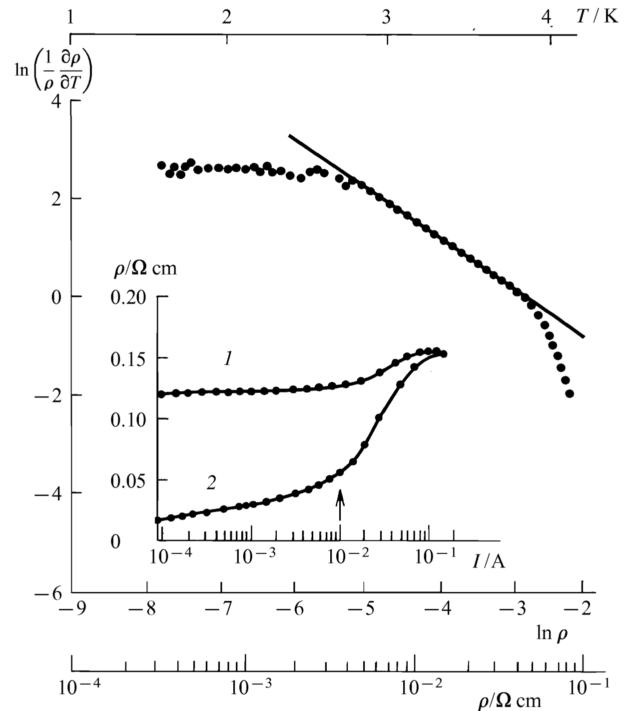

Figure 34. $\rho(T)$ curve for $T < T_m$ plotted in special coordinates (see text) to calculate the critical exponent q. The insert shows the current dependence of the resistivity at $T = 4.2$ K (*1*) and $T = 2.5$ K (*2*). The arrow shows the characteristic current which separates the region where the suppression of the weak links between the inclusions by the current is predominant from the region where the superconductivity of the inclusions is suppressed [82].

$$\ln\left(\frac{1}{\rho}\frac{\partial\rho}{\partial T}\right)$$

reaches saturation, which suggests a different type of dependence for this range. We attribute this effect to the presence of weak links between the superconducting inclusions. As we have previously shown [81], the existence of these links is confirmed by measurements of the current dependence $\rho(I)$ for $T \approx T_p \approx 2$ K (see insert to Fig. 34). In the vicinity of T_p we find, in addition to a steep increase of $\rho(I)$ for $I > 10^{-2}$ A (corresponding to the Joule heating of the medium and to the suppression of the superconductivity by the current [81]) a region of gradual increase in $\rho(I < 10^{-2}$ A) which is unrelated to the above effects but results from the breakdown of the weak links by the electric current. As can be seen from the insert in Fig. 34, the effect of the weak links increases as the temperature decreases. Therefore in the region of $\rho < 4.5 \times 10^{-3}\,\Omega$ cm $(T < 2.8$ K) it is reasonable to expect the power law (11) to be replaced by a stronger dependence, for example of the exponential kind $\rho \approx \rho_0 \exp(-\alpha V_s)$. It is easily seen that in this case

$$\ln\left(\frac{1}{\rho}\frac{\partial\rho}{\partial T}\right) \sim \ln\alpha\varphi(T),$$

and for a slowly varying $\varphi(T)$

$$\ln\left(\frac{1}{\rho}\frac{\partial\rho}{\partial T}\right) \approx \text{const}$$

(as is observed experimentally). We note that the effect of weak links is not allowed for in the derivation of formula (11) [55, 62, 63].

Let us now examine the region $\rho > 6 \times 10^{-2}\,\Omega$ cm ($T \approx 4$ K), where the concentration of inclusions is small and the conductivity of the medium can be expressed [53] by the linear asymptotic relation (5).

It follows from Eqn (5) that for $\varphi(T) \approx$ const, and $T \to T_m$, $\sigma(T)$ will have a linear asymptotic behaviour (see Fig. 35) differing (in general) from that of formula (11) for $V_s \to 0$. By extrapolating the linear part of $\sigma(T)$ (see Fig. 35) to $T \to T_p$ we determine $\Delta\sigma_{max} = 3\beta\sigma_0 V_s^c$. It follows from the results in Fig. 35 that in a-GaSb $\Delta\sigma_{max}/\sigma_0 \approx 0.6$. The value thus obtained is very close to the theoretical value for spherical superconducting inclusions ($\beta = 1$, $V_s^c = 0.17$), for which $\Delta\sigma_{max}/\sigma_0 \approx 0.51$.

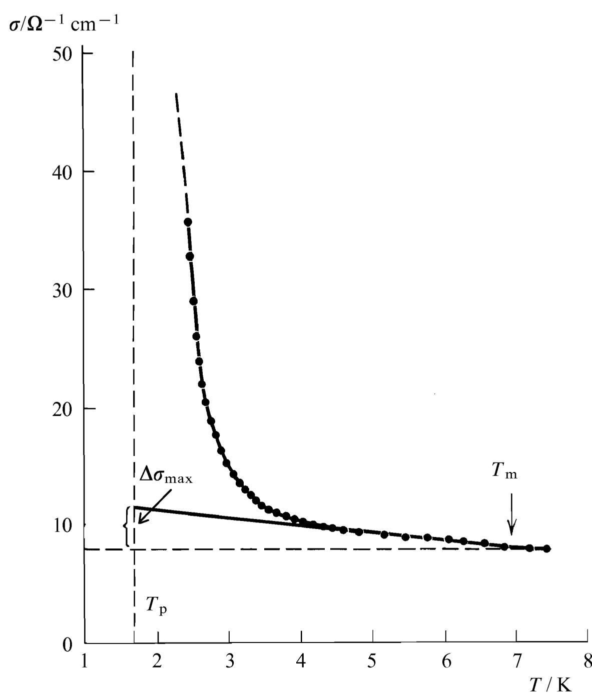

Figure 35. Linear conductivity asymptote in the limit of low concentrations of the superconducting inclusions and approach of the $\sigma(T)$ curve towards the critical behaviour described by formula (11) ($I = 0.5$ mA).

Thus the conductivity of a real system with superconducting inclusions can be described by already available theories [53, 55] for inhomogeneous media except for the immediate vicinity of the percolation threshold, where weak superconductivity effects are (apparently) important. This critical region is most satisfactorily described by the Efros – Shklovskii model [55].

6.4 Superconductivity in epitaxial GaAs layers

To conclude this section we shall briefly mention the special features of the development of superconductivity in binary, ternary, and other semiconducting compounds containing gallium.

We believe that the mechanism of formation of superconductivity discussed in Section 6, based on local changes in the short-range order structure, is common to many semiconductor materials, and that in materials containing gallium the nonstoichiometric regions responsible for the superconductivity contain an excess of gallium. These assumptions are confirmed by the recently observed superconducting anomalies in epitaxial layers of gallium arsenide containing an excess of arsenic [103]. We know that in epitaxial GaAs layers the spatial uniformity of the characteristics is perturbed on a distance scale of $\sim 0.5 - 1$ μm, controlled by changes in the stoichiometric composition of the material [104]. Since an excess of arsenic in the layer does not exclude the possibility of regions with a local excess of gallium, superconductivity in GaAs may be formed by the same mechanism as in GaSb.

This explanation is supported by the similarity between the critical temperature of GaAs ($T_c \approx 10$ K) and the corresponding values for amorphous gallium ($T_c \sim 8 - 9$ K) [98, 99]. It can easily be shown that for inclusions rich in gallium the values of the critical field H_c observed [103] in GaAs correspond to the Ginzburg – Landau parameter $\kappa \approx 20$, whereas in a-GaSb $\kappa \approx 80$ [81]. This discrepancy can be explained by noting that in a-GaSb the degree of disorder is higher, and therefore the coherence length is smaller than in epitaxial GaAs layers. However, the reasonably high values of κ assumed for GaAs are consistent with a significant level of disorder in the epitaxial layers, as has been found experimentally [103].

7. Conclusions

We have reviewed the currently available experimental data on the structure and physical properties of amorphous semiconductors prepared by high-pressure quenching of a melt. We believe that this class of noncrystalline materials can be used as a model of materials prepared by other methods of solid-state amorphisation, and therefore an analysis of the structure and properties of the ASHP should help to clarify both the fundamental mechanisms of solid-state amorphisation and the behaviour of complex multiphase systems. Special attention has been paid to the inclusions of submicrometre size formed during the synthesis of metastable phases, because in most cases these determine not only the properties of the amorphous matrix but also those of the crystalline phases of binary and ternary compounds.

An analysis of all the available experimental data on the ASHP leads to the conclusion that the models of multicomponent media are the most convenient and effective method of describing this type of material. However, in order to describe the critical behaviour of different systems in the immediate vicinity of the phase transition (amorphisation, crystallisation) we must introduce the scale theory and the percolation theory. A review of the metal – insulator transitions observed in ASHP and accompanying a phase transition is given in Section 4: it allows comprehensive tests of the validity of these theoretical approaches when applied to actual physical systems.

The use of other physical characteristics, in addition to structure methods, in studies of phase transformations offers (in most cases) information of great importance for the analysis of multicomponent systems having a complex phase composition. The dynamics of the relaxation of the metastable phases to the equilibrium state allow the phases to be identified and the sequence of transformations in the system to be established, and furthermore they allow the changes in size (and shape) and in composition of the submicrometre metallic inclusions in the amorphous matrix to be studied. One of the most striking phenomena observed in this class of semiconductor materials is superconductivity induced by amorphisation.

Acknowledgements

We are grateful to A A Abrikosov, V F Gantmakher, and E G Ponyatovskii for helpful discussions, which conributed to completion of the work. Sincere thanks are also due to S V Popova for her generous help during the planning and the preparation of this review and to V V Brazhkin for his valuable comments and interest in this work.

References

1. McDonald T R R, Sard R, Gregory E *J. Appl. Phys.* **36** 1498 (1965)
2. Belash I T, Ponyatovskii E G *High Temp. – High Press.* **7** 523 (1975)
3. Aptekar I L, Belash I T, Ponyatovskii E G *High Temp. – High Press.* **9** 641 (1977)
4. Belash I T, Ponyatovskii E G, *High Temp. – High Press.* **9** 645 (1977)
5. Belash I T, Ponyatovskii E G *High Temp. – High Press.* **9** 651 (1977)
6. Ponyatovskii E G, Barkalov O I *Mater. Sci. Rep.* **8** 147 (1992)
7. Mott N F, Davis E *Electronic Processes in Non-crystalline Materials* (Oxford: Clarendon Press, 1979)
8. Fritzche H (Ed) *Amorphous Silicon and Related Materials* (Singapore: World Scientific, 1989)
9. Joannopoulos J D, Lucovsky G (Eds) *The Physics of Hydrogenated Amorphous Silicon* (Berlin: Springer, 1984)
10. Schwarz R B, Johnson W L *Phys. Rev. Lett.* **51** 415 (1983)
11. Seyffert M, Siber A, Ziemann P *Phys. Rev. Lett.* **67** 3792 (1991)
12. Koch C C, Cavin O B, et al. *Appl. Phys. Lett.* **43** 1017 (1983)
13. El-Eskandarary M S, Aoki K, Suzuki K *J. Appl. Phys.* **71** 2924 (1992)
14. Shen T D, Wang K Y, et al. *J. Appl. Phys.* **71** 1967 (1992)
15. Volkert C A *J. Appl. Phys.* **70** 3521 (1991)
16. Gamarnick M Ya, Brick A B, *Fiz. Tverd. Tela* **33** 1293 (1991) [*Sov. Phys. Solid State* **33** 732 (1991)]
17. Fecht H J, Johnson W L *Phys. Rev. Lett.* **64** 1753 (1990)
18. Larchev V I, Mel'nik N N, Popova S V, et al. *Kratkie Soobshcheniya po Fizike (FIAN)* **1** 7 (1985)
19. Ponyatovskii E G, Belash I T, Barkalov O I *J. Non-Cryst. Solids* **117/118** 679 (1990)
20. Barkalov O I, Belash I T, Degtyareva V F, Ponyatovskii E G *Fiz. Tverd. Tela* **29** 1975 (1987)
21. Barkalov O I, Belash I T, Bol'shakov A I, Ponyatovskii E G *Fiz. Tverd. Tela* **30** 2724 (1988)
22. Barkalov O I, Belash I T, Gurov A F *Phys. Stat. Sol. A* **115** K19 (1989)
23. Degtyareva V F, Belash I T, Ponyatovskii E G, Rashchupkin V I *Fiz. Tverd. Tela* **32** 1429 (1990) [*Sov. Phys. Solid State* **32** 834 (1990)]
24. Gantmaker V F, Esipov S E, Teplinskii V M *Zh. Eksp. Teor. Fiz.* **97** 373 (1990) [*Sov. Phys. JETP* **70** 211 (1990)]
25. Barkalov O I, Belash I T, Esipov S E, Gantmakher V F, Ponyatovskii E G, Teplinskii V M *Physica B* **165–166** 311 (1990)
26. Teplinskii V M, Gantmaker V F, Barkalov O I *Zh. Eksp. Teor. Fiz.* **101** 1698 (1992) [*Sov. Phys. JETP* **74** 905 (1992)]
27. Gantmaker V F, Zverev V N, Teplinskii V M, Barkalov O I *Pis'ma Zh. Eksp. Teor. Fiz.* **56** 311 (1992) [*JETP Lett.* **56** 309 (1992)]
28. Brazhkin V V, Lyapin A G, Popova S V, Voloshin R N *Pis'ma Zh. Eksp. Teor. Fiz.* **56** 156 (1992) [*JETP Lett.* **56** 152 (1992)]
29. Brazhkin V V, Larchev V I, Popova S V, Skrotskaya G G *Usp. Fiz. Nauk* **150** 466 (1986) [*Sov. Phys. Usp.* **29** (11) 1066 (1986)]
30. Brazhkin V V, Popova S V *Metallofizika* **7** 103 (1985)
31. Mishima O, Calvert L D, Whalley E *Nature (London)* **310** 393 (1984)
32. Chen A L, Yu P Y, Pasternak M P *Phys. Rev. B* **44** 2883 (1991)
33. Goncharov A F, Makarenko I N, Stishov S M *Zh. Eksp. Teor. Fiz.* **96** 670 (1989) [*Sov. Phys. JETP* **69** 380 (1989)]
34. Goncharov A F *Zh. Eksp. Teor. Fiz.* **98** 1824 (1990) [*Sov. Phys. JETP* **71** 1025 (1990)]
35. Goncharov A F *Pis'ma Zh. Eksp. Teor. Fiz.* **51** 368 (1990) [*JETP Lett.* **51** 418 (1990)]
36. Stishov S V *Khim. i Zhizn'* (4–5) (1991)
37. Aleksandrova M M, Demishev S V, Kosichkin Yu V, Larchev V I, Popova S V, Skrotskaya G G *Pis'ma Zh. Eksp. Teor. Fiz.* **43** 182 (1986) [(*JETP Lett.* **43** 230 (1986)]
38. Clarke D R, Kroll M C, Kirchner P D, Cook R F, Hockey B J *Phys. Rev. Lett.* **60** 2156 (1988)
39. Vohra Y K, Xia H, Ruoff A *Appl. Phys. Lett.* **57** 2666 (1990)
40. Mokrovskii N P, Regel A A *Zh. Tekh. Fiz.* **22** 1281 (1952)
41. Glazov V M, Chizhevskaya S N, Glagoleva N N *Zhidkiye Poluprovodniki* (Liquid Semiconductors) (Moscow: Nauka, 1968)
42. Regel' A R, Glazov V M *Fizicheskie Svoistva Elektronnykh Rasplavov* (Physical Properties of Electron Melts) (Moscow: Nauka, 1980)
43. Brazhkin V V, Voloshin R N, Popova S V *J. Non-Cryst. Solids* **136** 243 (1991)
44. Sethna J P, Shore J D, Huang M *Phys. Rev. B* **44** 4943 (1991)
45. Hemley R J, Jephcoat A P, Mao H K, Ming L C, Manghani H H *Nature (London)* **334** 52 (1988)
46. Richet P *Nature (London)* **331** 56 (1988)
47. Fecht H J, Johnson W L *Nature (London)* **334** 50 (1988)
48. Massobrio C, Pontikis V *Phys. Rev. B* **45** 2484 (1992)
49. Thorpe M F, Cai Y *J. Non-Cryst. Solids* **114** 19 (1989)
50. Denisov V N, Mavrin B N, Podobedov V B, Skrotskaya G G *Pis'ma Zh. Teor. Fiz.* **50** 363 (1989) [*JETP Lett.* **50** 393 (1989)]
51. Popova S V, Skrotskaya G G, Larchev V I, Zentai G, Pogany L, Denisov V N, Mavrin B N *J. Non-Cryst. Solid* **135** 255 (1991)
52. Shklovskii B I, Efros A L *Elektronnye Svoistva Splavov Poluprovodnikov* (Electronic Properties of Alloyed Semiconductors) (Moscow: Nauka, 1979)
53. Balagurov B Ya *Zh. Tekh. Fiz.* **52** 850 (1982) [*Sov. Phys. Tech. Phys.* **27** 544 (1982)]
54. Balagurov B Ya *Zh. Eksp. Teor. Fiz.* **89** 1796 (1985) [*Sov. Phys. Tech. Phys.* **62** 1036 (1985)]
55. Efros A L, Shklovskii B I *Phys. Stat. Solidi B* **76** 475 (1978)
56. Skal A S *Zh. Eksp. Teor. Fiz.* **88** 516 (1985) [*Sov. Phys. JETP* **61** 302 (1985)]
57. Balagurov B Ya *Fiz. Tekh. Poluprovodnikov* **20** 1276 (1986) [*Sov. Phys. Semicond.* **20** 805 (1986)]
58. Shklovskii B I *Zh. Eksp. Teor. Fiz.* **72** 288 (1977) [*Sov. Phys. JETP* **45** 152 (1977)]
59. Landau L D, Lifshitz E M *Elektrodinamika Sploshnykh Sred* (Electrodynamics of Continuous Media) (Moscow: Nauka, 1982)
60. Ozhovan M I, Semenov K N *Zh. Eksp. Teor. Fiz.* **101** 1286 (1992) [*Sov. Phys. JETP* **75** 696 (1992)]
61. Zvyagin I P *Kineticheskie Yavleniya v Neuporyadochennykh Poluprovodnikakh* (Kinetic Phenomena in Disordered Semiconductors) (Moscow: Moscow State University, 1984)
62. Coniglio A, Stanley H E *Phys. Rev. Lett.* **52** 1068 (1984)
63. Stanley H, "Fractal surfaces and "thermite" model for two-component irregular materials" in *Fractals in Physics: Proceedings of the VI Trieste International Symposium* ICTP, 1985 (Eds L Pietronero, E Tosatti) (Amsterdam: North-Holland, 1986)
64. Sokolov I M *Usp. Fiz. Nauk* **150** 221 (1986) [*Sov. Phys. Usp.* **29** (10) 924 (1986)]
65. Brandt N B, Demishev S V, Moshchalkov V V, Rylik A S, Chudinov S M *Zh. Eksp. Teor. Fiz.* **81** 743 (1981) [*Sov. Phys. JETP* **54** 398 (1981)]
66. Brandt N B, Demishev S V, Dmitriev A A, Moshchalkov V V, Parchevskaya L N, Chudinov S M *Zh. Eksp. Teor. Fiz.* **86** 1446 (1984) [*Sov. Phys. JETP* **59** 847 (1984)]
67. Rosenbaum T F, Andres K, Thomas G A, Bhatt R N *Phys. Rev. Lett.* **45** 1723 (1980)
68. Gantmakher V F, Zverev V N, Teplinskii V M, Barkalov O I *Pis'ma Zh. Eksp. Teor. Fiz.* **57** 373 (1993) [*JETP Lett.* **57** 390 (1993)]
69. Gantmakher V F, Zverev V N, Teplinskii V M, Barkalov O I *Zh. Eksp. Fiz.* **103** 460 (1993) [*J. Exp. Theor. Phys.* **76** 714 (1993)]
70. Brandt N B, Demishev S V, Dmitriev A A, Moshchalkov V V *Pis'ma Zh. Eksp. Teor. Fiz.* **38** 323 (1983) [*JETP Lett.* **38** 386 (1983)]
71. Al'tshuler B L, Aronov A G *Pis'ma Zh. Eksp. Teor. Fiz.* **37** 349 (1983) [*JETP Lett.* **37** 410 (1983)]
72. Zvyagin I P *Phys. Stat. Solidi B* **120** 503 (1983)
73. Alexander S, Laermans C, Orbach R, Rosenberg H M *Phys. Rev. B* **28** 4615 (1983)
74. Orbach R *Science* **231** 814 (1986)
75. Demishev S V, Kosichkin Yu N, Larchev V I, Lyapin A G, Popova S V, Skrotskaya G G, Sluchanko N E *Pis'ma Zh. Eksp. Teor. Fiz.* **45** 574 (1987) [*JETP Lett.* **45** 733 (1988)]

76. Demishev S V, Kosichkin Yu V, Lyapin A G, Sluchanko N E, Aleksandrova M M, Larchev V I, Popova S V, Skrotskaya G G *J. Non-Cryst. Solids* **97 – 98** 1459 (1987)
77. Demishev S V, Kosichkin Yu N, Larchev V I, Lyapin A G, Popova S V, Skrotskaya G G, Sluchanko N E *Fiz. Tekh. Poluprovodnikov* **22** 1666 (1988) [*Sov. Phys. Semicond.* **22** (9) 1051 (1988)]
78. Demishev S V, Kosichkin Yu N, Lyapin A G, Sluchanko N E *Zh. Eksp. Teor. Fiz.* **47** 654 (1988) [*JETP Lett.* **47** 755 (1988)]
79. Demishev S V, Kosichkin Yu N, Lyapin A G, Sluchanko N E, Chernyak S E *Fiz. Tverd. Tela* **30** 3691 (1988) [*Sov. Phys. Solid State* **30** (12) 2119 (1989)]
80. Demishev S V, Kosichkin Yu N, LYapin A G, Sluchanko N E, Sharambeyan M S *Fiz. Tekh. Vysokikh Davlenii* **1** 17 (1991)
81. Demishev S V, Kosichkin Yu N, Luntz D G, Lyapin A G, Sluchanko N E, Sharambeyan M S *Zh. Eksp. Teor. Fiz.* **100** 707 (1991) [*Sov. Phys. JETP* **73** (2) 394 (1991)]
82. Demishev S V, Kosichkin Yu N, Lyapin A G, Lunts D G, Sluchanko N E *Pis'ma Zh. Eksp. Teor. Fiz.* **56** 379 (1992) [*JETP Lett.* **56** 45 (1992)]
83. Naidu B S, Reddy P J *Thin Solid Films* **61** 379 (1979)
84. Demishev S V, Kosichkin Yu N, Lyapin A G, Sluchanko N E, Sharambeyan M S *Zh. Eksp. Teor. Fiz.* **104** (1993) [*JETP* **77** (1) 68 (1993)]
85. Brazhkin V V, Demishev S V, Kosichkin Yu N, Lyapin A G, Sluchanko N E, Frolov S V, Sharambeyan M S *Zh. Eksp. Teor. Fiz.* **101** 1980 (1992) [*Sov. Phys. JETP* **74** (6) 1020 (1992)]
86. *Dvoinye i Mnogokomponentnye Sistemy na Osnove Medi Spravochnik* (Binary and Multi-component Systems Based on Copper Reference Book) (Moscow: Nauka, 1979) p. 14
87. Skryshevskii A F *Strukturnyi Analiz Zhidkostei i Amorfnykh Sred* (Structural Analysis of Liquids and Amorphous Media) (Moscow: Vysshaya Shkola, 1980) p 47
88. Essamet M, Hepp B, Proust N, Dixmier J *J. Non-Cryst. Solids* **97 – 98** 191 (1987)
89. Parton V Z *Mekhanika Razrusheniya* (Mechanics of Breakdown) (Moscow: Nauka, 1990) p 80
90. Edelin J, Mathiot D *Phil. Mag. B* **42** 95 (1980)
91. Brazhkin V V, Demishev S V, Kosichkin Yu N, Luntz D G, Lyapin A G, Popova S V, Sluchanko N E, Frolov S V *Zh. Eksp. Teor. Fiz.* **104** 3126 (1993) [*JETP* **77** (3) 465 (1993)]
92. Milns A *Deep Impurities in Semiconductors* (New York: Wiley, 1973)
93. *Spravochnik Khimika* (Handbook for Chemists) (Leningrad: Khimiya, 1971) vol. 1, p. 384
94. Kavanagh K L, Cargill G S *Phys. Rev. B* **45** 3323 (1992)
95. Tibballs J E, Feteric S M, Barnea Z *Aust. J. Phys.* **34** 689 (1981)
96. Brazhkin V V, Abstracts of Thesis for the Degree of Candidate of Physics-Mathematical Sciences, Moscow, 1987, p 18
97. Christian J W *The Theory of Transformations in Metals and Alloys* (Oxford: Pergamon, 1975)
98. Hauser J J *Phys. Rev. B* **11** 738 (1975)
99. Lazarev B G, Semenkov E E, Tutov B I *Voprosy Atomnoi Nauki i Tekhniki. Seriya: Fundamental'naya i Prikladnaya Sverkhprovodimost'* (Problems in Atomic Science and Technology. Series: Fundamental and Applied Superconductivity) Vol. 1, number 4, 1976, p. 3
100. McWhan D B, Hull G W, McDonald T R R, Gregory E *Science* **147** 1441 (1965)
101. McDonald T R R, Gregory E, Barberich G S *Phys. Lett.* **14** 16 (1965)
102. Abrikosov A A *Osnovy Teorii Normal'nykh Metallov* (Foundations of the Theory of Normal Metals) (Moscow: Nauka, 1987) p 287
103. Baranowski J M, Liliental-Weber Z , Yau W F, Weber E R *Phys. Rev. Lett.* **66** 3079 (1991)
104. Buyanov A V, Laurs E R, Peka G P, Semashko E I, Tkachenko V N *Fiz. Tverd. Tela* **33** 2744 (1991) [*Sov. Phys. Solid State* **33** 1551 (1991)]